ISSN 1000-9620

海洋通报

Marine Science Bulletin

NATIONAL MARINE DATD AND
INFORMATION SERVICE OF CHINA

2016
Volume 18
Number 1

MARINE SCIENCE BULLETIN

Vol. 18 No. 1 May 2016

CONTENTS

Numerical simulation of tides, tidal currents and residual currents in the Yellow River estuary ····· GAO Jia et al. (01)

Submonthly timescale oscillation characteristics of the East Asian winter monsoon and its effect on the temperature of southwest China in 2010 ····· QI Dong-mei et al. (09)

Experimental study on the wave pressure of liquefied silty soil ····· HUANG Zhe et al. (29)

Methods for determining the development space in the conservation and utilization planning of uninhabited islands ····· JI Hou-de et al. (43)

Preliminary aquatic life criteria development and ecological risk assessment of ammonia in seven major river basins in China ····· WANG Yi-zhe et al. (55)

A preliminary study on food consumption, preference and day-night predatory difference of *Asterias amurensis* on *Scapharca Broughtonii* ····· ZHANG Tian-wen et al. (69)

Effects of salinities on the growth and nutrient compostition in the muscle of *Exopalaemon carinicauda* ····· JIANG Ju-feng et al. (81)

Distribution of heavy metals in suspension in Bohai Bay ····· DONG Yu-bo (93)

LIBRARY
Pacific Islands Fisheries Science Center
NOAA Fisheries
Honolulu, Hawai'i

NOAA CENTRAL LIBRARY
JAN 27 2017
WITHDRAWN
National Oceanic & Atmospheric Administration
US Dept of Commerce

Numerical simulation of tides, tidal currents and residual currents in the Yellow River estuary

GAO Jia[1, 2], CHEN Xue-en[2], YU Hua-ming[2], Ming LI[3]

1. *National Marine Data and Information Service, Tianjin* 300171, *China;*

2. *College of Oceanic and Atmospheric Sciences, Ocean University of China, Qingdao* 266100, *Shandong province, China;*

3. *Department of Engineering, University of Liverpool, U.K. L*669 3*BX*

Abstract: A 3-D Finite-Volume Coastal Ocean Model was applied in the Bohai Sea, especially near the Yellow River estuary, to simulate the tides, tidal currents, residual currents and shear fronts, using unstructured triangular grids. In the case of an accurate simulation of the tides and tidal currents in the Bohai Sea, this article focuses on the Yellow River mouth. The type of tides is irregular semi-diurnal and the type of tidal currents is the reciprocating flow, mostly parallel to the coastline. The tide induced eulerian residual currents are a couple of eddies on each side of the river mouth, with the anticlockwise on the left side and clockwise on the other side, and both of the eddies are enhanced by the Yellow River runoff. Two patterns of shear fronts are identified at the conversion between the flood and ebb tidal phase. The results suggest that the shear fronts be generated in the shallow water because the tidal phase of the coastal area is ahead of the deeper seaward area, then moves seaward and finally disappears 1-2 hours later.

Keywords: Huanghe (Yellow River) mouth; numerical simulation; tides; tidal currents; shear fronts; residual currents

Introduction

At present, the Yellow River mouth is located in Yellow River town, Kenli county, Dongying city, Shandong province, intersected between the Bohai Bay and Laizhou Bay. The Yellow River began to run northwestward into the sea, after it diverted from Weilv to Chahe branch in 1996(Fig. 1). Large sediments deposited as soon as the sediments discharged into sea, and the water and sediment regulation prolonged the spit for 1.6 km into sea in 2005. In the recent 50 years, the sharp decrease of water and soil discharge into sea was caused by human activities and natural factors. Hao et al.[1] found that the

Received on Mar. 15, 2016

Corresponding author: gaojia109@163.com

location of amphidromic point had changed obviously in recent years, which resulted in different tides, tidal currents, tidal residual currents, and shear front distribution. The mathematical model is an effective way to study the hydrodynamics of the estuary, and can overcome the space-time limitation of field observation in a certain extent. This paper simulates the hydrodynamics in Yellow River estuary using a three-D model, trying to solve the problems in the point of physical oceanography.

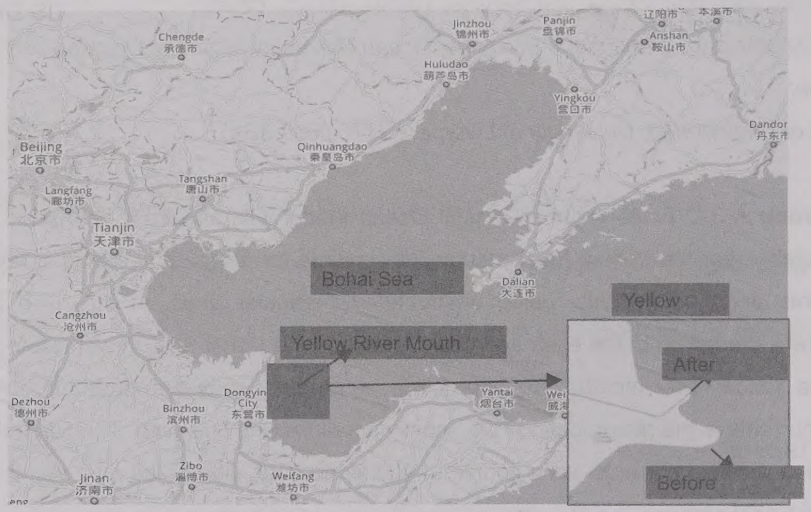

Fig. 1 Location of Yellow River estuary at present

1 Numerical model

This study is based on the unstructured grid and primitive equation, Finite Volume Coastal Ocean Model (FVCOM)[2] which applies the finite-volume discrete method using irregular triangular grids in the horizontal direction and a terrain-following coordinate in the vertical direction. FVCOM has been successfully used in the Bohai Sea by Chen et al.[3].

1.1 Model domain and topography

This paper focuses on the Yellow River estuary, therefore the model domain covers the entire Bohai and part of Huanghe, with the model grids and bathymetry shown in Fig. 2 and Fig. 3. The horizontal triangular mesh system includes 9 030 nodes and 16 989 triangular elements. The resolution near the estuary is 200 m and 12 km at the openboundary. In the vertical direction, a generalized terrain-following coordinate is used and 11 levels are applied. The model bathymetric data are obtained from Fang 2 mins.

1.2 Model forcing and initial conditions

The model is forced by tides and river discharge, and other forces such as surface

wind, atmospheric pressure and heat flux are not considered. The river discharge is used as 1 260 m^3/s, from Yellow River Sediment Bulletin 2007. The elevation at open boundary is predicted using t-tide software package by the main four tides, M_2, S_2, K_1 and O_1. The radiative boundary condition and standard non-slippery land boundary are used for the open boundaries and solid boundary, respectively.

2 Model validation

Harmonic analysis is applied to the tidal level outputs of the model. The iso-amplitude lines and iso-epoch lines of the main 4 tides are shown in Fig. 4, which is basically the same with atlas and former studies[4,5]. Compared with the tidal station in the Bohai Sea, the mean absolute errors of the 4 tides are 3.9 cm and 9.6° for amplitude and epoch respectively, indicating that the model meets requirements for hydrodynamics study in the Bohai Sea.

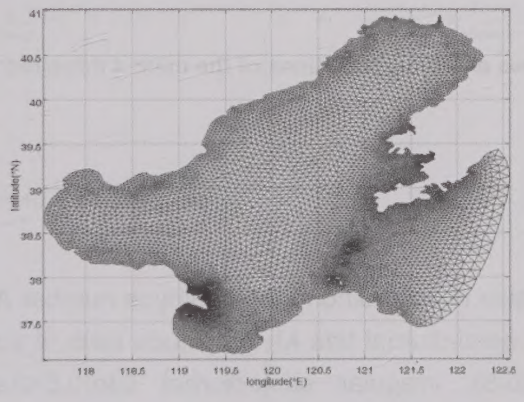

Fig. 2 Model domain and grids

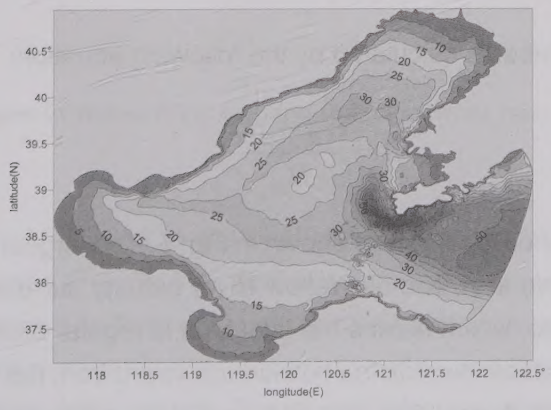

Fig. 3 Bathymetry of model domain

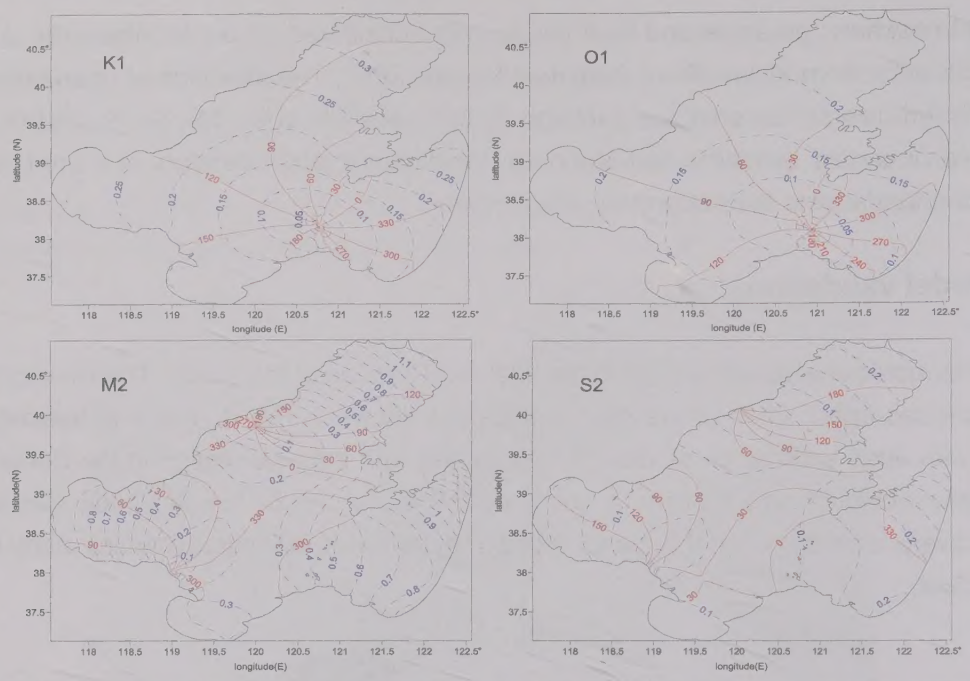

Fig. 4 Iso-amplitude lines and iso-epoch lines of the main 4 tides(red: epoch; blue: amplitude)

3 Model results

3.1 Tidal type

The tidal type division is according to the tidal type number A, the sum of diurnal tide K_1 and O_1 amplitude to semi-diurnal tide M_2 amplitude ratio. 4 tide types are the regular semi-diurnal tide($0<A\leq0.5$), irregular semi-diurnal tide($0.5<A\leq2.0$), irregular diurnal tide($2.0<A\leq4.0$), and regular diurnal tide($A\geq4.0$)[9]., reflecting relative importance of diurnal tide to semi-diurnal tide.

The tidal type number is calculated by the following equation:

$$A=\frac{H_{K_1}+H_{O_1}}{H_{M_2}} \tag{1}$$

The tidal type of the Bohai Sea is shown in Fig. 5. The largest tidal type number over 4 occurs in Qinhuangdao area and old Yellow River estuary surrounding the amphidromic point of semi-diurnal tide, which means the tidal type is regular diurnal tide in these areas. The tidal number decreases towards the outskirt backward from the amphdromic point, and it belongs to the irregular diurnal tide. The tidal type of the area east to the Bohai Strait and top of the Liaodong Bay is regular semi-diurnal tide. Other areas of the domain have

irregular semi-diurnal tides. For the Yellow River estuary, the tidal type west to the inlet is irregular diurnal tide as the number is over 2. The area southeast to the inlet has the irregular semi-diurnal tide in the Laizhou Bay.

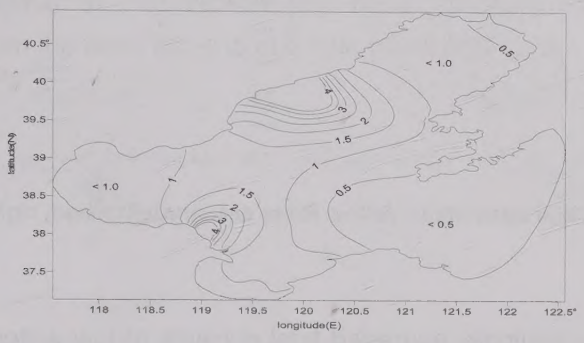

Fig. 5 Tidal type of the Bohai Sea

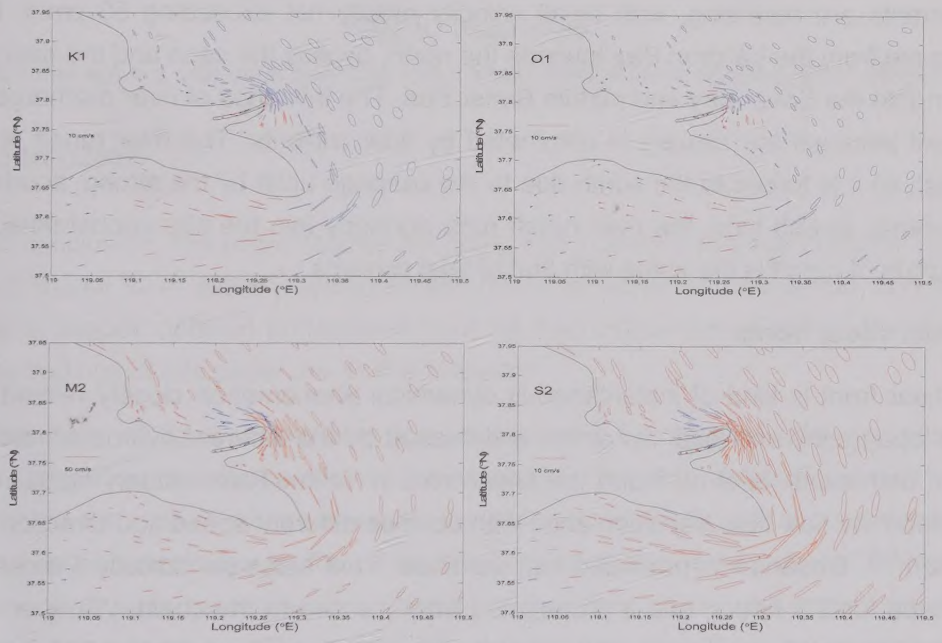

Fig. 6 Tidal ellipse in Yellow River estuary(red: clockwise; blue: anticlockwise)

3.2 Tidal ellipse

Harmonic analysis is applied to the tidal current output, obtaining the tidal ellipse distribution of the four tides (Fig. 6). The tidal ellipse is more flat as the reversing current near the coast and it is round far from coast as the rotating flow. In Yellow River estuary, the semi-diurnal tide is mostly anticlockwise. It is worth noting that the area northwest to the inlet is filled with clockwise tidal currents. The diurnal tides are mostly anticlockwise, while the area south to the inlet has clockwise tidal currents.

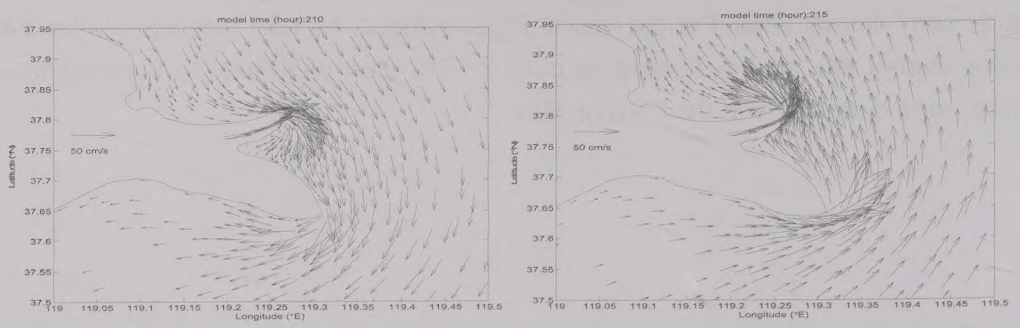

Fig. 7 Tidal currents in Yellow River estuary(left: flood, right: ebb)

3.3 Tidal currents

Fig. 7 shows the vertically averaged tidal currents of low water level, flooding, high water level and ebbing in Yellow River estuary. The tides flood from north to south, and the tidal currents are reversing, with small velocity mostly not exceeding 50 cm/s. Ebbing currents are from the Laizhou Bay towards the north, bypass the cape and the river mouth spit, turn into the Bohai Bay and middle Bohai Sea. The influence of river discharge is not significant because the estuary is dominated by tidal currents. The river runoff is to the northeast, so it is forced to the south due to the seepage uplift by the strong, southwardly tidal currents. In ebb time, the river runoff runs northerly into the sea unobstructed since the direction of runoff is the same with that of tidal currents.

3.4 Tidal shear fronts

Shear front is kind of instantaneous dynamical phenomenon closely related to the estuary topography and local dynamics and caused by the different hydrodynamic forces between both sides. Li et al. found the shear front in Yellow River estuary firstly in 1991, and defined the flow field transition zone with obvious different speed and direction as the shear front[13]. Observation produced that the shear front arose periodically 4 times a day and existed for 2-3 hours, and it propagated from the sea to the coast. Wang et al.[14,15] found the opposite results via tidal current observation in September 1995, and they believed that the shear front propagated from the coast to the sea and it lasted for 2 hours. This paper is consistent with Wang et al. We find two types of shear fronts, including the inner ebbing with outer flooding, and the inner flooding with outer ebbing. The shear front presents arc belt distribution, approximately parallel to the coast. It arises in the shallow water area and moves to the deeper water, with different duration about 1-2 hours. The discharge has not exercised a decisive influence on the shear front, only increased its intensity.

Because of the discharge, topography, friction and so on, the outer sea phase lags

behind the offshore at the tidal current transition time, with a shear belt between offshore and outer sea in different flow directions or velocities, thereby forming the shear front. The offshore area ebbs firstly and forms the inner ebbing with outer flooding when the ebb turns to flood tidal currents (Fig. 8). The offshore area floods firstly and forms the inner flooding with outer ebbing when the flood turns to ebb tidal currents (Fig. 9).

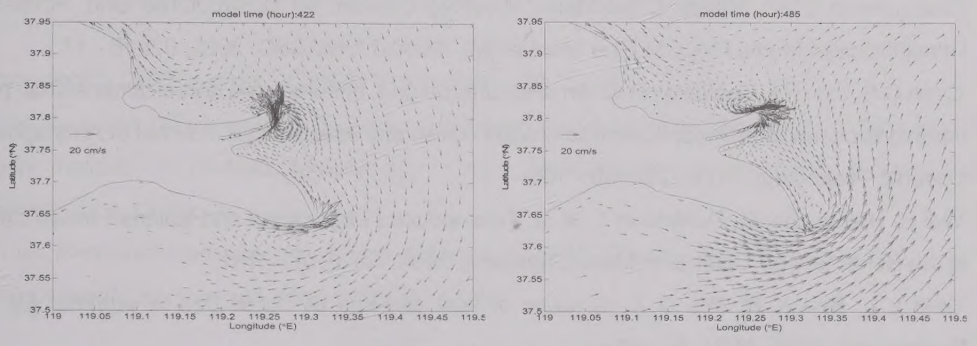

Fig. 8 Shear fronts

(left: inner ebbing with outer flooding; right: shear front of inner flooding with outer ebbing)

4 Conclusion

In conclusion, this paper studies the tides, tidal currents, residual currents and shear fronts of Yellow River estuary systematically based on numerical simulation, and helps us to have a deeper, detailed understanding of the hydrodynamics of Yellow River estuary. The key findings of this paper are as the following:

The type of tides is irregular semi-diurnal and the type of tidal currents is the reciprocating flow, mostly parallel to the coastline. The tide induced eulerian residual currents are a couple of eddies on each side of the river mouth, with the anticlockwise on the left side and clockwise on the other, and both of eddies are enhanced by the Yellow River runoff. 2 patterns of the shear fronts are identified at the conversion between the flood and ebb tide phase. The results suggest that the shear front be generated in the shallow area because of the tidal phase of the coastal area is ahead of the seaward area, then the shear front moves seaward and finally disappears 1-2 hours later.

Acknowledgements

This work was supported by National Key Technology Research and Development Program of the Ministry of Science and Technology of China (2014BAB12B02); Key Technologies Research and Development Program of Tianjin (14ZCZDSF00012).

References

[1] Hao Y, Le K T, Liu X Q. Numerical prediction of the tide wave distribution of Yellow River estuary in 2010 [J]. Marine Sciences, 2000, 24(6): 43 - 46.

[2] Changsheng Chen, Robert C.Beardsley, Geoffrey Cowles. An Unstructured Grid, Finite-Volume Coastal Ocean Modle FVCOM User Manual [M]. SMAST/UMASSD. 2006, 02: 16 - 17.

[3] Chen C S, Liu H D, Beardsley R C. An unstructured grid, finite-volume, three-dimensional, primitive equations ocean model: application to coastal ocean and estuaries [J]. Journal of Atmospheric and Oceanic Technology, 2003, 20: 159 - 186.

[4] Wei H, Hainbucher D, Pohlmann T, et al. Tidal-induced Lagrangian and Eulerian mean circulation in the Bohai Sea [J]. Journal of Marine Systems, 2004, 44(3):141 - 151.

[5] Qiao L L, Bao X W, Wu D X. Analysis of tidal currents of Bohai Sea in summer [J]. Ocean Engineering, 2006, 24(2): 38 - 44.

[6] Gao J, Chen X E, Yu H M, et al. Numerical simulation of tides, tidal currents, residual currents and shear front in estuary [J]. Periodical of Ocean University of China, 2010, 40(S): 41 - 48.

[7] Li G X, Cheng G D. Flow field shear front in Yellow River estuary at present [J]. Chinese Science Bulletin, 1994, 39(10): 928 - 932.

[8] Li G X, Tang Z S, Yue S H, et al. Sediment in the shear front off the Yellow River mouth [J]. Continental Shelf Research, 2001, 21(S6-7): 607 - 625.

[9] Wang H J, Yang Z S, Li Y H, et al. Dispersal pattern of suspended sediment in the shear frontal zone off the Huanghe mouth [J]. Continental Shelf Research, 2007, 27: 845 - 871.

黄河口海域潮汐、潮流、余流、切变锋数值模拟

高 佳[1,2]，陈学恩[2]，于华明[2]，李 明[3]

（1. 国家海洋信息中心，天津 300171；2. 中国海洋大学 海洋与大气学院，山东 青岛 266100；
3. 英国利物浦大学工程学院，利物浦 L669 3BX）

摘 要：采用有限体积三维近岸海洋模型，建立无结构三角形网格，对当今地形下的黄河口海域进行高分辨率数值模拟，在成功模拟渤海潮汐潮流的情况下，重点研究了黄河口海域。当前黄河口附近海域潮汐为不规则半日潮，潮流为往复流，方向近似平行于岸界，潮致欧拉余流在岬角两侧存在成对的涡旋，涡旋的方向为南顺北逆，黄河径流对此涡旋有加强的作用。由于地形等复杂因素的影响，河口海域附近在涨落潮转换过程中存在内涨外落型和内落外涨型切变锋，其首先出现在浅水区域，然后向深水区域传播，1～2 h 后消失，它的产生是由于近岸海域潮汐相位领先于外海海域潮汐相位。

关键词：黄河口；数值模拟；潮汐；潮流；余流；切变锋

Submonthly timescale oscillation characteristics of the East Asian winter monsoon and its effect on the temperature of southwest China in 2010

QI Dong-mei[1], LI Yue-qing[1], CHEN Yong-ren[2], DE Qing[3]

1. *Heavy Rain and Drought-Flood Disasters in Plateau and Basin Key Laboratory of Sichuan Province, Chengdu Institute of Plateau Meteorology, China Meteorology Administration, Chengdu* 610072, *Sichuan province, China;*

2. *Sichuan Provincial Meteorological Office, Chengdu* 610072, *Sichuan province, China;*

3. *Tibet Meteorological Bureau, Lhasa* 850000, *China*

Abstract: Using NCEP/NCAR R2 reanalysis daily data and daily meteorological observational data of southwest China in 2010, this paper studied the submonthly timescale oscillation characteristics of the East Asian winter monsoon (EAWM) and its effect on the temperature of southwest China in 2010 by bandpass filtering, wavelet transformation, composite analysis and correlation analysis. The main conclusions are as follows: The EAWM in 2010 was dominated by low-frequency oscillations of about 7-, 12-, and 30-day periods. There existed obviously negative correlation between the EAWM and the winter temperature in southwest China on submonthly, quasi-weekly and quasi-biweekly timescales, and negative correlation was more obvious on the quasi-biweekly than the quasi-weekly timescale. There was significant difference in the distribution of high, middle and low layer of the troposphere when the EAWM was on the submonthly, quasi-one-week and quasi-two-week timescales in the positive and negative phase. In the positive EAWM phase, the upper-level subtropical westerly jet is stronger and the East Asia trough is deeper, thus it is favorable for the dominance of more powerful north wind and lower temperature in southwest China. On the contrary, in the negative EAWM phase, the upper-level subtropical westerly jet is weaker and the East Asia trough is shallower, thus unfavorable for the north wind and lower temperature in southwest China.

Keywords: East Asian winter monsoon; submonthly timescales; southwest China; winter temperature; low-frequency oscillation

Received on Feb. 10, 2016

Corresponding author: qidongmei@163.com

1 Introduction

Monsoon refers to the phenomenon that the prevailing winds in near surface layer are opposite in winter and summer and the relative climate characteristics are significantly different, which is caused by the interaction of land-sea distribution, overall terrain and planetary wind belt, and its intensity and space structure changes closely in line with the changes of atmospheric circulation. China locates in East Asian monsoon region that has typical summer monsoon and also prominent winter monsoon. The East Asian winter monsoon, with large control area and long influence time, is one of the most active circulation systems in the winter of the northern hemisphere. The East Asian winter monsoon breaks out in terms of cold wave, not only brings on eastern Asian regional disastrous weather like cold damage, strong wind, freezing hazard and etc., but also influences the later circulation and weather significantly, for example, spring dust weather and flood and water logging disasters at northern China in summer, even leads to the global atmospheric circulation abnormality and thus significantly influences the global climate[1-7]. It has great science and social value to do research on the change and development rule of the monsoon. As a result, scholars pay great attention to the research on the East Asian winter monsoon.

There has been various researches on the East Asian winter monsoon and these researches define the East Asian monsoon index from various angles, namely the pressure difference of land and sea[8, 9], wind field[10-18], 500 hPa potential height field size[19-21], and these definition angles are all according to the change characteristics of the aspects of winter monsoon system, and all have the ability to characterize the abnormality of the East Asian winter monsoon though there are differences in the ability to reflect. The abnormality of the East Asian winter monsoon system directly influences the winter weather and climate in the monsoon region. According to the researches[22-25], the East Asian winter monsoon activity closely relates to the cold air activity in middle and high latitudes of Eurasian continent. As a result, when the winter monsoon is strong (weak), the subtropical North Wind Flow is strong (weak), and the winter temperature in China is low (high). Guo Qiyun[4] has researched on the relations between the changes of East Asian winter monsoon and the abnormality of temperature in China, he claims that the changes of winter monsoon is the direct cause of winter temperature changes in China, and that strong winter monsoon can influence south China. The result of statistical analysis shows that the East Asian winter monsoon is abnormally strong both in the extreme cold month during winter and all the winter months of south China[26]. The East Asian winter monsoon influences not only the winter temperature of the north China, but also the middle and lower

reaches of the Yangtze River, and even the south China and southwest China. A lot of researches show that the East Asian winter monsoon influences the synchronous circulation and climate, and also influences the circulation and climate in spring and summer [19, 21, 27-29]. In addition, there are also various researches on the temporal and spatial evolution of East Asian winter monsoon and the relations between the evolution and ENSO or AO[30, 31].

The researches on the East Asian winter monsoon in the past mainly focused on the seasonal, inter-annual and inter-decadal changes and their effects, not on the changing characteristics of winter monsoon on submonthly timescales, and a little on the East Asian winter monsoon's effect on the southwest China. To do research on the relations between the submonthly timescale oscillation characteristics in the East Asian winter monsoon and the winter temperature of southwest China has important value for the estimation of regional weather and climate phenomenon of the southwest China in short time period. From the autumn of 2009 to the winter of 2010, southwest China suffered great drought, which had large influence areas and caused great economic loss, and at the same time, caused the abnormal high temperature in southwest China in the winter of 2010. In this paper, it chooses the East Asian winter monsoon of 2010 as a typical example, and researches on the relations between the submonthly timescale oscillation characteristics of East Asian winter monsoon and winter temperature in southwest China, and also discusses the effect of the submonthly timescale oscillation characteristics of East Asian winter monsoon on the synchronize atmospheric circulation. In addition, in the year of 2010, the East Asian winter monsoon was typically weak and the temperature was higher than the usual one in southwest China, therefore, the East Asian winter monsoon in 2010 reflects its changing characteristics on submonthly timescales.

2 Data and methods

2.1 Data

The research resources are the average daily temperature, precipitation data of 107 sites in southwest China from 1980 to 2010 provided by National Meteorological Information Center and the NCEP/NCAR R2 daily reanalysis data, of which the reanalysis data includes the geo-potential height, horizontal zonal level, meridional wind level and temperature of the 12 isobaric surface in the troposphere, and the horizontal resolution of the data is 2.5 °×2.5 °. The paper defines the December of the previous year and January and February of the current year as the winter months, that is to say, the winter months of 2010 was December of 2009, January and February of 2010.

2.2 Methods

Wavelet analysis is a kind of signal time-frequency analysis method. Morlet wavelet is complex wavelet, it can be used to do periodic analysis that is better to inflect the local feature of the signal compared with Fourier and can widely be used in climate diagnosis[32-34]. The paper uses Morlet wavelet function to determine the main submonthly timescales of the East Asian winter monsoon activity in 2010. In order to extract the oscillation characteristics of East Asian winter monsoon in the submonthly timescale, this paper uses Butterworth filter function on East Asian winter monsoon daily sequence bandpass filter index[35]; at the same time, synthetic analysis, correlation analysis and other statistical methods are used to do research on the relations between the submonthly timescale oscillation characteristics and winter temperature in southwest China. The southwest China researched in this paper refers to the region (97 - 110 °E, 21 - 32 °N), it mainly includes Yunnan, Sichuan, Chongqing, Guizhou, and most parts in Guangxi(Tab. 1).

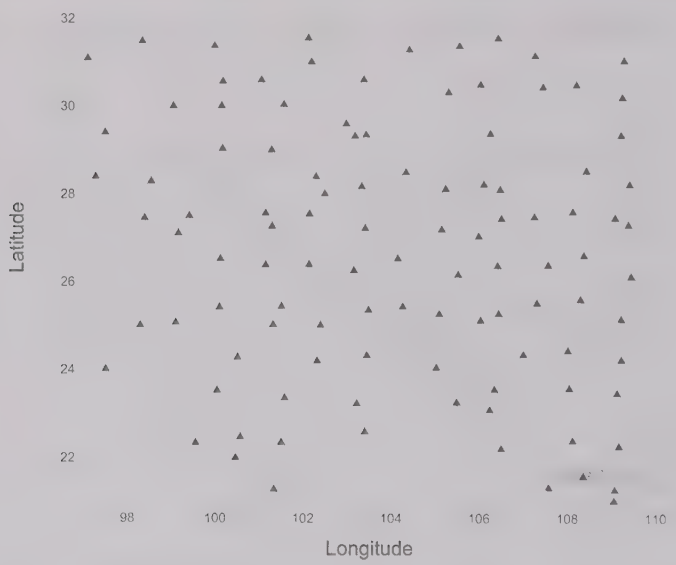

Fig. 1 Distribution of meteorological sites in southwest China

2.3 The determination of East Asian winter monsoon

To do research on the changing of East Asian winter monsoon, first step is to determine how to quantitatively describe winter monsoon activity, that is to say, what index to represent the East Asian winter monsoon. There are various definitions of East Asian winter monsoon. For example, Shineng et al.[8] used thermal difference between the land and sea to represent the changing of East Asian winter monsoon index; Ji et al.[10] used the average 1000 hPa meridional wind field in the area of 115 - 130 °E, 10 - 30 °N to define the

East Asian winter monsoon index; Sun Shuqing et al.[19] took the average 500 hPa geo-potential height field size among the area 125 - 145 °E, 30 - 45 °N as the index to show the strength of the East Asian winter monsoon; Jhun et al.[16] used anomaly of upper troposphere westerly jet to show the changing of East Asian winter monsoon. The above indices are from different angles with different features, and all can reflect the changing characteristics of East Asian winter monsoon.

The physical process of the upper and lower troposphere in the high latitude and low latitude regions can be used to predict the monsoon changes, and under the premise of considering the ocean change characteristics of low latitude area (ENSO) and high latitude atmospheric variations (AO). Li Yueqing et al.[18] defined a new East Asian winter monsoon index using the upper troposphere 200 hPa average zonal wind shear in the tropics (90 - 160 °E, 5 °S - 10 °N), subtropical (90 - 160 °E, 30 - 35 °N) and temperate zone(70 - 170 °E, 50 - 60 °N), and concrete calculating methods are as follows:

$$I=[U_{200}(90 - 160\ °E/30 - 35\ °N)- U_{200}(70\text{-}170\ °E/50 - 60\ °N)+ U_{200}(90\text{-}160\ °E/30\text{-}35\ °N)- U_{200}(90\text{-}160\ °E/5\ °S\text{-}10\ °N)]/2,$$

The larger (smaller) the index is, the stronger (weaker) the East Asian winter monsoon will be.

3 Main submonthly timescales of the East Asian winter monsoon

From the autumn of 2009 to the winter of 2010, southwest China has suffered the greatest drought disaster since 1951, with higher than usual temperature in the area, durative low precipitation, long period of drought and wide range of influence. The drought disaster has caused severe economic damage, largely affected people's daily life and national economy. Fig. 2 is the anomaly distribution of temperature and precipitation in the southwest China during the winter of 2010, and it can be seen from the Fig. 2a that the temperature in the whole winter of 2010 was higher than that in previous years, and high value centers concentrated in eastern Yunnan, southwestern Guizhou and northwestern Guangxi; precipitation of the southwest China were negative anomaly in addition to the southwest part of Guangxi, and there were low value centers in Yunnan, Guizhou and in the northern part of Guangxi (Fig. 2b), showing that the high temperature and drought disaster in southwest China has wide influence area, large range and strong intensity. Huang Ronghui et al.[36] studied the cause of the severe drought and pointed out that the winter and spring drought in southwest China was closely related to the anomaly winter and summer circulation in the tropical western Pacific and the bay of Bengal and the Indochina Peninsula, and also had a certain relationship with the middle and high latitude

circulation in the northern hemisphere. The paper takes the East Asian winter monsoon of 2010 as a typical case, to further study the relationship between the submonthly timescale oscillation characteristics of the East Asian winter monsoon and winter temperature in southwest China, and to discuss the effect of the submonthly timescale oscillation of the East Asian winter monsoon on the atmospheric circulation over the same period.

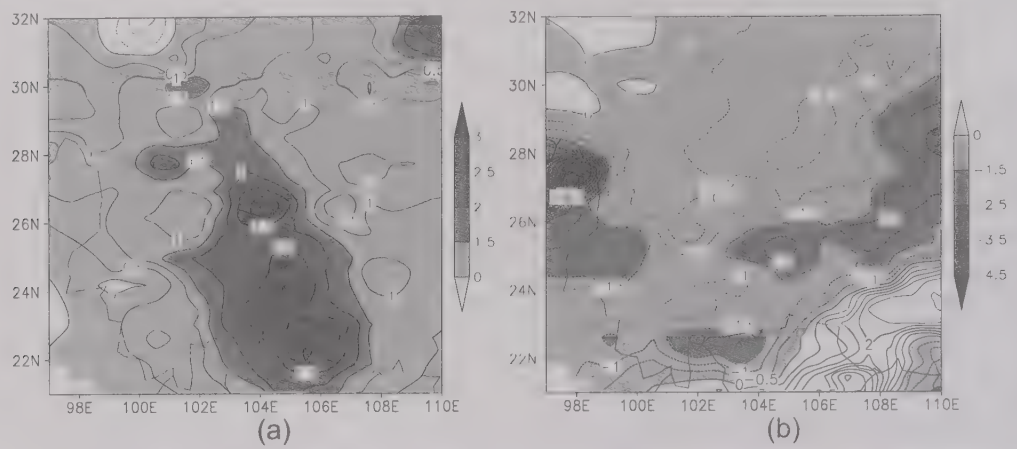

Fig. 2 Anomaly distribution of the temperature (a, Unit: °C) and precipitation (b, Unit: mm) in the southwest China during the winter of 2010

Based on the determination of East Asian winter monsoon in the previous section, the paper calculated the index of East Asian winter monsoon of 2010 and also carried out wavelet analysis of the East Asian winter monsoon index by using the wavelet function, determining the main time scale of its activities within the month. As can be seen in Fig. 3, the East Asian winter monsoon had mainly low frequency oscillation with about 7 days, 12 days and 30 days of period in a month, in addition, it can be seen from the wavelet variance in the frequency domain (Fig. 4) that the wavelet variance of the East Asian winter monsoon in 2010 had a maximum value at 7 days, 12 days and 30 days. The author of this paper ever calculated the main submonthly timescales of East Asian winter monsoon activities from 1980 to 2012, and found that there was a significant changing period mainly with the period of quasi-week(5 - 10 days), quasi-two-weeks(10 - 20 days) and quasi-three-weeks (20 - 30 days).

4 Submonthly timescale oscillation characteristics of the East Asian winter monsoon and its effect on the temperature in Southwest China

After analyzing the previous section, it can be found that the periodic submonthly timescale activity characteristics of 2010 East Asian winter monsoon is significant, then what is the submonthly timescale changing characteristics? What is the relationship

between the changing character and the winter temperature of southwest China? Following parts will further discuss these questions. Fig. 5 shows the daily variation of the East Asian winter monsoon index in 2010, indicating that during the activities of 2010 East Asian winter monsoon, the winter monsoon constantly becomes stronger from 6th of December, and the monsoon strong stage starts from 15th of December and peaks at 12nd of January, then lasts till 6th of February, afterward it will be weaker and weaker.

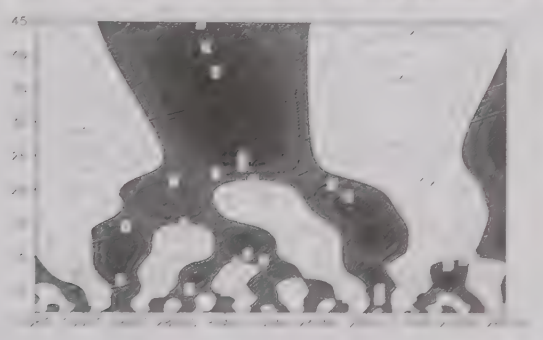

Fig. 3 The diagram of Morlet wavelet real part coefficient for analyzing the East Asian winter monsoon in 2010 (the shadow area denoting the positive phase)

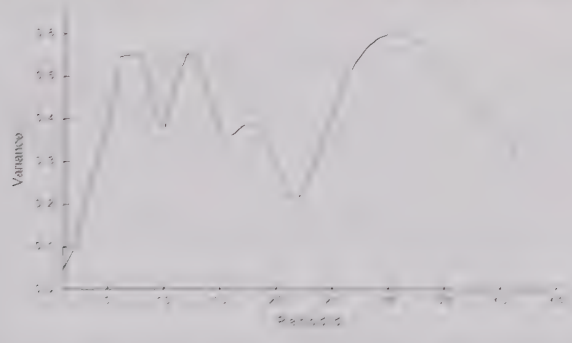

Fig. 4 The diagram of Morlet wavelet variance for analyzing the East Asian winter monsoon in 2010

The East Asian winter monsoon index submonthly timescales (5 - 30 days), quasi-week (5 - 10 days), quasi-two-weeks (10 - 20 days) and quasi-three-weeks (20 - 30 days) were treated with band-pass filter according to the wavelet analysis in the previous section, and the processed time series and the daily temperature of southwest China in 2010 are drawn in the same figure (Fig. 6). It can be seen from the figure that the submonthly, quasi-week, quasi-two-week, and quasi-three-week oscillation of the Asian Winter Monsoon are very active, and amplitude and oscillation peak in quasi-two-week. The submonthly, quasi-week, quasi-two-week and quasi-three-week oscillation index of the East Asian winter monsoon as well as the correlation coefficients of winter temperature in southwest China are calculated respectively, and the results show that the correlation

coefficient of the index after 5 - 30 days of band-pass filter processing and the daily air temperature in the southwest China is as high as -0.53, and it passes the 0.001 reliability test; the correlation coefficient of the index after 5 - 10 days of band-pass filter processing and the daily air temperature in the southwest China is -0.29, which passes the 0.01 reliability test; the correlation coefficient of the index after 10 - 20 days of band-pass filter processing and the daily air temperature in the southwest China is as high as -0.55, passing the 0.001 reliability test; the correlation coefficient of the index after 20 - 30 days of band-pass filter processing and the daily air temperature in the southwest China is -0.1, which fails to pass the significant test. The above analysis shows that there is a good correlation among the submonthly, the quasi-week and quasi-two-week timescales of the East Asian winter monsoon index of strong stage, and the period of low temperature in southwest China, as a result, the oscillation feature of the East Asian winter monsoon on submonthly, the quasi-week and quasi-two-week timescales can excellently indicate the strong low temperature process in the southwest China of the same time. The winter low temperature in southwest China is mainly affected by the oscillation of East Asian winter monsoon on submonthly, the quasi-week and quasi-two-week timescales.

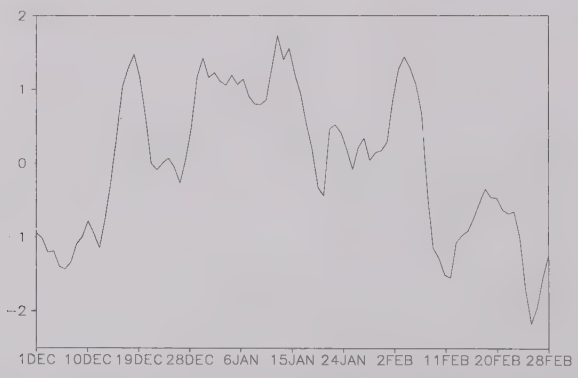

Fig. 5 Changes in the daily indices of East Asian winter monsoon in 2010

5 The corresponding atmospheric circulation characteristics of positive and negative phase in the East Asian winter monsoon of submonthly oscillation period

The analysis in the previous section found that the East Asian winter monsoon in 2010 is periodically active mainly of quasi-week, quasi-two-week and quasi-three-week, and there is a good corresponding relationship between the oscillation of East Asian winter monsoon on submonthly, quasi-week and quasi-two-week timescales and the winter temperature in the southwest of China. Then, what are the corresponding atmospheric circulation characteristics of positive and negative phase in the East Asian winter monsoon

submonthly oscillation period? What is its influencing process and mechanism on the winter temperature of Southwest China? The following part will discuss theses questions in detail.

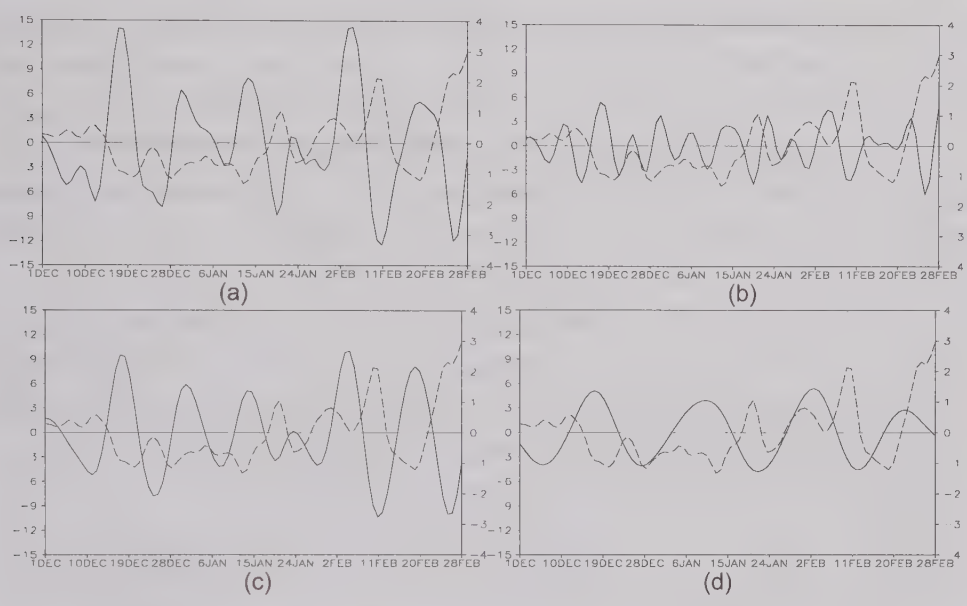

Fig. 6 Changes of the indices of East Asian winter monsoon (solid line) and the daily winter temperature in southwest China (dotted line) on submonthly(a), quasi-one-week (b), quasi-two-week(c) and quasi-three-week(d) time scales in 2010

5 - 30 days of time scale can represent the overall or average activity characteristics of East Asian winter monsoon, and the analysis of the scale characteristics of the quasi-week and quasi-two-week is conducive to more detailed understanding of the main characteristics of activity on submonthly timescales. The following parts, first of all, will analyze the distribution characteristics of tropospheric circulation in the positive and negative phases on submonthly timescales (5 - 30 days) of the East Asian winter monsoon, including the distribution characteristics of the potential height field, wind field and temperature advection, and secondly to discuss the differences characteristics of each time scale (quasi-week, quasi-two-week).

5.1 The corresponding atmospheric circulation characteristics of positive and negative phase in the East Asian winter monsoon on submonthly timescales

The paper uses the method of Maloney et al.[37] to carry out the phase synthesis, and to select 5 positive wave peak value (17, 30, 44, 66, 80) and 5 negative wave peak value (12, 26, 50, 72, 87) among the submonthly timescales (5 - 30 days) of East Asian winter monsoon index to carry out synthetic analysis.

Firstly, the 200 hPa zonal wind anomaly synthetic features are analyzed corresponding to the positive and negative phase of the East Asian winter monsoon on submonthly timescales (Fig. 7a and 7b). It can be seen from the figure that the anomaly synthetic features corresponding to the positive and negative phase of the East Asian winter monsoon on submonthly timescales are opposite. That is to say, when the East Asian winter monsoon is in the positive phase, the subtropical westerly jet is stronger and the center intensity is stronger than mean value about 12 m/s and the zonal wind on north side will weaken, which may cause East Asia cold and dry air popular as well as frequent cold air activities, and this change may lead to low temperature through the influence on East Asian meridional secondary circulation and strengthen the low layer weather disturbances[38, 39]. Fig. 7b reflects that when the East Asian winter monsoon is in the negative phase, the subtropical westerly jet is weaker and the center intensity is weaker than mean value about 24 m/s, and the zonal wind on both sides will be strengthened, which is not conducive to the low temperature in the southwest China.

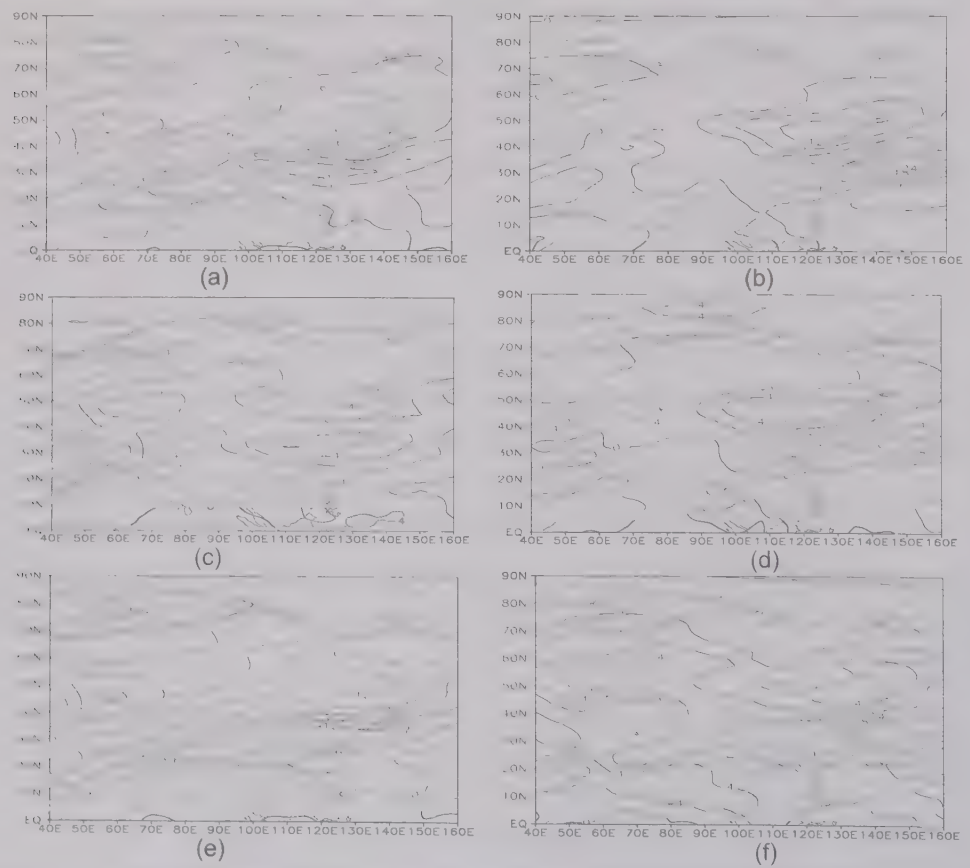

Fig. 7 The 200 hPa zonal wind anomaly fields corresponding to the positive(a, c, e) and negative(b, d, f) phase of the East Asian winter monsoon on submonthly(a, b), quasi-one-week (c, d), and quasi-two-week(e, f) time scales (unit: m/s)

Secondly, the 500 hPa height anomaly fields in the middle troposphere corresponding to the positive and negative phase of the East Asian winter monsoon on submonthly timescales are opposite (Fig. 8a and 8b). In Fig. 8a, 500 hPa height anomaly synthetic field near the East Asia trough shows obvious negative anomaly, indicating that the East Asian winter monsoon in the positive phase, the East Asian trough is stronger; the airflow of the upper reaches of the north-west is also strong; cold air activity is active in East Asia region; it is advantageous to the low altitude cold air south to affect the southwest China, and prone to the low temperature. In Fig. 8b, 500 hPa height anomaly synthetic field near the East Asia trough shows obvious positively anomaly, indicating that when the East Asian winter monsoon is in the negative phase, the East Asian trough is weaker; the airflow of the upper reaches of the north-west is also weak; cold air activity is inactive in East Asia region; it is not advantageous to the low altitude cold air south to affect the southwest China.

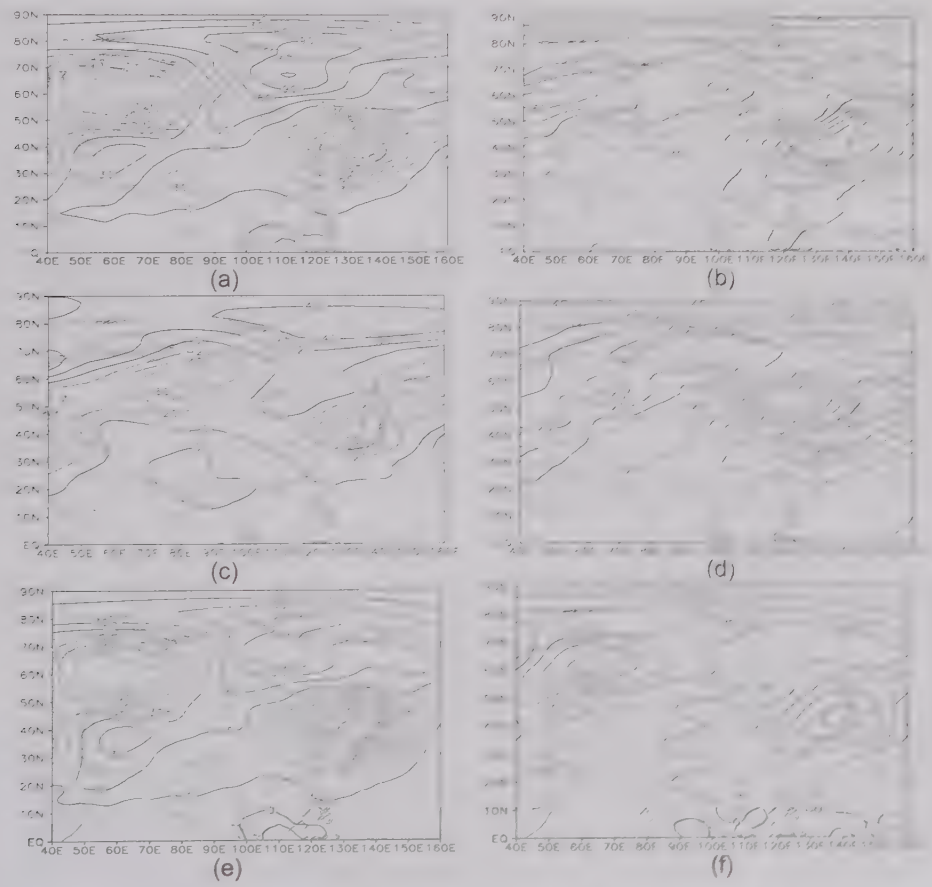

Fig. 8 The 500 hPa height anomaly fields corresponding to the positive(a, c, e) and negative(b, d, f) phase of the East Asian winter monsoon on submonthly(a, b), quasi-one-week (c, d), and quasi-two-week(e, f) time scales (unit: gpm)

In addition, it is worth to note the 850 hPa wind fields in the lower troposphere corresponding to the positive and negative phase of the East Asian winter monsoon on submonthly timescales (Fig. 9a and 9b). From Fig. 9a, when the East Asian winter monsoon is in the positive phase, the southwest China is consistent with partial strong northeast wind anomaly, indicating that the northeast wind is strong over the southwest China, which is conducive to the delivery of cold air near the surface layer to the southwest China, causing low temperature in southwest China in winter; when the East Asian winter monsoon is in the negative phase (Fig. 9b), the southwest China is consistent with the southwest wind anomaly, which is not conducive to the delivery of cold air near surface layer to the southwest China, unlikely to cause low temperature in southwest China in winter.

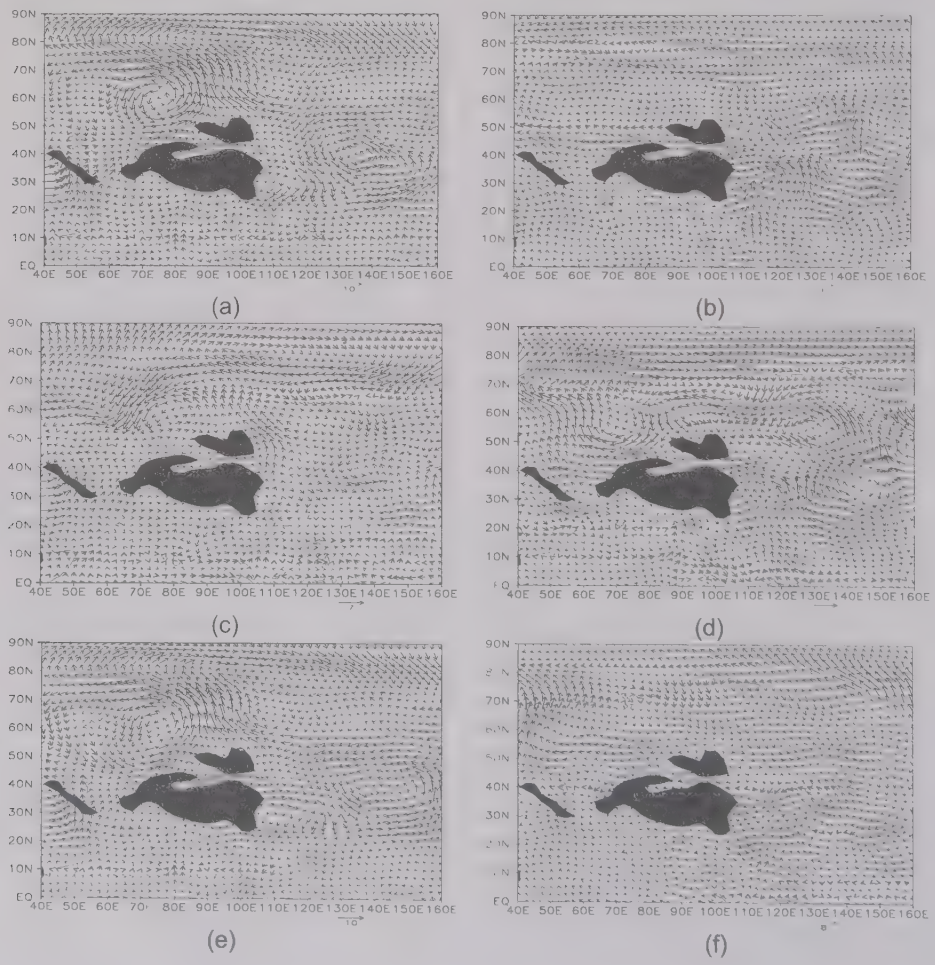

Fig. 9 The 850 hPa wind anomaly fields corresponding to the positive(a, c, e) and negative(b, d, f) phase of the East Asian winter monsoon on submonthly(a, b), quasi-one-week (c, d), and quasi-two-week(e, f) time scales (unit: m/s)

At last, from the 850 hPa temperature advection anomaly synthetic fields corresponding to the positive and negative phase of the East Asian winter monsoon on submonthly scale (Fig. 10a and 10b), the variation features of temperature advection in southwest China are completely opposite. That is to say, when the East Asian winter monsoon is in the positive phase (Fig. 10a), the 850 hPa is controlled by the cold advection over most of the southwest China, which is advantageous to the low temperature in southwest China in winter. When the East Asian winter monsoon is in the negative phase (Fig. 10b), the 850 hPa is controlled by the warm advection over most of the southwest China, which is advantageous to the high temperature in southwest China in winter.

In summary, when the East Asian winter monsoon on submonthly timescale is in positive and negative phase, there are significant differences in the distribution of the upper, middle and lower layer of the troposphere. When the East Asian winter monsoon is in the positive phase, the subtropical westerly jet in the upper troposphere is strong, and the cold air activities in East Asia are frequent; when East Asian trough in the middle troposphere is strong, its upper reach of the northwest airflow is strong, which is conducive to guiding the cold air southward; when the Northeast wind in the lower troposphere is strong over the southwest China, it is conducive to the transport of cold air from surface layer to the southwest China, leading to low temperature in the southwest China. When the East Asian winter monsoon is in the negative phase, the subtropical westerly jet in the upper troposphere is weaker; middle troposphere with a weak East Asian Trough causes the upper reaches of the northwest airflow weak, which is not conducive to guide the cold air southward, and East Asia cold air activity is weak; when the southwest China of the lower troposphere wind field is the southwest wind anomaly, it is not conducive to the transmission of cold air from the near surface layer to the southwest China, causing high temperature in southwest China in winter.

5.2 The corresponding atmospheric circulation characteristics of positive and negative phase in the East Asian winter monsoon on main submonthly timescales

In this paper, we select 8 positive wave peak value (9, 17, 30, 44, 53, 66, 84, 90) and 9 negative wave peak value (6, 13, 21, 27, 40, 50, 62, 71, 87) of the East Asian winter monsoon for quasi-week (5-10 days) as well as 5 positive wave peak value (17, 31, 44, 66, 80) and 6 negative wave peak value (11, 24, 38, 59, 72, 87) for that of quasi-two-week (10 - 20 days) on the main submonthly timescale feature of East Asian winter monsoon, then these values are synthesized respectively.

As to the anomaly synthetic features of the East Asian winter monsoon on the main submonthly timescales corresponding to positive and negative phase of the 200 hPa zonal

wind (Fig. 7c-f), the features are opposite for quasi-week and quasi-two-week. The central intensity of the subtropical westerly jet is strong and the center intensity is stronger than mean value about 8 m/s for the quasi-week in the positive phase and stronger than mean value about 12 m/s for quasi-two-week in the positive phase. Comparing these two values, it's found that the value is stronger for quasi-two-week than that for quasi-week. The central intensity of the subtropical westerly jet is weak and the center intensity is weaker than mean value about 8 m/s for quasi-week and quasi-two-week in the negative phase, however, the value range of quasi-two-week is larger than that of quasi-week, which indicates that the subtropical westerly jet of quasi-two-week is weaker than that of quasi-week in negative phase. The above analysis shows that when the East Asian winter monsoon is in the positive phase for quasi-week and quasi-two-week, the subtropical westerly jet is strong, and the cold air activity is frequent, which is conducive to the low temperature in the southwest China and vice versa. The effect of the phases for quasi-two-week on the southwest temperature is more significant than that for quasi-week.

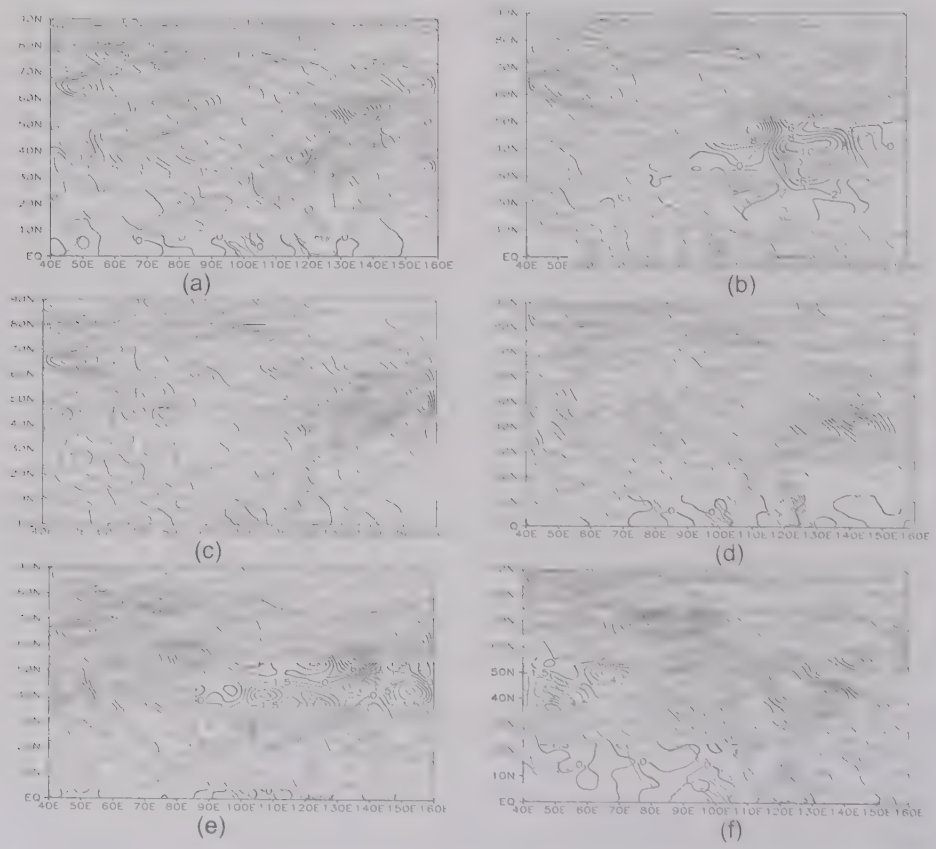

Fig. 10 The 850 hPa temperature advection anomaly fields corresponding to the positive(a, c, e) and negative(b, d, f) phase of the East Asian winter monsoon on submonthly(a, b), quasi-one-week (c, d), and quasi-two-week(e, f) time scales (unit: 10^{-5} K/s)

From the figure of 500 hPa height anomaly fields corresponding to the positive and negative phase of the East Asian winter monsoon on the main submonthly timescales (Fig.8c-8f), it's found that when the East Asian winter monsoon on the quasi-week and quasi-two-week is in positive phase (Fig. 8c and 8e), the 500 hPa height anomaly field is obviously negative in the vicinity of East Asian trough, and the East Asian trough is strong and among the northwest air flow that behind the trough of southwest China, cold air is active and more likely to cause low temperature weather. Comparing Fig. 8c and 8e, it can be found that the anomaly range of 500 hPa height near East Asian trough for quasi-two-week is larger and the low value center is stronger than those of quasi-week in positive phase. That is to say, the East Asian trough and the cold air behind it are stronger for quasi-two-week than those for quasi-week in positive phase, and more conductive to low temperature weather for southwest China. When the East Asian winter monsoon on the quasi-week and quasi-two-week is in negative phase (Fig. 8d and 8f), the 500 hPa height anomaly field is obviously positive in the vicinity of East Asian trough, and the East Asian trough is weak and cold air is inactive thus less likely to cause low temperature weather in southwest China. In addition, the anomaly range of 500 hPa height near East Asian trough for quasi-two-week is larger and positive anomaly center is larger than those for quasi-week when it is in negative phase. That is to say, the East Asian trough is weaker for quasi-two-week than that for quasi-week when it is in negative phase.

Look at the 850 hPa wind field corresponding to the positive and negative phase of the East Asian winter monsoon (Fig. 9c-9f), it can be seen that when the East Asian winter monsoon on quasi-week is in positive phase (Fig. 9c), the region over southwest China is controlled by easterly wind anomaly; when the East Asian winter monsoon on quasi-two-week is in positive phase (Fig. 9e), the region over southwest China is controlled by northeast wind anomaly, which is conductive to the transmission of cold air from high latitude to southwest China; when the East Asian winter monsoon on quasi-week and quasi-two-week is in negative phase (Fig. 9d and 9f), the region over southwest China is controlled by southwest wind anomaly, which is not conductive to the transmission of cold air to the southwest China. Comparing figure 9c and 9e, it can be found that the northeast wind for quasi-two-week is stronger than that for quasi-week when it is in positive phase, which is more likely to cause low temperature weather in southwest China.

From the 850 hPa temperature advection anomaly synthetic field corresponding to the positive and negative phase of the East Asian winter monsoon (Fig. 10c-10f), when the East Asian winter monsoon on quasi-week is in positive phase (Fig.10c), the region over southwest China has cold advection, and when the East Asian winter monsoon on quasi-two-week is in positive phase (Fig.10e), the region over southwest China has also

cold advection and it is more stronger than that for quasi-week, which is more likely to cause low temperature weather. When the East Asian winter monsoon on quasi-week and quasi-two-week is in negative phase (Fig. 10d and 10f), the region over southwest China has warm advection, which is unlikely to cause low temperature weather.

The above analyses come to the summary that when East Asian winter monsoon on quasi-week and quasi-two-week is in positive phase, the circulation fields of upper, middle, and lower layer troposphere are likely to cause low temperature in southwest China in winter, and when it is in negative phase, it is unlikely to cause low temperature weather in southwest China. It is worth noting that the effect of East Asian winter monsoon for the quasi-two-week is more obvious than that of the quasi-week on winter temperature in southwest China, consistent with the results of the previous section.

6 Conclusions and discussion

The paper studies the submonthly timescale oscillation characteristics of the East Asian winter monsoon and the relationship between the oscillation characteristics and winter temperature in southwest China as well as the atmospheric circulation through various analysis methods, leading to the following results.

(1) It's found that the East Asian winter monsoon in 2010 is mainly low frequency oscillation with about 7 days, 12 days and 30 days of periods on submonthly timescale with wavelet analysis. The East Asian winter monsoon Index on submonthly timescale (5 - 30 days), quasi-week (5 - 10 days), quasi-two-weeks (10 - 20 days) and quasi-three-weeks (20 - 30 days) were treated with band-pass filter according to the wavelet analysis in the previous section and then it's found that the oscillation for all these time scales are active in the whole winter monsoon period, amplitude and oscillation peak and most active on quasi-two-weeks.

(2) Through the correlation analysis, we find that there is an obvious negative correlation among the East Asian winter monsoon index on submonthly, quasi-weekly, and quasi-biweekly timescales and the period of low temperature in southwest China, as a result, the oscillation feature of the submonthly, quasi-weekly, and quasi-biweekly timescales can excellently indicate the strong low temperature process in southwest China of the same time. The winter low temperature in southwest China is mainly affected by the oscillation of the East Asian winter monsoon on submonthly, quasi-weekly, and quasi-biweekly timescales.

(3) With the analysis of the phase synthesis, the paper finds that there are

significant differences in the distribution of the flow field in the upper, middle, and lower layer of the troposphere when the East Asian winter monsoon on submonthly timescale in positive phase and negative phase. When the East Asian winter monsoon is in the positive phase, the subtropical westerly jet in the upper troposphere is strong, and the cold air activities in East Asia are frequent; when the East Asian trough in the middle troposphere is strong, its upper reaches of the northwest airflow is strong, which is conducive to guiding the cold air southward; when the Northeast wind is strong over the southwest China in the lower troposphere, it is conducive to the transport of cold air from surface layer to the southwest China, leading to low temperature in the southwest China. When the East Asian winter monsoon is in the negative phase, the subtropical westerly jet in the upper troposphere is weaker; middle troposphere with a weak East Asian trough causes the upper reaches of the northwest airflow weak, which is not conducive to guide the cold air southward, and East Asia cold air activity is weak; when the southwest China of the lower troposphere wind field has the southwest wind anomaly, it is not conducive to the transmission of cold air from the near surface layer to the southwest China, causing high temperature in southwest China in winter.

(4) When East Asian winter monsoon is in positive phase in the scale of quasi-week and quasi-two-week, the circulation fields of upper, middle, and lower layer troposphere are likely to cause low temperature in southwest China in winter, and when it is in negative phase, it is unlikely to cause low temperature weather in southwest China. It is worth noting that the effect of East Asian winter monsoon for the quasi-two-week is more obvious than that of the quasi-week on the winter temperature in southwest China.

References

[1] ZHU Quangen, LIN Jinrui, SHOU Shaowen, et al. Principles and methods of synoptic meteorology [M]. Beijing: Chinese Meteorological Press, 2000: 565 - 599.

[2] CHEN Jun, SUN Shuqing. Eastern Asian winter monsoon anomaly and variation of global circulation part Ⅰ: A comparison study on strong and weak winter monsoon [J]. Chinese Journal of Atmospheric Sciences, 1999, 23(1): 101 - 111.

[3] HE Shengping, WANG Huijun. An Integrated East Asian Winter Monsoon Index and Its Interannual Variability [J]. Chinese Journal of Atmospheric Sciences, 2012, 36(3): 523 - 538.

[4] GUO Qiyun. Relationship between the variations of East Asian winter monsoon and temperature anomalies in China [J]. Journal of Applied Meteorological Science, 1994,5(2): 218 - 225.

[5] LI Yueqing, TONG Wenlin. Anomalies of East Asian winter monsoon and ENSO and its prediction value [J]. Journal of Chengdu Institute of Meteorology, 1999,14(1): 14 - 19.

[6] HUANG Ronghui, WEI Ke, CHEN Jilong, et al. The East Asian winter monsoon anomalies in the

winter of 2005 and 2006 and their relations to the Quasi-stationary planetary wave activity in the Northern hemisphere [J]. Chinese Journal of Atmospheric Sciences, 2007,31(6): 1 033 - 1 048.

[7] GAO Hui, LIU Yunyun, WANG Yong. Influences of the East Asian winter monsoon on the sand storm days in Northern China in boreal spring [J]. Plateau and Mountain Meteorology Research, 2012, 32(1): 18 - 21.

[8] SHI Neng, LU Jianjun, ZHU Qiangen. East Asian winter/summer monsoon intensity indices with their climatic change in 1873-1989 [J]. Journal of Nanjing Institute of Meteorology, 1996,19(2):168 - 177.

[9] ZHAO Ping, ZHANG RenHe. Relationship of Interannual Variation Between an Eastern Asia-Pacific Dipole Pressure Pattern and East Asian Monsoon [J]. Chinese Journal of Atmospheric Sciences, 2006, 30(2): 307 - 316.

[10] JI L R, SUN S Q. Model Study on the interannual variability of Asian winter monsoon and its influence [J]. Adv. Atmos. Sci., 1997, 14(1): 1 - 22.

[11] CHEN W, Graf H F, HUANG R h. The interannual variability of East Asian winter monsoon and its relation to the summer monsoon [J]. Adv. Atmos. Sci., 2001, 17(1): 48 - 60.

[12] LIANG Hongli, Xiao Ziniu, YAN Hongming. Relationship between the bay of Bengal winter monsoon and the summer climate change in Asia [J]. Journal of Tropical Meteorology, 2004, 20(5): 537 - 547.

[13] YANG S, LAU K M, KIM K M. Variations of the East Asian jet stream and Asian-Pacific-American winter climate anomalies [J]. J. Climate, 2002, 15(3): 306 - 325.

[14] WANG Huijun, JIANG Dabang. A new east Asian winter monsoon intensity index and atmospheric circulation comparison between strong and weak composite [J]. Quarternary Sciences, 2004, 24(1): 19 - 27.

[15] HUANG Xianxiang, SHI Neng, YAN Lijun. Anomalous winter circulation at 1 000 hPa over east Asia and its relation to climate change over China [J]. Journal of Tropical Meteorolog, 2007, 23(6): 623 - 628.

[16] JHUN J G, LEE E J. A new East Asian winter monsoon index and associated characteristics of the winter monsoon [J]. J. Climate, 2004, 17(4): 711 - 726.

[17] KUANG Xueyuan, ZHAGN Yaocun, LIU Jian. Relationship between subtropical upper-tropospheric westerly jet and East Asian winter monsoon [J]. Plateau Meteorology, 2008, 27(4): 701 - 712.

[18] LI Y Q, YANG S. A dynamical index for the East Asian winter monsoon [J]. J. Climate, 2010, 23(15): 4 255 - 4 262.

[19] SUN Shuqing, SUN Bomin. The relationship between the anomalous winter monsoon circulation over East Asia and summer drought/flooding in the Yangtze and Huaihe river valley [J]. Acta Meteorologica Sinica , 1995, 53(4): 438 - 450.

[20] CUI Xiaopeng, SUN Zhaobo. East Asian winter monsoon index and its variation analysis [J]. Journal of Nanjing Institute of Meteorology, 1999, 22(3): 321 - 325.

[21] YAN Hongming, DUAN Wei, XIAO Ziniu. A study on relation between East Asian winter monsoon and climate change during raining season in China. Journal of Tropical Meteorology. 2003,19(4): 367 - 376.

[22] CHEN Longxun, ZHU Qiangen, LUO Huibang, et al. East Asian monsoon [M]. Beijing: Chinese Meteorological Press, 1991:25-27.

[23] ZHU Qiangen, XIE Lian. 1986-87 Northern winter Asia/Australia circulation anomalies with their relation to the Western Pacific SST [J]. Journal of Tropical Meteorology . 1988, 4 (4): 254 - 262.

[24] SHI Neng. Features of the East Asian winter monsoon intensity on multiple time scale in recent 40 years and their relation to climate [J]. Journal of Applied Meteorological Science. 1996, 7 (2): 175 - 182.

[25] YANG Xuan, LI Dongliang. Variation of winter temperature in China and its responding to the anomalies in East Asian winter monsoon and surface heating field over Qinghai-Xizang plateau [J]. Plateau Meteorology, 2009, 28(4) : 731 - 737.

[26] WU Shangsen, LIANG Jianyin. Schematic predictive model for extremely severe cold months in South China winter- physical factors of general circulation, polar sea ice and perpetual snow [J]. Journal of Tropical Meteorology, 2000,16 (4) : 289 - 296.

[27] GAO Hui. Comparison of four East Asian winter monsoon indices [J]. Acta Meteorologica Sinica, 2007, 65(2): 272 - 279.

[28] LIU H. TOSI E. Tibaldi S. On the relationship between northern hemispheric weather regimes in wintertime and spring precipitation over China [J]. Q. J. R. Meteo. Soc., 1994, 120(515): 185 - 194.

[29] SUN B M. SUN S Q. The analysis on the features of the atmospheric circulation in preceding winters for the summer drought and flooding in the Yangtze and Huaihe river valley [J]. Adv. Atmos. Sci., 1994, 11(1): 79 - 90.

[30] ZHANG Jing, LI Yueqing, JIANG Xingwen. Review of study on the change of East Asian winter monsoon and its relationship with ENSO and AO [J]. Plateau and Mountain Meteorology Research, 2012,32(3):89 - 96.

[31] LIU Yuyun, ZHAO Di, CAO Jie. A mechanism for the impact of sea surface temperature anomaly over tropical Pacific and Indian Ocean on East Asian winter monsoon [J]. Plateau and Mountain Meteorology Research, 2008, 28 (1): 24 - 29.

[32] Hu Zengzhen, Shi Wei. Application study of wavelet transform in atmospheric sciences [J]. Chinese Journal of Atmospheric Sciences, 1997, 21(1): 58 - 72.

[33] Wu Hongbao, Wu Lei. Methods for diagnosing and forecasting climatic variability [M]. Beijing: Chinese Meteorological Press, 2005:208 - 225.

[34] Wang Zhaoli, Chen Xiaohong, Huang Guoru, et al. Wavelet analysis of rainfall series during flood season in Dongjiang river basin [J]. Yangtze River, 2010, 41(2): 52 - 55.

[35] Murakami M. Large scale aspects of deep convective activity over the GATE area [J]. Mon. Wea. Rev., 1979, 107(8): 994-1 013.

[36] HUANG Ronghui, LIU Yong, WANG Lin, et al. Analyses of the causes of severe drought occurring in Southwest China from the fall of 2009 to the spring of 2010 [J]. Chinese Journal of Atmospheric Sciences, 2012, 36(3): 443 - 457.

[37] Maloney E D, Hartmann D L. Frictional moisture convergence in a composite life cycle of the Madden-Julian Oscillation [J]. J. Climate, 1998, 11(9): 2 387 - 2 403.

[38] MAO Rui, GONG Daoyi, FANG Qiaomin. Influences of the East Asian jet stream on winter climate in China [J]. Journal of Applied Meteorological Science, 2007, 18(2): 137 - 146.

[39] ZHANG Ziyin, GONG DAOyi, GUO Dong, et al. Anomalous winter temperature and precipitation events in Southern China [J]. Acta Geographica Sinica, 2008, 63(9): 899 - 912.

2010 年东亚季风月内尺度振荡特征及其与西南地区冬季气温的关系

齐冬梅[1]，李跃清[1]，陈永仁[2]，德 庆[3]

（1. 中国气象局成都高原气象研究所 高原与盆地暴雨旱涝灾害四川省重点实验室，四川 成都 610072；
2. 四川省气象台，四川 成都 610072；3. 西藏自治区气象台，西藏 拉萨 850000）

摘 要：利用 NCEP/NCARR2 逐日再分析资料和西南地区气象台站逐日气温资料，通过带通滤波、小波分析、相关分析和合成分析等统计方法，研究了 2010 年东亚冬季风月内尺度振荡特征及其与西南李区冬季气温的联系。结果表明，2010 年东亚冬季风在月内时间尺度上主要存在 7 天左右、12 天左右以及 30 天左右为主要振荡周期的低频振荡。东亚冬季风月内尺度，准 1 周、准 2 周时间尺度内的振荡特征可以很好指示出同期西南地区较强的低温过程，且在准 2 周尺度比准 1 周尺度对西南地区冬季低温的影响更明显。月内尺度、准 1 周、准 2 周尺度上东亚冬季风正、负位相时，无论是对流层高层、中层、低层环流场分布形势均有显著差别，当东亚冬季风正位相时对流层从高层到低层环流场形势均有利于西南地区冬季低温，而负位相时环流形势相反，不利于西南地区低温。

关键词：东亚冬季风；月内时间尺度；西南地区；冬季气温；低频振荡

Experimental study on the wave pressure of liquefied silty soil

HUANG Zhe [1, 2], XU Guo-hui[1], MENG Qing-sheng[1]*, WANG Gang[1]

1. *Department of Environmental Science and Engineering, Ocean University of China, Qingdao* 266100, *Shandong province, China*;

2. *Institute for Sedimentation on River and Coastal Engineering, Tianjin University, Tianjin* 300072, *China*

Abstract: A number of studies focus on the pore-water pressure in seabed under the waves and seabed instability induced by liquefaction, but rarely on the wave pressure of liquefied soil. In this paper, flume tests were performed at varying wave heights under both conditions of liquefied and stable seabed. The total pressures equal to soil pressures and pore water pressures were measured and analyzed at each depth. The results showed that the liquefied seabed had little difference from the stable seabed on the peak pressures. However, the pressure amplitude of the liquefied soil increased by several to 10 times and decreased faster with increasing soil depths, compared with the stable soil. According to the experiments and further analysis, an empirical equation between pressure amplitude of the liquefied soil and wave parameters was put forward under the flume test. The results provide a valuable reference for engineering applications.

Keywords: silty soil; wave pressure; liquefaction; water flume test

Introduction

Many disastrous events occurring in nearshore development (e.g. capsized oil rig and damaged breakwater) may be closely associated with seabed instability [1]. Under extreme waves, soil liquefaction occurs in the seabed and leads to the instability of pile foundation, which affects the safety of nearshore structures grievously and may cause huge economic loss[2-5]. Quantitative characterization of seabed soil liquefaction and understanding of liquefaction process under wave loading are essential to provide information necessary for the safe design of marine structures.

The waves propagating in water can induce a dynamic response in the seabed, including the pore pressure accumulation within the seabed [3,6-9]. Liquefaction may be caused when the pore water pressure builds up progressively to the level equal to the

Received on Nov. 12, 2015

*Corresponding author: qingsheng@ouc.edu.cn

vertical effective stress.

Since the wave-induced liquefaction was proposed by Bjerrum in the structure foundation design in the North Sea[10], a number of studies have been conducted to analyze the wave-induced liquefaction in the sandy soil under various conditions [11-14]. Cohesive soil liquefaction is still poorly understood. Few studies about the cohesive soil liquefaction focus on characterization of liquefaction and its mechanism. Foda and Tzang[15] identified the resonant liquefaction of silty soil in the laboratory during the complex soil liquefaction induced by water waves. Effective stresses still existed when the mud was liquefied, which was different from the sandy soil[16]. However, little attention has been paid to the analysis of liquefied soil, especially the liquefied silty soil.

Once liquefaction occurs, soil grains become unbound and completely free from each other, and the liquefied soil acts like the fluid[17]. Then the water and the liquefied sediments form a two-layer liquid system [18]. Within this system, the liquefied sandy sediments behave in a wavy way similar as the water [19]. In cohesive soils, the cohesiveness weakens the liquefaction depth, which affects the amplitude and speed of soil wavy motion [20]. The motion of soil may produce a dynamic pressure significantly higher than the wave pressure, exerting additional pressure on the marine structures and potentially causing excessive damage [21, 22].

The dynamic pressure of liquefied soil is a key factor in the design of marine structures, but few studies focus on characterizing the dynamic pressure of wave-induced liquefied soil. An indoor flume test was performed in this study using the soils collected from the Yellow River delta, where most soil liquefaction and marine structure damages were recorded and reported. The objectives are to: 1) characterize the vertical distribution of total dynamic pressure along the depth of soil bed; 2) and develop an empirical equation to quantify the dynamic pressure related to the liquefied soil and wave parameters.

1 Methods

1.1 Soil bed preparation for the flume test

A series of experiments were carried out in a wave flume (structure and size shown in Fig. 1), which was equipped with a piston wave maker at one end and a 1:4 slope spending beach at the other end. The wave maker was capable of producing a range of wave frequency and wave height.

The silty soil was collected from a harbor basin of Yellow River delta, and during the preparation, all grass roots were cleared away. The gradation test was performed using a

small amount of soil from the flume and it was confirmed that the soil mass was clay-floury silt (Tab. 1). The air-dried silty soil was put into a container and water was added under sufficient stirring to create the uniform slurry. Then the slurry was poured into the flume via a plastic barrel and a funnel attached to the side wall to avoid producing bubbles. The soil in the flume formed a soil bed of 0.6 × 2.6 × 0.5 m (depth × length × width). In-house pressure transducers were calibrated in a water container (shown in Fig. 2) with known pressures before fixation inside the flume prior to laying the soil bed. The transducers with the correlation coefficients of measured voltages and the known pressures larger than 0.99 could only be used in the test. The pressure transducers were located at 0 (surface), 10, 20 and 35 cm below the bed surface (Fig. 3).

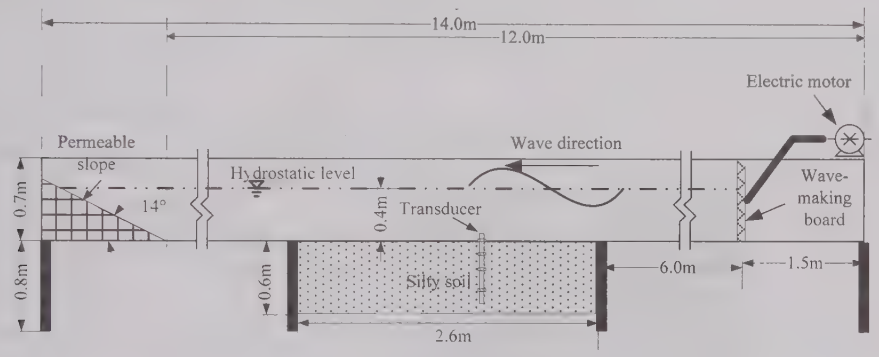

Fig. 1 Layout of wave flume

Tab. 1 Physical properties of the soil bed in the flume test

ω (%)	ρ (g/m^3)	Grain sizes / mm		
		>0.075	0.005~0.075	<0.005
32.2	1.69	<6.4%	>92.5%	<1%

Then water was slowly added into the flume at the spending beach located at one end of the flume. The final water depth in the flume was 40 cm. To approximate the in-field seabed state, the silt bed in the flume was consolidated for 10 days.

After the consolidation, the transducer originally positioned at the soil-water interface was relocated above the soil surface in water and used to measure the pressure equal to the water pressure for comparison with the total pressures equal to the water pressures and the soil pressures measured using the transducers in the soil bed.

After ten days of consolidation, a soil sample with diameter 32 mm and length of 32 cm was collected from the middle of the bed. The average water content ω and the density ρ

of the soil are listed in Tab. 1.

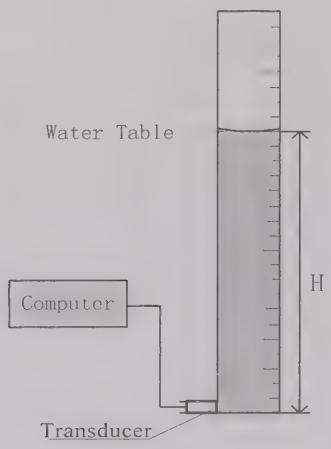

Fig. 2 Transducers calibration

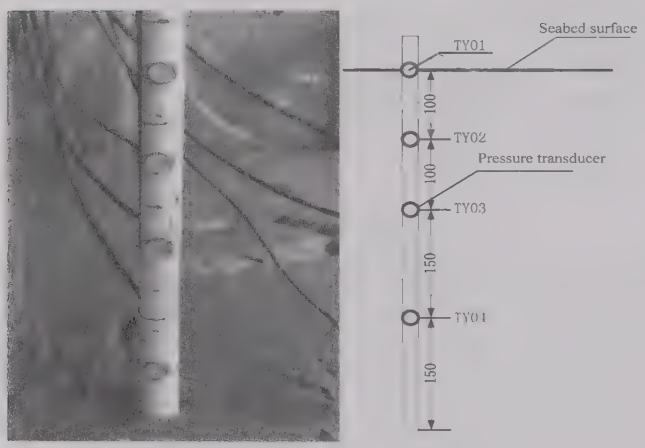

Fig. 3 Positions and numbers of pressure transducers

1.2 Wave parameters in the test

The wave generator was capable of generating a range of waves with varying wave height (H) and wave period (T). Because of the limitation of the wave maker, larger waves were of shorter periods, and 4 wave height scenarios were chosen with the highest wave height at 0.16 m (Tab. 2).

1.3 Experimental procedures and measurements

The flume test was conducted in 2 phases. The first phase was performed after the soil bed was adequately consolidated and before the test bed was liquefied. Waves were acted on the soil bed in a sequence of four scenarios, from the low to high wave height

(Tab. 2). Each wave lasted for 30 min. The pressures were measured using the pre-installed transducers, which were allowed to be in adequate contact with the soil during the consolidation. The frequency of the transducers was set at 500 hz. Two measurements each lasting for 5 min were made at the start and before the end of each wave loading.

After the first phase, the bed was manually disturbed to allow the upper-layer of the soil bed to be liquefied, and then the second phase was carried out. Under Phase II, the transducers originally positioned at 10 and 20 cm depth were relocated in the liquefied soil, while the transducer at 35 cm depth was still relocated below the liquefied soil. 4 experiment scenarios each started with a liquefied soil bed. The same wave parameters (Tab. 2) were also used in this phase, but each scenario lasted for 120 min so that the bottom interface of the liquefied soil layer could reach its stable depth under each wave loading. The pressures were measured at 30 min interval and lasted for 5 min, and the depth of the liquefied soil layer was also observed and recorded. The depth of liquefaction was measured using a scale following Sassa and Sekiguchi once soil liquefaction was observed [14].

Tab. 2 Wave parameters in the flume test

Wave Height / m	Wave Period / s	Wave Length / m
0.08	1.97	3.18
0.11	1.55	1.79
0.14	1.28	1.31
0.16	1.18	1.3

1.4 Verification test

A verification test was designed to validate the accuracy of the empirical equation developed to quantify the total dynamic pressure related to the liquefied soil and wave parameters based on the second phase test. 4 transducers were located at 13 cm, 18 cm, 23 cm, and 28 cm below the bed surface. A new set of 4 scenarios with different wave parameters was selected while the other test conditions were the same as Phase II (Tab. 3). The depth of liquefaction under each wave height was also observed (Tab. 3). Waves in each scenario were acted for 240 min.

2 Results

2.1 Phenomenon of the test

Visual observations were made during the test. Under Phase I, ripples were formed

on the non-liquefied soil bed surface after the wave acted for a few minutes. With the increased wave height, the turbidity of the flume water was elevated and the ripples on the soil bed surface grew deeper, which was similar to the results observed by Sumer, et al.[18]. Under Phase II (after the soil bed was disturbed), the bed liquefaction was noted through the side wall of the flume. The interface between the liquefied soil and non-liquefied soil constantly expanded at horizontal and vertical directions after the beginning of phase II, and eventually was relatively stabilized at an intermediate depth. The phenomenon that liquefied soil grains migrated elliptically as a fluid was also observed (Fig. 4), which was similar to the phenomenon reported by Sassa, et al. [19].

Tab. 3 Wave parameters and the depth of liquefaction in verification test

Wave Height / m	Wave Period / s	Wave Length / m	Depth of Liquefaction/ m
0.08	2.23	4.73	0.36
0.10	2.20	4.03	0.32
0.13	1.71	3.23	0.28
0.15	1.39	2.42	0.255

2.2 Results of pressure

The total pressure changed in a wave sequence with time for both liquefied and non-liquefied soil beds. Trough and crest values of total pressure were observed (Fig. 5). The dash line in Fig. 5 was the average total pressure, which nearly represented the static fluid pressure at the observation depth, and apparently, the wave-induced total pressure fluctuated around the average total pressure. When the total pressure was at the crest value, the soil in motion exerted additional pressure to any object it contacted, such as the marine structure foundations in the water. Here, we define the crest value as the peak pressure and the amplitude of total pressure as total dynamic pressure.

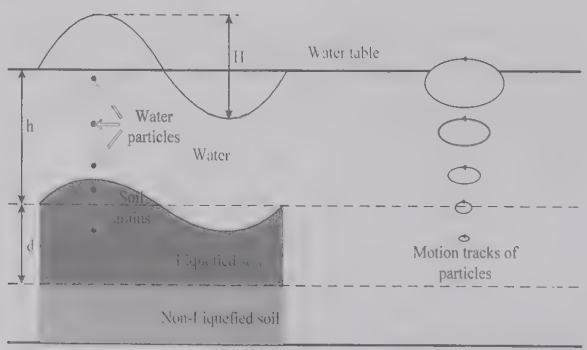

Fig. 4 Motion tracks of the liquefied soil and the water particles

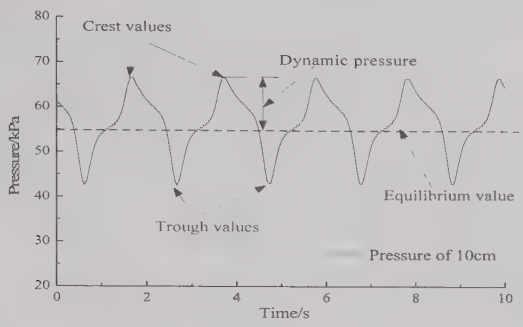

Fig. 5 Total pressure observed at 10 cm in liquefied soil bed with time

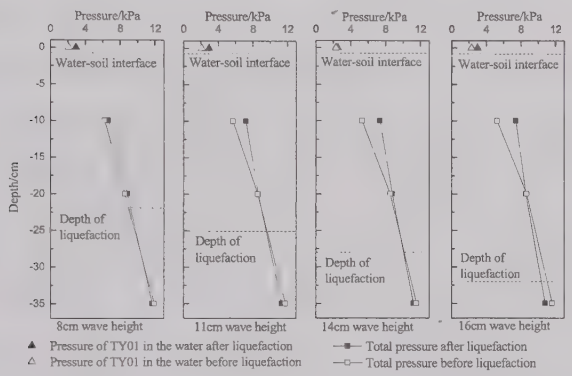

Fig. 6 Distribution of peak pressure along soil profile under different wave-action scenarios

The peak value of total pressure increased with depth generally in a linear manner under both liquefied and non-liquefied phases. The peak value of total pressure in the liquefied soil was essentially higher than that in the non-liquefied soil, especially at shallow depth (Fig. 6). However, the total dynamic pressures in liquefied soil increased significantly by several to more than 10 times, especially in the shallower liquefied soil layers compared with the non-liquefied soil observed at the same depth. On the other hand, total dynamic pressure in the non-liquefied soil layer beneath the liquefied soil changed little in total dynamic pressure (Fig. 7).

2.3 Quantification of total pressure

The peak value of total pressure changed little in the liquefied soil compared with the non-liquefied soil, because the increase of total dynamic pressure at certain depth after soil bed liquefaction did not affect the static pressure of soil, which accounted for the major proportion of the peak value of total pressure. The soil at 10 cm depth vibrated more severely compared with deeper soil, or namely, and the dynamic total pressure was higher while the static pressure was lower at this depth. The peak value of total pressure

increased obviously due to the increase of total dynamic pressure.

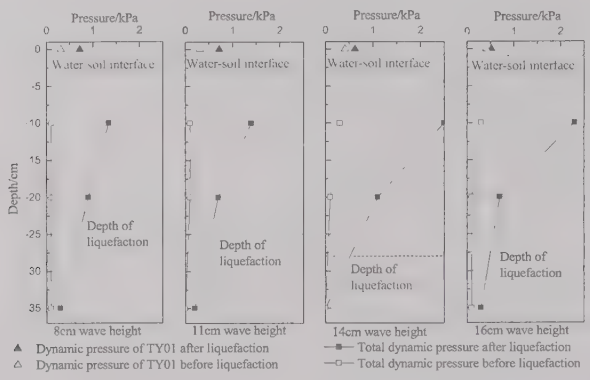

Fig. 7 Distribution of dynamic pressure along soil profile under different wave-action scenarios

In terms of the liquefied soil in this test, the dynamic pressures increased significantly. Marine structures, such as superficially buried cables or pipelines, were in the static equilibrium under no-wave conditions. The wave-induced dynamic pressure could cause the instability of the structures. Our observation indicated that when soil was liquefied and started to move with waves, it exerted additional pressure - total dynamic pressure, which depended on the liquefaction depth, and it can be high enough to unstabilize the structural foundations. Since no quantification method is available in the practical application, a method is developed based on the flume test data and presented here.

The movement soil particles in liquefied soil were consistent with water particles and followed an ellipse track with the amplitude damps exponentially with the depth, meaning that the dynamic pressure of the liquefied soil will decay exponentially with depth as follows [23]:

$$P=a\cdot e^{b\cdot z} \tag{1}$$

where a and b are constants related to wave parameters; P is the dynamic pressure of the liquefied soil; z is the depth starting from the water-soil interface. Using the total dynamic pressure measured in each wave height scenario at the depth of 10 cm and 20 cm, a and b can be calculated as shown in Tab. 4.

Tab. 4 Values of a and b in each wave condition

Wave Height/cm	8	11	14	16
a	2.03	2.8	5.68	7.56
b	-4.05	-6.93	-8.21	-11.90

As a and b are related to wave parameters, the relationship between a, b and wave parameters was explored according to experience and theories. In the above table, a is

positively correlated with the wave height and negatively correlated with the wave period, and b is positively correlated with wave height and negatively correlated with the water depth. It is also negatively correlated with the result of water depth plus the depth of liquefied soil. Obviously, under the experimental conditions, the empirical equation of the wave-induced liquefied total dynamic pressure can be obtained:

$$P = 52.05\frac{H}{T}e^{-17.6\frac{z}{d+h}\frac{H}{h}} \tag{2}$$

where H is the wave height of the water; T is wave period; d is the depth of the liquefaction; h is the water depth and z is the depth calculated from the water-soil interface. In this test, the regression relationships between a, b and the wave parameters are shown in Fig.8.

In the verification test, the liquefaction depth was shallower when the wave was higher, because wave acted for such a long time that the pore pressure dissipated and the liquefied interface moved upwards. The difference between the calculated value and the measured value of liquefied total dynamic pressure is shown in Fig. 10.

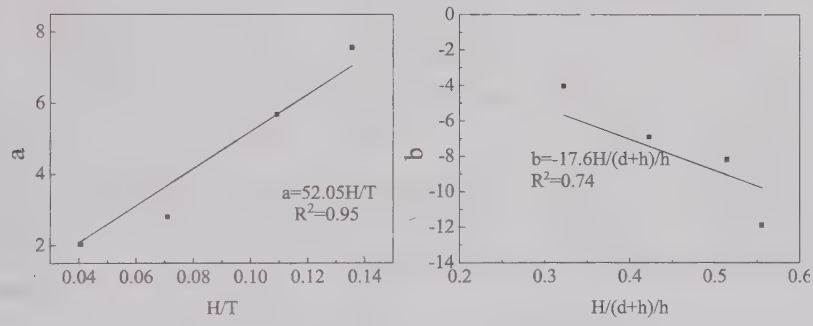

Fig. 8 Correlations of a, b and wave parameters

Equation (2) was used to calculate the total dynamic pressures under various experiment conditions and the equation fit the experiment data well (Fig. 9).

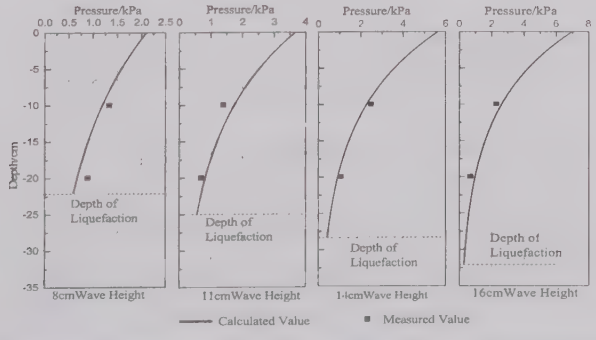

Fig. 9 The difference between calculated values and the measured values of the liquefied total dynamic pressure

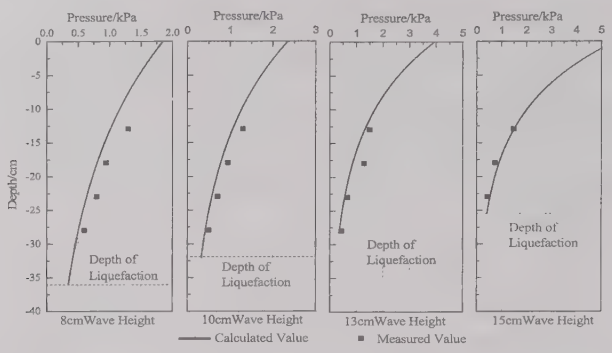

Fig. 10 The difference between calculated value and the measured value of the liquefied total dynamic pressure in verification test

The error of the empirical equation is obtained as follows:

$$\text{Error} = \frac{|M\text{-}C|}{C} \tag{3}$$

where M is the measured value and C is the calculated value.

The error distributions of the empirical equation in the two tests are shown in Fig. 11. The errors in two types of test are between 1.3% - 49.4%, mostly between 0% - 30%. Only one error is far more than 30%, accounting for less than 5% of all the observations. The largest error is 49.4%, in the verification experiment at depth of 18 cm under the 13 cm wave height, probably due to some accidental factors. Therefore, it can be judged that the error of the empirical equation may be around 30%.

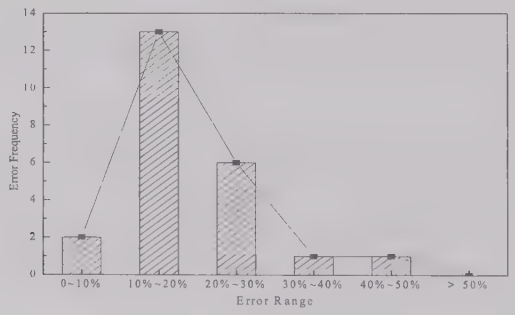

Fig. 11 Distribution of errors

Tab. 5 The wave parameters in the field[24]

H/m	T/s	h/m	L/m
3	8	8	65

In the field, the wave pressure on non-liquefied bed can be calculated by Eq. (4), and

the result is 11.2 kPa under 3 m wave height. The dynamic pressure before liquefaction in the seabed can be calculated by Eq. (5)[6], and the dynamic pressure in the bed at the depth of 0 m is 11.2 kPa. In liquefaction cases, according to the measured results of total dynamic pressure in the test, the speed and acceleration of liquefied soil particles can greatly increase the dynamic pressure and the dynamic pressures decay more rapidly with depth, which are consistent with the test observation (Fig. 7). The dynamic total pressure also accounts for less proportion of the peak value of total pressure, which is also consistent with the test observation (Fig. 6). Also, we can see in Fig.12 that the total dynamic pressures in the non-liquefied soil are not much smaller than these in the liquefied soil, which come from the empirical formula calculation results. This is due to that the total dynamic pressure in non-liquefied soil is equal to the water dynamic pressure through the soil pores. Yamamoto took the sand soil as the research objects. Water went through the soil pores more smoothly. So the water dynamic pressure should be higher than that in the silt soil. The total dynamic pressure in non-liquefied soil in Fig.12 is much higher than the actual value. To sum up, it is reasonable and credible that the empirical formula is usable in the field.

$$P_0 = \frac{\gamma_\omega H}{2\cosh(k_0 h)} \tag{4}$$

$$P_s = P_0 e^{k_0 z} \tag{5}$$

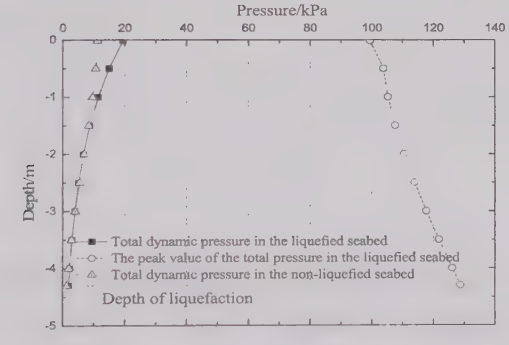

Fig.12 The peak value of total pressure and total dynamic pressure of liquefied soil calculated in the field

In practice, the stability of marine structures such as the pile foundation is mainly determined by the dynamic pressures of the upper water and the lower soil. The soil before liquefaction as a fixed end helps to stabilize the pile foundation, but the liquefied soil applies the additional forces on the pile foundation, which is not conducive to the stability of pile foundation. Even worse, the liquefied total dynamic pressure increases substantially. Hence, in design of marine structures, it is necessary to consider the phenomenon that total dynamic pressure increases greatly when the soil is liquefied.

4 Conclusions

Through the flume experiment, total pressures before and after soil liquefaction at varying wave heights, different depth and time points are recorded. The distribution rules of peak value of total pressure and total dynamic pressure are given preliminarily under the wave-caused soil liquefaction. Then, a calculation scheme of the wave-induced liquefied total dynamic pressure that is simple and easy to use is provided:

(1) For liquefied soil layer, the liquefied peak value of total pressure changes little. The total dynamic pressure increases by several to more than 10 times compared with that of ono-liquefaction, especially in the shallower depth. And the total dynamic pressure damps with the depth more rapidly with the increase of wave height.

(2) Through the analysis, the empirical equation of the liquefied total dynamic pressure induced by waves is given as:

$$P = 52.05\frac{H}{T}e^{1.76\frac{z}{d+h}\frac{H}{h}}$$

The actual availability of the equation was discussed and analyzed.

(3) Based on the comparison of the total dynamic pressures before and after the liquefaction in the flume test, one can draw a conclusion that attention during the design of structure set in coastal foundation soil should be paid to the phenomenon that liquefied total dynamic pressure will increase significantly.

Acknowledgements

This study was supported by National Natural Science Foundation of China (Grant No. 41576039) and the Scientific Research Projects of Marine Public Welfare Industry (Grant No. 201305026).

References

[1] Barends F B J, Spierenburg S E J. Interaction between ocean waves and sea-bed. In: Proceedings of the International Conference on Geotechnical Engineering for Coastal Development-Theory and Practice on Soft Ground [J], Yokohama, Japan, 1991, (2): 1 091 - 1 108.

[2] Lee, K L, Focht, J A. Liquefaction potential at Ekofisk tank in North Sea [J]. Journal of the Geotechnical Engineering Division, ASCE, 1975, 101(1): 1-18.

[3] Seed H B, Rahman M S. Wave-induced pore pressure in relation to ocean floor stability of cohesionless soils [J]. Marine Georesources & Geotechnology, 1978, 3(2): 123 - 150.

[4] Zen K, Umehara Y, Finn W D L. A case study of the wave-induced liquefaction of sand layers under damaged breakwater [C]. In: Proceedings 3rd Canadian Conference on Marine Geotechnical Engineering, St John's, Newfoundl, Canada, 1985, 505 - 520.

[5] De Groot M B, Meijers P. Liquefaction of trench fill around a pipeline in the seabed [C]. Proc., BOSS' 92: Behavior of Offshore Structures, London , UK, 1992, 1 333 - 1 344.

[6] Yamamoto T, Koning H L, Sellmeijer H, et al. On the response of a poro -elastic bed to water waves [J]. Journal of Fluid Mechanics, 1978, 87(1): 193 - 206.

[7] Tsui Y, Helfrich S C. Wave-induced pore pressures in submerged sand layer [J]. Journal of Geotechnical Engineering, 1983, 109(4), 603 - 618.

[8] Van Kessel T, Kranenburg C. Wave-induced liquefaction and flow of subaqueous mud layers [J]. Coastal engineering, 1998, 34(1): 109 - 127.

[9] Chang S C, Lin J G, Chien L K, et al. An experimental study on non-linear progressive wave-induced dynamic stresses in seabed [J]. Ocean Engineering, 2007, 34(17): 2 311 - 2 329.

[10] Bjerrum L. Geotechnical problems involved in foundations of structures in the North Sea [J]. Geotechnique, 1973, 23(3): 319 - 358.

[11] Nataraja M S, Gill H S. Ocean wave-induced liquefaction analysis [J]. Journal of Geotechnical Engineering, 1983, 109(4): 573 - 590.

[12] Zen K, Yamazaki H. Mechanism of wave-induced liquefaction and densification in seabed [J]. Soils and Foundations, 1990, 30(4): 90 - 104.

[13] Zen K, Yamazaki H. Oscillatory pore pressure and liquefaction in seabed induced by ocean waves [J]. Soils and Foundations, 1990, 30(4): 147 - 161.

[14] Sassa S, Sekiguchi H. Wave-induced liquefaction of beds of sand in a centrifuge [J]. Geotechnique, 1999, 49(5): 621 - 638.

[15] Foda M A, Tzang S Y. Resonant fluidization of silty soil by water waves [J]. Journal of Geophysical Research: Oceans, 1994, 99(C10): 20 463 - 20 475.

[16] De Wit P J, Kranenburg C. The wave-induced liquefaction of cohesive sediment beds [J]. Estuarine, Coastal and Shelf Science, 1997, 45(2): 261 - 271.

[17] Sumer B M, Fredsoe J, Christensen S, et al. Sinking/floatation of pipelines and other objects in liquefied soil under waves [J]. Coastal Engineering, 1999, 38(2): 53 - 90.

[18] Mutlu Sumer B, Hatipoglu F, Fredsøe J, et al. The sequence of sediment behaviour during wave-induced liquefaction [J]. Sedimentology, 2006, 53(3): 611 - 629.

[19] Sassa S, Sekiguchi H, Miyamoto J. Analysis of progressive liquefaction as a moving-boundary problem [J]. Geotechnique, 2001, 51(10): 847 - 857.

[20] Liu Z, Jeng D S, Chan A H C, et al. Wave - induced progressive liquefaction in a poro - elastoplastic seabed: A two-layered model [J]. International journal for numerical and analytical

methods in geomechanics, 2009, 33(5): 591 - 610.

[21] Zakeri A. Submarine debris flow impact on suspended (free-span) pipelines: Normal and longitudinal drag forces [J]. Ocean Engineering, 2009, 36(6): 489 - 499.

[22] Zakeri A, Høeg K, Nadim F. Submarine debris flow impact on pipelines—Part I: Experimental investigation [J]. Coastal engineering, 2008, 55(12): 1 209 - 1 218.

[23] Wang Xin. Experimental Study on Movement Characteristics of Liquefied Silty Seabed under Waves: [Ms Dissertation], Qingdao: Ocean University of China, 2010. 33 - 34.

[24] Xu G, Sun Y, Wang X, et al. Wave-induced shallow slides and their features on the subaqueous Yellow River delta [J]. Canadian Geotechnical Journal, 2009, 46(12): 1 406 - 1 417.

List of symbols

H	Wave height/m
h	Water depth over the bed/m
T	Period of waves/s
L	Wave length/m
d	Depth of liquefaction/m
z	Depth starting from the water-soil interface/m
P	Total dynamic pressure of the liquefied soil/kPa
P_0	Wave pressure on the bed/kPa
P_S	Dynamic pressure in the bed of no liquefaction/kPa
γ_w	Unit weight of the water/$N \cdot m^{-3}$
k_0	Wave number/m^{-1}

液化粉质土波动压力试验研究

黄 哲[1,2]，许国辉[1]，孟庆生[1*]，王 刚[1]

（1. 中国海洋大学 环境科学与工程学院，山东 青岛 266100；2. 天津大学 河流海岸工程泥沙研究所，天津 300072）

摘 要：海床土对波浪响应以及波致海床液化失稳的问题，已经有很多研究成果，而波浪作用海床液化土波动压力的研究还未见报道。采用波浪水槽实验，在未液化和液化两种情况下，分别施加不同波高的波浪，对底床各层位采集土体土压力，进行分析，实验结果表明，液化前后总土压力变化不明显，液化后的土动压力比液化前增大几倍到十几倍，且沿着深度的衰减速度更快。根据试验获得结果，进一步分析，提出了在水槽试验条件下的土动压力与波浪要素之间的经验公式。同时指出，在工程设计中应注意因底床液化引起的土动压力的增加的现象。

关键词：粉质土；波压力；液化；波浪；水槽试验

Methods for determining the development space in the conservation and utilization planning of uninhabited islands

JI Hou-de, LUO Mei-xue, YANG Shun-liang, SUN Qin-qin

Fujian Institute of Oceanography, Laboratory of Coast and Island Management Technology Study, Xiamen 361013, Fujian province, China

Abstract: The conservation and utilization planning of uninhabited islands is an important part of island management system, which is also the link between island administrators and users. How to scientifically and reasonably determine the development space is the core and difficulty in the planning. In this paper, taking the conservation and utilization planning of the Dashan Island and Ding Island as the example, methods of determining the development space for the highly sensitive ecological islands in the premise of ensuring ecological safety space are explored. According to the ecological status of islands, intensity of human disturbance is confirmed as the main assessment factor and assigned based on different space uses, which is used to assess the status of human disturbance. Results suggest the status of island human disturbance is on the slight level and the magnitude is very low, which is consistent with the reality. Also the results show the adaptability of the model. The threshold is used to calculate the development space of the island, which is the slight level of human disturbance in the model. Finally, the applicable scope of this method is discussed.

Keywords: uninhabited islands; conservation and utilization planning; development space; human disturbance

As a vital part of marine territory, the uninhabited island is a bridge tower for marine economy development[1]; and how to realize the sustainable utilization of uninhabited islands and protect islands effectively in the process of their development has become a core problem which attracts attention from island administrators, users and researchers. The eco-system of islands is featured with particularity, vulnerability and being difficult to be recovered, etc., which restricts the growth of island economy[2-4]. However, thanks to its unique resource advantages, marine development gives priority to islands so that the contradiction between island eco-environment protection and island development and

Received on Apr. 13, 2016

Corresponding author: applecoe@126.com

utilization becomes increasingly prominent[5,6]. With the implementation of Islands Protection Act of the People's Republic of China (hereinafter referred to as the "Islands Act"), island development and protection begins to be abided by laws. In line with this Act, management systems for national, provincial, municipal and county-level island protection planning (national and provincial planning is mandatory) as well as uninhabited island protection and utilization planning (hereinafter referred to as the "Single Island Planning") have been established gradually[7-9]. The "Single Island Planning" in such systems is the "controlled planning" and "conceptual planning" compiled in the national and provincial framework of island protection planning, and is a key level connecting the macroscopic and the microscopic as well as the entirety and the locality [10]. The planning is a critical carrier connecting island administrators with island users, and is a core link in uninhabited island development management. It directly reflects details of island development, such as directions, spatial distributions and protective measures, etc.; moreover, it is also a precondition for the establishment of a specific island development and utilization scheme, and an island utilization argument [11].

High expectations are placed on "Single Island Planning" as it occupies an important position in the island development and management; at the beginning of its establishment, it even became "Detailed Controlled Planning", however, the reality is so unsatisfactory that such expectations are dampened. Fundamentally, it is hard for the "Single Island Planning" which is established in accordance with a Primacy of Protecting Principle to cope with diversified market demands and complicated development modes. Up to the end of 2014, concerning the first batch of 176 uninhabited islands for development utilizations published by the State Oceanic Administration, only 10 Island Use Right Certificates were issued[12]; enthusiasm for island development is far from the expectation. The fact of island development utilization forces the "Single Island Planning" to change from being "Active" to "Passive"[13]. Concerning the current "Passive Planning", most of them take advantage of the status quo layout to delimit planning zones, and the engineering layout to determine spatial planning arrangement so as to customize the "Single Island Planning" for applicants of island utilizations. Shortcomings of such a method are unapparent in islands where the contradiction between eco-environmental stress and island development is not sharp, while they are just like stalks in the throat in terms of islands with sharp conflicts. Therefore, it is a difficulty for both island administrators and island users. At present, researches on methods about how to determine the island development space quantitatively are rather rare domestically. The paper writer encounters a similar problem during the work. It will be taken as an instance to discuss the island use space determination method hoping to provide a reference for the "Single Island Planning".

1 Background of the case study

In April 2011, list for the first batch of 176 uninhabited islands which could be developed and utilized was published, including Dashanyu Island that is adopted for the case study in this paper. Exploitable and available uninhabited islands from this list as well as those mentioned in the *Island Protection Planning of Fujian Province (2011-2020)* are all determined to be islands for the tourism and recreation[14]. Developers of Dashanyu Island planned to construct a certain number of tourist facilities on the island and open up certain space to perform "pro-island" activities so as to integrate into its natural landscapes and "enjoy" economic benefits brought by the eco-tourism of this island. On the Dashanyu Island with dense vegetation, the horsetail beefwood is dominant and it is the favorite habitat of ardeidae. In recent years, ardeidae birds benefit from advantaged original ecological environment in Dashanyu Island and adjacent sea area together with abundant food obtained from nearby mud flat, and their seasonal activities become perched reproductions so that they are changed into resident birds gradually from migrant ones. For islands whose ecological sensitivity is so high, managers do not know what to do with the determination of development space; moreover, as island development may give rise to damages of bird habitats so as to further lead to investment failures, island users are afraid of those problems and hence become irresolute. Consequently, how to determine the development space is the first question to solve the contradiction between eco-environment protection and development of islands. It is impossible for the method of development space determination based on engineering layout to pre-estimate the scale of island protection; therefore, such a method is infeasible obviously. Methods that can be utilized to determine the island development zone haven't been clearly given in relevant guidance documents of "Single Island Planning" compilation as well. As a result, other methods are introduced in this paper to delimit island development zones.

2 Introduction to the island background

2.1 Brief introduction to the island

Dashanyu Island and Dingyu Island are located to the south bank of the Quanzhou Bay, in a sea area at the northeast of Gufu Village, Xiangzhi Town in Shishi City of Quanzhou, Fujian Province (Fig. 1). Geographical coordinates of their central points are (24°47′02″ N, 118°45′07″ E) and (24°47′04″ N, 118°45′16″ E); moreover, horizontal projected areas are 20,324 m^2 and 11,541 m^2 respectively; and their coastline lengths are 816 m and 506 m; the closest approaches of them to the mainland are 320 m and 450 m. It

can be seen from Fig. 1, both islands are very close to each other. To be specific, during the low tide, they are even linked together; while during the high water, they are only a few meters apart. Therefore, both islands are treated as a whole in this research to perform zonal studies.

Dashanyu Island and Dingyu Island are both constituted by metamorphic rocks. On the surface of the former which has a denudation hilly landform, rocks are exposed and vegetation is rather developed. In addition, on the edge of this island, a marine abrasion landform including sea cliffs, sea caves and benches has developed; a small area of beach exists in the northern bay and its eastern reef pan is linked to the Dingyu Island, where vegetation is scarce, and altitude is low, and terrain of knap slightly fluctuates and its top is strongly weathered. At present, such two islands are basically in a natural and undeveloped state; only the Dashanyu Island has a tablet of island name and an abandoned stone house.

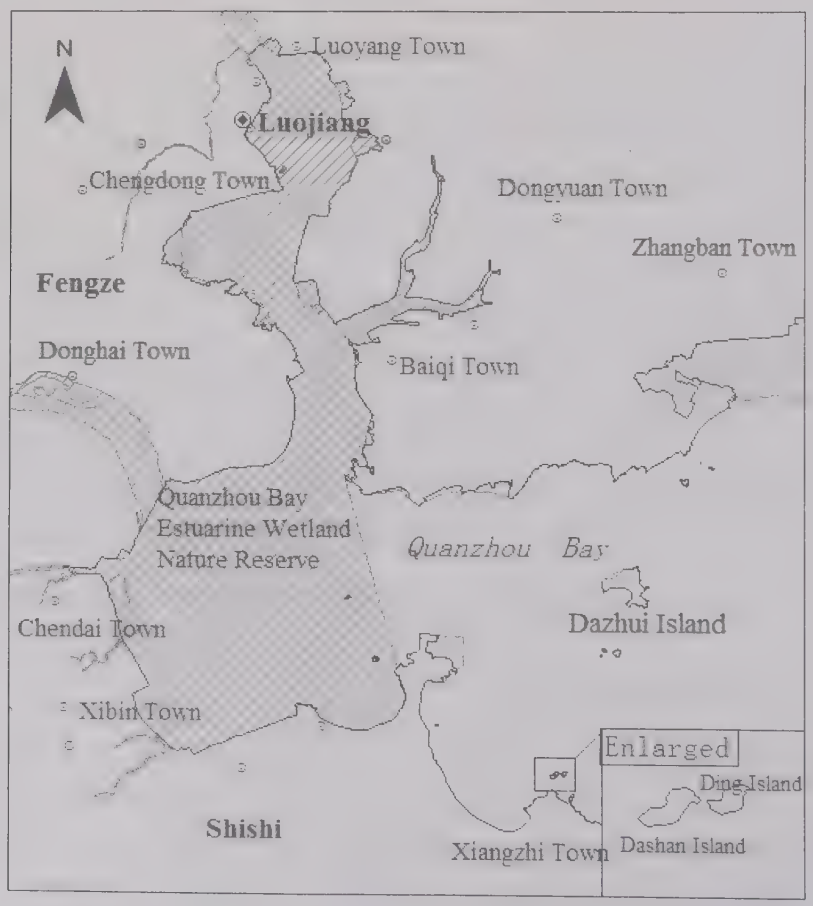

Fig. 1 Geographical location map of islands

2.2 Status quo of vegetation

According to field investigation of vegetation, 55 island protophytes have been reserved on both Dashanyu and Dingyu islands; and that is a large number for them whose areas are very small. In detail, among them, 7 endemic plants grow on the islands or in the coastal zone, while 3 are exotic species; and they are not dominant species. As under the long-term actions of tides, waves, ocean currents and predominant northerly strong winds, the vegetation canopy has an evident NW-SE ridge structure on islands with dense upper vegetation. Especially on the Dashanyu Island, terrestrial vegetation coverage above the high-water line even reaches 77.2% and the region with the vegetation coverage of 100% takes a percentage of 49.9% in the total area. The vegetation with the largest area on Dashanyu Island is the arbor community of horsetail beefwood; height of tree-crown generally ranges from 4 m to 6 m which serves as an essential condition to become a bird habitat.

2.3 Status quo of birds on islands

In line with related data[15], great and little egrets predominate the Dashanyu Island where multiple emphasized protective animals of Fujian Province can be seen as well, such as herons, Chinese pond-herons, Pacific reef herons, fairytale herons and cattle egrets, etc.; in addition, other bird populations include grand coucals, long-tailed shrikes, fork-tailed sunbirds, oyster catchers, masked laughingthrushes, sparrows and crows, etc.. Among them, Pacific reef herons and grand coucals are national second class protected birds. At present, the number of them is within the limit of a hundred all over Fujian Province. As one of the 11 highly endangered birds in China, Pacific reef herons have been listed into *Migrant Bird and Habitat Environment Protection Agreement between the People's Republic of China and Australian Government*. Depending on preliminary conservative estimations, over 5 000 birds inhabit the islands.

2.4 General situations for the adjacent sea environment of islands

Broad mudflat aquaculture areas are distributed around islands to provide rich sources of food for birds. In a sea area which is about 4.2 km on the west of islands, the Quanzhou Bay Estuarine Wetland Nature Reserve (in a level of province) has been established with an area of 70.46 km^2. In the reserve, there are 213 varieties of birds including egretta eulophotes and Pacific reef herons, etc.; hence, vast space for activities and reproductions can be offered to birds. Thanks to the improvement of surrounding marine environment, movement areas for birds have been expanded gradually, making the Dashanyu Island become a bird habitat step by step.

3 Island planning zones

3.1 Planning guidelines

According to field investigation data of the island, main objects of protection are determined to be the natural coastline, the vegetational type and the birds on the Dashanyu Islands, and the natural coastline and the vegetational type on the Dingyu Island. From the perspective of objects of protection, it is clear that birds are the core for all objects of protection and other objects of protection can be seen as their auxiliary objects. In other words, effective protections of bird resources and their habitats directly manifest the effective protection of islands. Therefore, an island partition method for the purpose of core objective protection is determined. The formation of a bird habitat is resulted from synthetic actions of geographic position, vegetation, landform and bird feeding field, etc.. Considering this, the protection over habitats should take influences of islands, adjacent sea environment and even the landfall into a comprehensive account [16]. In conformity with such a thought, it is considered that whether activities including natural sightseeing of island, bird watching and others can be conducted on Dashanyu Island provided that the bird habitat is protected to the greatest extent. Regarding Dingyu Island, it serves as a hinderland for the tourism development of Dashanyu Island to provide the growth space for tourism so that an equilibrium point can be found between island development demands and island environment protection.

3.2 Method selection

Birds on islands are predominated by ardeidae animals. As a result, egrets are selected as the representative to perform researches. According to features of island development and research data given by foreign and domestic scholars about the influences of human activities on birds [17-27], disturbances over habitats of egrets are primarily derived from human development activities and noises generated by such activities at the time of island development. Birds have strong recognition capabilities for their own stridulation. In the habitat of egrets, the average background noise value of various frequency bands is very low. As noise values are able to impact egrets to different degrees, especially the amplitude noise of low and medium frequency from 20 Hz to 2 000 Hz, the exchange and reproduction of them can be impacted substantially [28].

In order to carry out quantitative analysis for the relation between island development space and egret habitat further, the calculation method for human disturbance degree which is adopted by Egret Ecological Security Evaluation System in Xiamen Nature

Reserve is brought in [29] so as to assess the human disturbance degree of the sea area adjacent to Dashanyu Island; furthermore, the maximum exploitable space of island can be derived reversely.

Tab. 1 Estimation scale and assignment range for human disturbance degrees over egrets

Human Disturbance Degree	1 - 0.8	0.8 - 0.6	0.6 - 0.4	0.4 - 0.2	0.2 - 0
Estimation Scale	Very strong	Strong	Moderate	Marginally	Slight

Tab. 2 Evaluation coefficients for the human disturbance of different utilization types

Utilization Type	Disturbance Degree				
	Very strong	Strong	Moderate	Marginally	Slight
Commercial or Esidential Zone	0.9				
Industry Zone		0.8			
Main TrafficRoad	0.9				
Navigation Route			0.4		
Landscape Ground					0.1
Green Space/Cultivated Land				0.2	
Waters/Mud Flat					0

The corresponding calculation formula is as follows.

$$D=1/S_1\sum(S_{1i}\times di)+1/2S_2\sum(S_{2i}\times di) \quad (1)$$

where, D refers to the evaluation coefficient of human disturbance, S_1 to the center of a habitat, S_2 to peripheral area of a habitat, S_{1i} and S_{2i} to areas of different utilization types within S_1 and S_2, and d_i to the evaluation coefficients for human disturbance degrees of different utilization types.

3.3 Calculation results

3.3.1 Acquisition of basic data

By referring to research achievements related to bird tolerance level to human disturbances and combined with characteristics of natural environment adjacent to the island, the central point of Dashanyu Island is adopted as the base point and two areas ranging from 0m-600m and 600 m - 1 200 m respectively (including sea area, island and land) are selected as the central and the peripheral areas to perform human disturbance

researches; moreover, islands are located within the central area. Based on remote sensing images with a resolution of 5m×5m and field investigation data, Arcgis is employed to process the utilization type of research areas.

3.3.2 Current situation evaluation

In order to verify the adaptability of the established evaluation system, current situations of human disturbance scales over Dashanyu Island and areas next to it are assessed. In line with the corresponding calculations, the current human disturbance scale is 0.06. After checking Tab. 1, it can be seen that the grade of such an influence is slight, while its magnitude is rather low; this is in good agreement with current ecological status of islands and surrounding areas.

3.3.3 The maximum exploitable area

For the purpose of calculating the maximum exploitable area of the island, upper limits of 0.2 and 0.4 which refer to marginal and slight influences are selected to respectively calculate the maximum tolerance area of different human disturbance factors; that is the exploitable area of the island. In conformity with development characteristics of islands, Commercial and Residential Zone, Industrial District and Channel mentioned in Tab. 2 are selected to conduct computation separately. The computational results are shown in Tab. 3.

Tab. 3 Maximum tolerance areas of Dashanyu Island and Dingyu Island under the influence of human disturbance

Development Type	Marginally Influence (0.2) Maximum Tolerance Area / m^2	Slight Influence (0.4) Maximum Tolerance Area / m^2
Commercial or residential zone	2 308	424 683
Industry zone	6 357	477 768
Navigation route	5 193	955 536

With an aim to improve the compatibility of panning zone results, the commercial and residential zone which has the greatest impact is chosen to be the typical type; meanwhile, in order to improve the security level for objects of protection, 0.2, the upper limit of minor influence is adopted as the threshold. Hence, the exploitable and available maximum area on the island is 2 308 m^2.

Although the development area can be determined based on such a method, it is impossible to define development positions because weight coefficients of all points within the central area are identical, which is a shortcoming of this method. Generally, the closer

the distance to habitat is, the stronger the influence of human disturbance will be, so is the weight; moreover, the bigger the development intensity is, the greater the influence on birds will be; the faster the shipping sail speed is, the greater the influence intensity of it will be. As a result, the development zone should be on the east of Dingyu Island where the slope segment is rather gentle and vegetation is scarce. By taking the above factors into a comprehensive consideration, the island development zone is delimited, as shown in Fig. 2.

Fig. 2 Schematic diagram for the space utilization type surrounding islands and determined island development zones

4 Result discussions and reflections

(a) One factor from the Egret Ecological Security Evaluation System which has been established by Lin Tao et al. is brought into this paper to evaluate the status quo of island ecological security. Considering that evaluation results are in conformity with realities, the adaptability of such an algorithm is verified. In addition, the pressure threshold of this algorithm is utilized to derive the maximum exploitable area of island reversely so that a feasible approach can be provided for the quantitative determination of island use space.

(b) At present, there are still no available mature theories or models that can be used

to carry out island planning. This paper aims to tentatively explore into the service space determination method for islands with high ecological sensitivity. As the algorithm used in this paper is rather coarse, it is very difficult to determine development positions, intensities and approaches, etc. in an accurate manner. Despite that universality of the research achievement is improved to a certain extent, it still lacks pertinence. Therefore, controlling index system which combines with factors such as building density, capacity, height and development mode, etc. will be further studied so as to improve the corresponding scientificity and pertinence. Hopefully, more scientific and perfect micro planning method can be constructed for islands.

(c) With regard to objects of protection on the island selected as research instances of this paper, their "advantages" are extremely prominent. Island partition of this type can be performed by referring to planning guidelines described in this paper. For uninhabited islands where core objects of protection are lacking in outstanding "Merits", such a spatial zonal approach is infeasible apparently. Therefore, more spatial zonal approaches should be probed into to quantitatively delimit the service zone of islands, determine island protection zone and use district in a more reasonable way and give more scientific guidance to island development directions.

(d) "Single Island Planning" is a new subject before managers and scientific researchers; partition shouldn't be carried out by copying methods used for urban planning as they are different from each other in essence from multiple aspects. As a result, the "Single Island Planning" cannot be defined in detail according to indices of urban planning. At least, on the premise of incomplete island planning theories and technologies, it is unscientific and lacking in vitality for the single island planning to be positioned as a detailed plan mandatorily. On the contrary, control planning should be performed for islands based on research assessment of island's resources carrying capacity and health bearing capacity and guidance planning for island use so as to cope with diversified markets and fulfill market-oriented allocation for island use.

References

[1] Chen Qiu-ming. A Study on the Adaptability of Uninhabited Island Development Based on Ecology-economy [D]. Xiamen University, 2009, Master Dissertation.

[2] Chen Ke-xin, Chen Jia-gang. Sustainable Utilization of Island Resources in China [J]. Journal of Tianjin Normal University (Natural Science Edition), 2002, 22(l): 60 - 63.

[3] Yang Yi. A Study on Uninhabited Island Management in China Based on Eco-system Management. Ocean University of China [D]. 2012, Master Dissertation.

[4] Leng Yue-shan, Sun Shu-xian, Wang Zong-ling, et al. Analysis on Vulnerability of Ecological Environment of the Island and Controlling Countermeasures [J]. Ocean Engineering, 2008, 2(27): 58 - 64.

[5] Liu Shu-xi, Wang Wei-ping, Sun Shu-yan, et al. A Study on Evaluation Method for Adaptability of Uninhabited Island Development and Utilization [J]. Marine Environmental Science, 2013, 32(5): 783 - 786.

[6] Lu Wen-hai, Zeng Rong, Xiang Xian-quan.. A Study on Marine Ecosystem Health Evaluation for Coastal Regions [J]. Marine Science Bulletin, 2013, 32(5): 580 - 585.

[7] Li Xiang-li. A Study on Uninhabited Island Protection Laws and Regulations of China [D]. Harbin Engineering University, 2013, Master Dissertation.

[8] Liao Lian-zhao. A Study on Compilation of Uninhabited Island Protection Planning and the Case of Xiamen [J]. Ocean Development and Management, 2007, 24(4): 27 - 31.

[9] Zhang Yun-feng, Zhang Zhen-ke, Zhang Jing, et al. A Study on Progresses of Ocean Space Planning Researches in Europe and America [J]. Marine Science Bulletin, 2013, 32(3): 352 - 360.

[10] Fu Shi-feng, Chen Peng, Wu Hai-yan, et al. Difficulties Associated with Uninhabited Island Protection and Utilization Planning [J]. Marine Environmental Science, 2013, 32(4): 325 - 328.

[11] Chang Li-xia, Dai Ling-yan Qu Lin-jing, et al. Analysis on the Relation of Single Island Planning, Scheme and Argument [J]. Ocean Development and Management, 2014, 2(31): 27 - 31.

[12] State Oceanic Administration People's Republic of China. List of Islands for Development and Utilization [EB/OL]. http://www.chinaislands.gov.cn /utils/searchhd.aspx, 2014.

[13] Shen Jian, Chang Li-xia, Wang Si-ru. Analysis on Differences in Island Planning Compilations of Various Types [J]. Ocean Development and Management, 2014, 1(31): 27 - 29.

[14] Fujian Provincial Department of Ocean and Fisheries. Island Protection Planning of Fujian Province [C]. Fuzhou: Fujian Provincial Department of Ocean and Fisheries, 2012.

[15] Lin Fu-rong. Sorry for Disturbing, Dashanyu Island [N]. Shishi Daily, 2014.

[16] Wang Chang-ying, Zhang Jie, Xin Hong-mei, et al. Potential Ecological Risk Assessment of Island Development Based on Landscape Pattern [J]. Acta Ecologica Sinica, 2008, 6(28): 2 811 - 2 817.

[17] Chen Xiao-lin, Song Xiao-jun. Ecological Analysis on Spring Bird Community in Xiamen Intertidal Zone [J]. Chinese Journal of Ecology, 1999, 18(4): 36 - 39.

[18] Chen Shui-hua, Ding Ping, Zheng Guang-mei, et al. A Study on Abundance and Influencing Factors of Bird Community on Island Habitat [J]. Acta Ecologica Sinica, 2002, 22(2): 141 - 149.

[19] Wu Lie, Chen Xiao-lin, Hu Hui-juan, et al. A Study on Spatial Distribution of Ardeidae Breeding in Xiamen Egret Nature Reserve [J]. Journal of Xiamen University (Natural Science Edition), 2001, 40(4): 979 - 983.

[20] Smith J P. Nesting Season Food Habits of 4 Species of Herons and Egrets at Lake Okeechobee [J]. Colonial Waterbirds, 1997, 20(2): 198 - 220.

[21] Lombardini K, Benntetts R E, Toutenq C. Foraging Success and Foraging Habit At Use by Cattle

Egrets and Little Egrets in the Camargue [J]. Condor, 2001, 103(1): 38 - 44.

[22] Wong L C, Corlett R T, Young L, et al. Comparative Feeding Ecology of Little Egrets on Intertidal Mudflats in Hong Kong, South China [J]. Waterbirds, 2000, 23(2): 214 - 225.

[23] Stolen E D. The Effects of Vehicle Passage on Foraging Behavior of Wading Birds [J]. Waterbirds, 2003, 26(4): 429 - 436.

[24] Burton N H K, Armttage M J S, Musgrove A J, et al. Impacts of Man-made Landscape Features on Numbers of Estuarine Water Birds at Low Tide [J]. Environmental Management, 2002, 30(6): 857 - 864.

[25] Wang Yan-ping, Chen Shui-hua, Ding Ping. Flushing Distance－A Study on Adaptability of Common Birds to Human Disturbances in Hangzhou [J]. Zoological Research, 2004, 25(3): 214 - 220.

[26] Wang Rong, Zhang Yong. An Investigation on Wintering Waterfowl in Coastal Areas of Fujian [J]. Chinese Journal of Wildlife, 2012, 33(5): 271 - 274.

[27] Fang Wen-zhen, Chen Zhi-hong, Chen Xiao-lin, et al. A Study on Diversity of Winter Avian Community in Coastal Wetlands of Xiamen [J]. Marine Sciences, 2007, 31(1): 10 - 16.

[28] Dai Yi-ling. A Preliminary Investigation on Structure and Habitat of Ardeidae in Shibanya Village of Chongqing [J]. Journal of Chongqing Normal University (Natural Science/JCQNU), 2002, 19(1): 57 - 61.

[29] Lin Tao, Xue Xiong-zhi, Lu Chang-yi, et al. Egret Ecological Security Evaluation for Xiamen National Nature Reserve [J]. Acta Ecologica Sinica, 2006, 26(12): 3 998 - 4 006.

无居民海岛保护和利用规划中开发空间的确定方法

姬厚德，罗美雪，杨顺良，孙芹芹

（福建海洋研究所 福建省海岛与海岸带管理技术研究重点实验室，福建 厦门 361013）

摘 要： 无居民海岛保护和利用规划是海岛使用管理体系的重要组成部分之一，是承接海岛管理者和海岛使用者之间的重要载体。如何科学的、合理的确定开发空间是规划的核心问题，也是规划的难点。以大山屿、顶屿海岛保护和利用规划为实例，探索对生态敏感度高的海岛在保证生态安全的前提下确定开发空间的方法。根据海岛生态现状，确定人为干扰度为主要评估因子，按照不同空间利用类型对人为干扰度进行赋值，并对海岛人为干扰现状进行评估。计算结果显示，海岛人为干扰现状处于轻微等级且量级很低，与实际情况吻合，验证了引入模型的适应性。最后，利用模型中人为干扰度轻微的阈值推算海岛可开发空间，并讨论了此方法的适用范围。

关键词： 无居民海岛；保护和利用规划；旅游娱乐用岛；开发空间；人为干扰

Preliminary aquatic life criteria development and ecological risk assessment of ammonia in seven major river basins in China

WANG Yi-zhe[1], YAN Zhen-guang[1]*, ZHENG Xin[1], ZHAO Ying[2], ZHANG Ya-hui[1], YANG Ni-yun[1]

1. *Key Laboratory of Ecological Effect and Risk Assessment of Chemical of MEP, Chinese Research Academy of Environmental Sciences, Beijing* 100012, *China*

2. *China Emission Vehicle Control, Chinese Research Academy of Environmental Sciences, Beijing* 100012, *China*

Abstract: Ammonia is one of the basin indices which are nation-controlled in the water environmental management. In order to assess the differences of ammonia criteria in different basins, 7 major basins are used for the study object, including Songhua River, Liaohe River, Haihe River. Yellow River, Huaihe River, Yangtze River and Zhujiang River, referring the water environmental criteria technology of the United States Environmental Protection Agency, based on the effects of water characteristics on the ecotoxicity of ammonia, and in summer and non-summer situation, aquatic life criteria is derived for ammonia. The results showed that: (a) The differences between the criteria values in different basins and different seasons were significant. The differences between the criteria values in different basins were greater than 6 times, while those in different seasons in the same basin were greater than 2 times. (b) The summer acute and chronic criteria for Huaihe River were 0.37 mg/L and 0.06 mg/L while the non-summer values were 0.81 mg/L and 0.15 mg/L. Both the summer and the non-summer values were lowest in all of the seven basins. (c) The preliminary assessment of Ammonia exposure ecological risk indicated that was the lowest in Zhujiang River, and it was much lower in Songhua River, Liaohe River and Yangtze River, and was higher in Yellow River, and the highest in both Haihe River and Huaihe River. Haihe River has 7 sections while 2 in high risk, and Huaihe River has 27 sections while sixteen in high risk. According to the differences of the criteria values for ammonia in seven basins in different seasons and difference of ammonia ecological risk assessment, it is suggested that it should be managed by different policies.

Keywords: seven basins; ammonia; aquatic life criteria; ecological risk assessment; risk quotient

Received on Mar. 3, 2016

*Corresponding author: zgyan@craes.org.cn

The water quality criteria (WQC) were used as the scientific basis for the water quality standard. United States, European Union and other countries have carried out the WQC studies for many years and formed a relative mature technology system of water quality criteria and standards. The WQC study in China is relatively backward, and the relevant standards still refer to foreign standards mainly. Because of some differences in different countries or regions, both the characteristics of water environment(such as temperature, pH, hardness, ρ(DO), etc.) and the differences of aquatic biota in different areas could cause different criterion values of the same pollutant[1, 2]. Therefore, some domestic scholars carried out the native WQC studies recently, based on the native characteristics of water environment and aquatic biota, and they proposed some local pollutant criteria values, such as 2, 4-dichlorophenol[3], 2, 4, 6-Trichlorophenol [4], Nitrobenzene [5], metals [6, 7], ammonia [8] and etc., which provided scientific basis for the scientific revision of water quality standards in China.

Ammonia is one of the important indicators of water environment monitoring in China, and its main source is the production that is decomposed by microbial action from the nitrogenous organic compound in domestic sewage, some industrial wastewater and agricultural drainage[9]. In 2013, "China Environmental Status Bulletin"[10] pointed out that the total amount of ammonia was one of the most important water pollutants in China whose amount reached 245.7×10^4 t nationwidely. Ministry of Environmental Protection (MEP) issued "Planning of Water Pollution Prevention and Control in Key Drainage Basins (2011-2015)"[11], which proposed the target of the total quantity control of ammonia directly: ammonia emission would be controlled in 120.7×10^4 t by 2015. Therefore, it is very important to aim at developing the typical basin WQC and water quality standard for ammonia in China, which could both provide a theoretical basis for further reduction of the total quantity of ammonia emission and be important for the protection of the basin ecological safety in China.

In 2013, the United States Environmental Protection Agency (U.S. EPA) published the newest technical document "Aquatic Life Ambient Water Quality Criteria For Ammonia -Freshwater", which was combined with the latest international research results and proposed new ammonia[12] WQC benchmark functions and the reference value. In China, the current ammonia water quality standards refer to foreign WQC mainly [13], and there is no specific basin water quality standard now. A large number of studies [14-20] by scholars at home and abroad indicate that under different pH and different temperature conditions, the toxicity effects of ammonia on aquatic organisms are different. The China is vast in territory, where the climatic conditions and water quality conditions of different basins have obvious differences and these may bring significant impact on WQC of ammonia. Some

researchers have developed the WQC of ammonia in Liaohe River basin and Taihu basin, and found that WQC values in different basins reflected the difference [8, 21, 22]. However, the development of specific basin WQC was rarely reported because our parameter data of major basins were based on the state monitoring water quality. This study is on the basis of previous studies, both deriving the WQC for ammonia under different season conditions in Songhua River basin, Liaohe River basin, Haihe River basin, Yellow River basin, Huaihe River basin, Yangtze River basin and Zhujiang River basin and desiring to provide a reference for the differential management of the water environment in China.

1 Materials and methods

1.1 Source of water quality paramenters and ammonia environmental exposure data

PH data and ammonia monitoring data came from MEP's website "Water quality automatic monitoring weekly report of key section of major river basin" (http://datacenter.mep.gov.cn/report/getCountGraph.do?type=runQianWater, from December 31, 2012 to December 8, 2013, and Recorded 1 times the pH and ρ(ammonia) data from total 90 sections of the 7 basins each 4 weeks, and pH of each basin selected the average value of the 3 highest values of all sections.

Water temperature data came from the Local Records of seven basins [23-29] and literature [30-33], and the basins which have no record will be based on its average temperature by literature method [34]. Water temperature will be divided into summer water temperature and non-summer water temperature in the study, in which the summer water temperature means that the average water temperature from June to August and the non-summer water temperature means the average water temperature of the others. If the data is not incomplete, it could use the average water temperature of April, July, October and January to replace the average water temperature of four seasons, while the water temperature of the frozen winter period is calculated at 4 ˚C.

1.2 Deriving the WQC for ammonia in basins

At present, the method of deriving the WQC for ammonia is mainly based on "Guidelines for deriving numerical national water quality criteria for the protection of aquatic organisms and their uses" [35], which was published by U.S. EPA in 1985. Functional relation of water temperature and pH refer to the document "Aquatic Life Ambient Water Quality Criteria for Ammonia – Freshwater" [12] which was published by U.S. EPA in 2013.

The study refers to the results [8] from previous researchers to derive the WQC for

ammonia in seven basins.

Criteria maximum concentration (CMC) is as the following:

$$CMC = 0.643 \times \left(\frac{0.0489}{1+10^{7.204-pH}} + \frac{6.95}{1+10^{pH-7.204}}\right) \times MIN(10.40,\ 6.018 \times 10^{0.036 \times (25-T)}) \quad (1)$$

Criteria continuous concentration (CCC) is as the following:

$$CCC = 0.502 \times \left(\frac{0.0676}{1+10^{7.688-pH}} + \frac{2.912}{1+10^{pH-7.688}}\right) \times MIN(2.852,\ 0.914 \times 10^{0.028 \times (25-MAX(T,7))}) \quad (2)$$

where, T stands for the water temperature, ˚C.

1.3 Ecological risk assessment of ammonia exposure

Risk quotient (RQ) method is used to assess the ecological risk of ammonia in seven basins [36]. RQ is a simple and conservative approach to the risk characterization, which characterizes the ecological risk of pollutants through comparing the environmental exposure concentrations (EEC) with WQC. The calculation method is as the following:

$$RQ=EEC/WQC \quad (3)$$

where, EEC stands for the environmental exposure concentrations, mg/L; WQC stands for the water quality criteria, mg/L.

The study used the data of ρ(ammonia) measured from all the sections of the 7 basins as EEC, and each 4 weeks recorded once, respectively the first week, the fifth week, the ninth week, the thirteenth week, the seventeenth week, the twenty-first week, the twenty-fifth week, the twenty-ninth week, the thirty-third week, the thirty-seventh week, the forty-first week, the forty-fifth week and the forty-ninth week. When the ecological risk is assessed, the exposed time would correspond to the seasonality of WQC. Judging the ecological risk level according to the value of the risk quotient, when RQ < 1, there is nearly no risk; when 1≤RQ＜10, there is risk; when RQ≥10, there is the highest risk [36, 37].

1.4 Date analysis

The study used SPSS software 18.0 to analyze the significant differences of CMCs and CCCs in the summer season and non-summer season of ammonia, and samples with normal distribution used independent samples t test while samples in no conformity with normal distribution used Mann-Whitney test in non parametric test.

2 Results and analysis

2.1 WQC values for ammonia in seven basins

According to the pH and water temperature in summer season and non-summer season of 7 basins, the CMCs and CCCs in summer season and non-summer season of ammonia were calculated separately. The results were shown in Tab. 1. It can be known that the differences of the WQC values of ammonia in different basins were great, and WQC in Huaihe River basin was lowest in seven basins while the difference of CMCs in Huaihe River basin and Zhujiang River basin was more than 6 times; the differences of the WQC values of ammonia in the same basin during different seasons were also great, and the differences of the CCCs of ammonia in the same basin during different seasons, such as Songhua River basin, Haihe River basin, Yellow River basin and Huaihe River basin, were more than 2 times at all. Using software to analyze the significant differences of CMCs and CCCs in summer season and non-summer season of ammonia, the results were as follows: the CMCs of ammonia in summer season of ammonia were not conformed to the normal distribution, so it used Mann-Whitney test in non parametric test, and the results showed that there was no significant difference between two groups(P>0.05); the CMCs in summer season and non-summer season of ammonia were consistent with normal distribution, so it used independent samples t test, and the results showed that the difference was significant between two groups(P<0.05).

Tab. 1 Aquatic life criteria for ammonia in the seven basins

Basin	pH	Water temperature /℃		Criteria values in summer /(mg/L)		Criteria values in non-summer /(mg/L)	
		Summer	Non-summer	CMC	CCC	CMC	CCC
Songhua River	8.57	21	11	1.80	0.24	2.23	0.45
Liaohe River	8.64	23	13	1.34	0.18	1.96	0.35
Haihe River	8.94	29	13	0.48	0.08	1.16	0.22
Huaihe River	9.18	28	14	0.37	0.06	0.81	0.15
Yellow River	8.80	28	14	0.66	0.10	1.47	0.25
Yangtze River	8.71	23	17	1.18	0.16	1.72	0.24
Zhujiang River	8.11	28	19	2.45	0.32	5.16	0.57

2.2 Ecological risk assessment of ammonia exposure in 7 basins

According to the CCCs in summer season and non-summer season of ammonia in seven basins, RQ method was used to assess the ecological risk of the measured *ρ*(ammonia) in monitoring sections of each basin. The results were shown in Tab. 2.

Tab. 2 Amount of basin sections with risk or high risk

Basin	Section number	Ecological risk	Non-summer										Summer		
			1 weeks	5 weeks	9 weeks	13 weeks	17 weeks	21 weeks	37 weeks	41 weeks	45 weeks	49 weeks	25 weeks	29 weeks	33 weeks
Songhua River	16	In risk	8	7	8	8	6	3	4	3	2	3	11	8	8
		In high risk	0	0	0	0	0	0	0	0	0	0	0	0	0
Liaohe River	9	In risk	4	3	2	2	2	3	3	2	3	2	5	5	4
		In high risk	0	0	0	0	0	0	0	0	0	0	0	0	0
Haihe River	7	In risk	3	2	2	3	2	2	3	2	2	3	4	3	4
		In high risk	2	2	2	1	1	0	0	0	1	1	2	2	2
Huaihe River	27	In risk	19	20	19	14	19	20	21	20	20	21	22	19	21
		In high risk	6	7	7	8	5	4	2	3	2	2	4	8	6
Yellow River	12	In risk	7	9	9	8	7	2	6	3	5	7	9	8	10
		In high risk	3	3	2	1	1	2	0	1	2	3	2	2	1
Yangtze River	21	In risk	13	13	14	6	7	2	3	5	8	10	5	6	7
		In high risk	0	0	0	1	0	0	0	0	0	0	0	0	0
Zhujiang River	8	In risk	1	1	1	1	1	1	0	1	0	2	1	1	1
		In high risk	0	0	0	0	0	0	0	0	0	0	0	0	0

Note. Because of the large amount of data and limited length, it only showed the numbers of sections in risk or in high risk in seven basins

The results of ecological risk assessment showed that: the water quality situation in Zhujiang River basin was the best in 7 basins, and Guiyang Shizui section at the forty-ninth week and Guangzhou Changzhou section in part of the month were in risk, and the others had no risk. Those in Songhua River basin, Liaohe River basin and Yangtze River basin were moderate, and most sections in majority months had no risk and a few sections were in risk; There was no high risk in the sections of Songhua River basin and Liaohe River basin, while Leshan Minjiangdaqiao section in Yangtze River basin was in high risk at the thirteenth week with RQ of 15.17 and that might be due to a one-time centralized discharge by some enterprises in this month. The water quality in Yellow River basin was relatively poor, and Haidong Minheqiao section, Yuncheng Hejindaqiao section and Weinan Tongguandiaoqiao section were in higher risk during majority months. The highest risk occurred in Yuncheng Hejindaqiao section, where ammonia concentration exceeded 68 times in the forty-ninth week, and other sections were in risk during majority months, only a few with no risk. The water quality situation in Haihe River basin and Huaihe River basin were the worst. Haihe River basin has 7 monitoring sections, that the most serious pollution occurred in Tianjin Sanchakou section and Liaocheng Chenggouwan section, which continued in high risk during most months and other sections were in risk about half of the month; Huaihe River basin has 27 monitoring sections while 16 in high risk, the

others almost in risk, and only a few sections in some months were in no risk. Fuyang Zhangdaqiao section, Bozhou Yanji section and Suzhou Yangzhuang section were nearly in high risk at half a year, and the highest risk occurred in Fuyang Zhangdaqiao section, with RQ up to 159.17 at the twenty-fifth week, and it was hundreds of times over than other basins.

3 Discussion

3.1 Selection of the method for deriving basin WQC

At present, there are 3 types of Species Sensitivity Distribution (SSD) model used for WQC: the Species Sensitivity Rank (SSR) method based on log trigonometric function model[38], the method based on log normal distribution function[39], and the method based on log logistic distribution function[40]. On the basis of WQC for ammonia, the mainstream SSD model does not consider the influence of water quality parameters, so the SSD model is not suitable for deriving WQC for ammonia. US EPA established the methodology of aquatic life ambient water quality criteria for ammonia based on the empirical mathematical model, and released the latest version of the ammonia criteria technical documents in 2013. Therefore, this study mainly draw lessons from the ammonia criteria technical documents by USA, and derived the WQC for ammonia under different season conditions in 7 basins.

In addition, the data for water species distribution in different basins are not detailed enough, which is temporarily unable to support the establishment of the function formula of the WQC for ammonia separately in each basin, so this study used a unified functional relationship to derive the WQC for ammonia. With the further development of the research on the ammonia toxicity in the native species in China, if we have specific function formulae of different basins, the studies on the difference of the WQC for ammonia in different basins can be further promoted.

3.2 Selection of the data for pH and water temperature in seven basins

PH data came from MEP's website "Water quality automatic monitoring weekly report of key section of major river basin", including totally 90 sections from 7 basins and these can reflect the pH level of 7 basins basically. Considering the current monitoring site distribution of main basins may have differences, which do not fully reflect the true pH level of basins, the data could be supplemented and corrected by adding monitoring sites and other methods in the future. In addition, since the basins may have accidental emergencies and cause an abnormal elevation of pH values at some time point, and in order to reflect the true pH level of seven basins and ensure the reliability of data, we select the average

value of the 3 highest values of all sections in this study.

The geographical area of each basin has large span and the difference between the upper reaches and lower reaches is large, which lead to a great difference in water temperature at different sections of the same basin. Because of the different topography and water depth, the temperatures of the different water layers have a greater difference. Therefore, there is some uncertainty of the basin water temperature selection in the summer season and non-summer season. In order to reduce the uncertainty, following conservative principle, this study refers to local records or relevant published articles as a relatively reliable source of data, and makes a preliminary estimate of the average water temperature in the summer season and non-summer season of 7 basins. In the future, with the development of research, we can carry out the studies for the measurement of water temperature in some basins or the studies on section level and water layer level, which could further reduce the uncertainty of water temperature data.

3.3 Comparative analysis of the WQC values for ammonia in 7 basins and other WQC values

From Tab. 1 we can see that the WQC for ammonia in different basins was very different at different water temperature and pH conditions. Considering the geographical distribution of the basins, it indicated that the WQC values of higher latitude and lower latitude basins (Songhua River basin, Liaohe River basin, Zhujiang River basin) were greater than those of the middle latitude basins (Haihe River basin, Yellow River basin, Huaihe River basin, Yangtze River basin); considering the seasonal distinction, it indicated that the WQC values in the non-summer season were greater than those in summer season. The largest difference was in Huaihe River basin and Zhujiang River basin, and the differences of CMCs in summer season and non-summer season were 6.9 times and 6.4 times respectively, and the differences of CCCs were 6.9 times and 6.4 times respectively. The difference of CMCs was greater than CCCs, and the difference of WQC in summer season was greater than that in non-summer season. The reason is that the pollution of Huaihe River basin is very serious, with water pH of 9.18 and it has the highest value in 7 basins; and Zhujiang River basin water quality is better, with water pH of 8.11 and it has the lowest value in 7 basins. Based on reasons above, great difference of CMCs and CCCs is caused between 2 basins under the same summer average water temperature condition (6.62 times and 5.33 times, respectively). Non-summer average water temperature in Zhujiang River basin is higher than that in the Huaihe River basin, and the difference of CMCs and CCCs between two basins is slightly less than that in summer. Supposing the non-summer water temperature of two basins unchanged, and adjusting pH to the same level, the differences of CMCs and CCCs were 1.05 times and

1.38 times respectively. Therefore, it can be inferred that the difference of pH is the main important factor of the river basins. In addition, the differential analysis results showed that the CMCs of a few basins was relatively closed with each other and with no significant difference, so that we can use a unified threshold in principle except that the basins can be used cautiously with too large difference; the CCCs had significant difference, therefore, it had important significance and necessity to implement the management of ammonia according to different basins and different seasons in China.

According to the previous research results[8] and similar data from the United States[12], in the range of pH from 6.5 to 9 ,and the temperature from 0 °C to 30 °C, the WQC values were from 0.403 to 38.9 mg/L (CMCs) and from 0.066 4 to 3.92 mg/L (CCCs) respectively in China, while the values were from 0.299 to 57.0 mg/L (CMCs) and from 0.037 1 to 2.24 mg/L (CCCs) respectively in the United States. Compared with each other, the CMC and CCC in summer season of Huaihe River basin in this study were both less than the range of Chinese WQC values for ammonia, which were in the range of WQC values in the United States. Because of the calculation formula of ammonia in this study was directly used by the previous research results, without being derived in different basins respectively, in the case of the Huaihe River basin's pH beyond 9, and the result of the calculation was less than the WQC values in China. If the pH value is expanded to 9.18, the range of CMCs will become 0.309 to 38.9 mg/L and the range of CMCs will be from 0.052 to 3.92 mg/L, and the WQC values for ammonia in summer season of Huaihe River basin will be covered in the range of Chinese WQC values for ammonia, so the difference of the calculation results is reasonable. In addition, there have differences in the distribution and research status of aquatic organisms between China and the United States. The calculation of CMCs and CCCs for ammonia adopted the data of 67 genus and 12 genus respectively in the United States, which were much more than 27 genus and 7 genus in China. Furthermore, data of the most sensitive genus in the process of calculation in the United States (*Lampsilis*, 0.344 mg/L [12]) was far lower than data of the most sensitive genus in China (average value of shellfish, 0.914 mg/L [8]), which lead to the WQC values for ammonia in the United States lower than those in China.

According to "Environmental quality standards for surface water" (GB 3838-2002), the ρ(ammonia) standard limit values of Class Ⅰ to Class Ⅴ surface water are 0.15, 0.5, 1.0, 1.5 and 2.0 mg/L[41] respectively. Compared with the results of this study, the current standard limit values of the surface water ammonia in China are too general and lack of practical operability. According to water standard for ammonia, the CCCs in summer season and non-summer season in seven basins are almost divided into Class Ⅰ and Class Ⅱ, while the CMCs are most divided into Class Ⅱ to Class Ⅳ, so the CCCs can be

used as a reference for more detailed ammonia water quality standards in future and the CMCs can be used to apply to the water quality emergency management in China.

3.4 Ecological risk assessment of ammonia exposure in 7 basins

The risk level of ammonia exposure in 7 basins showed the same trend of pH. When the basins had lower pH values, the ammonia risk level was lower (in the Zhujiang River basin, Songhua River basin, Liaohe River basin and Yangtze River basin), and to the contrary, when the basins had higher pH values, the ammonia risk level was greatly increased (in the Yellow River basin, Haihe River basin and Huaihe River basin). From the geographical distribution of the basins, it indicated that the risk level of higher latitude and lower latitude basins was less than that of the middle latitude basins, which presented a trend that was opposite to the WQC values in 7 basins. From the seasonal distinction, it indicated that there had no significant impact on the risk of different months by seasonally calculating RQ in 7 basins. Through analyzing the reasons, due to the impact of pH, the WQC values will be smaller when pH values are higher, and it might lead to differences in risk levels of the same ammonia exposure concentrations. But Haihe River basin and Huaihe River basin had the highest RQ values that exceeded the ρ(ammonia) standard limit values tens of times or even a hundred times, much larger than those of other basins. In addition, affected by temperature factors, the WQC values in summer season were lower than those in non-summer season, and the risk assessment results showed that there had no significant impact on the risk of different months by seasonally calculating RQ. Therefore, we infer that the basin risk level is mainly affected by the concentration of environmental exposure (actual monitoring of ammonia concentration), and the basin risk level is high while ρ(ammonia) is high, and the basin risk level is low while ρ(ammonia) is low. This inference is almost the same as that for the water quality of major basins that is reported by "China Environmental Status Bulletin" in 2013[10]. A slight difference is that in "China Environmental Status Bulletin", it's reported that the water pollution of Haihe River basin is the most serious in 7 basins, but because there are only 7 sections' monitoring data in Haihe River basin, while Huaihe River basin have 27 sections , the number of cross sections which in high risk and RQ values of Haihe River basin are both lower than that of Huaihe River basin. The uncertainty due to monitoring site layout can be further improved in the follow-up study.

It is suggested that according to the results of risk assessment, it should be managed according to different basins and different seasons. For the basins at low risk or no risk, we can carry out water quality routine monitoring; for the basins at risk, in addition to the routine monitoring, the risk assessment should be carried out regularly, and if the risk is increased, the corresponding management measures should be taken to reduce the risk

level in time; for the basins and sections at high risk, we need to carry out comprehensive analysis on the pollution situation, and to reduce the risk to a lower level through a series of measures, such as real-time monitoring, strict control, total quantity control and so on.

4 Conclusions

A) The differences between the criteria values in different basins and different season were both significant. The differences between the criteria values in different basins were greater than 6 times, while those in the same basin during different seasons were more than two times. The summer CMC and CCC for Huaihe River were 0.37 mg/L and 0.06 mg/L while the non-summer values were 0.81 mg/L and 0.15 mg/L, respectively. Both the summer and the non-summer values were lowest in all of the 7 basins. The results of difference analysis showed that the CMC had no significant difference in summer and non-summer season, but the CCC had. It is suggested that according to the differences of the criteria values for ammonia in 7 basins, it should be managed according to different seasons and different policies.

B) The results of ecological risk showed that: Zhujiang River basin had better water quality, and the ecological risk was lowest in all basins; those in Songhua River basin, Liaohe River basin and Yangtze River basin were moderate, with some sections in risk; the water quality in Yellow River basin was relatively poor, with majority sections in risk and some sections in high risk; and the highest risk occurred in Haihe River basin and Huaihe River basin, and Haihe River basin had 7 sections while 2 in high risk, and Haihe River basin had 27 sections while 16 in high risk.

Acknowledgements

This paper was supported by the National Water Pollution Control and Treatment Science and Technology Major Project(Grant No.2012ZX07501-003); Science and technology basic work(Grant No.2014FY120606).

References

[1] YAN Zhenguang, WANG Hong, WANG Yizhe, et al. Developing a national water quality criteria system in China [J]. Water Policy, 2013, 15(6): 936 - 942.

[2] MENG Wei, WU Fengchang. Introduction to the theory and methodology of water quality standards [M]. Beijing: Science Press, 2010, 23 - 45.

[3] JIN Xiaowei, ZHA Jinmiao, XU Yiping, et al. Derivation of aquatic predicted no-effect concentration

(PNEC) for 2, 4-dichlorophenol: Comparing native species data with non-native species data [J]. Chemosphere, 2011, 84: 1 506 - 1 511.

[4] JIN Xiaowei, ZHA Jinmiao, XU Yiping, et al. Derivation of predicted no effect concentrations (PNEC) for 2, 4, 6-trichlorophenol based on Chinese resident species [J]. Chemosphere, 2012, 86: 17 - 23.

[5] YAN Zhenguang, ZHANG Zhisheng, WANG Hong, et al. Development of aquatic life criteria for nitrobenzene in China [J]. Environ. Pollut., 2012, 162: 86 - 90.

[6] Wu Fengchang, Mu Yunsong, Chang Hong, et al. Predicting water quality criteria for protecting aquatic life from physicochemical properties of metals or metalloids [J]. Environ. Sci. & Technol., 2013, 47(1): 446 - 453.

[7] YAN Zhenguang, MENG Wei, LIU Zhengtao, et al. Biological criteria for freshwater Cd in China [J]. Acta Scientiae Circumstantiae, 2009, 29(11): 2 393 - 2 406.

[8] YAN Zhenguang, MENG Wei, LIU Zhengtao, et al. Development of freshwater aquatic life criteria for ammonia in China [J]. Environmental Science, 2011, 32(6):1 564 - 1 570.

[9] XI Danli, SUN Yusheng, LIU Xiuying, et al. Environmental monitoring (Revised) [M]. Beijing: Higher education press, 1996.

[10] Ministry of Environmental Protection. China Environmental Status Bulletin [R]. Beijing: Ministry of Environmental Protection. 2013:13 - 20.

[11] Ministry of Environmental Protection. Planning of Water Pollution Prevention and Control in Key Drainage Basins (2011-2015) [R]. Beijing: Ministry of Environmental Protection. 2012.

[12] US EPA. Aquatic life ambient water quality criteria for ammonia-freshwater 2013 [R]. Washington DC: US EPA, Office of Water, 2013: 40-52.

[13] XIA Qing, CHEN Yanqing, LIU Xianbing. Water quality criteria and water quality standards [M]. Beijing: China Standard Press. 2004.

[14] Thurston R V, Russo R C, Vinogradov G A. Ammonia toxicity to fishes: effect of pH on the toxicity of the un-ionized ammonia species [J]. Environ. Sci. & Technol., 1981, 15(7): 837 - 840.

[15] Emrson K, Russo R C, Lund R E, et al. Aqueous ammonia equilibrium calculations: effect of pH and temperature [J]. J. Fish. Res. Board. Can., 1975, 32(12): 2 379 - 2 383.

[16] LV Yonglin, ZHANG Yongpu, SHAN Saisai, et al. Acute toxic effects of ammonia-N to Tegillarca granosa at different temperatures [J]. Journal of Zhejiang Ocean University(Natural Science), 2012, 31(1): 54 - 68.

[17] ZHANG Yongpu, XIAO Guoqiang, LIN Lizhu, et al. Effects of pH and ammonia-N on tolerance of Estellarca olivacea [J]. Sichuan Journal of Zoology, 2009, 28(1): 73 - 76.

[18] SHEN Chenggang, YANG Feng, LIU Changfa, et al. A study on the acute toxicity of ammonia to fishes in low temperature [J]. Journal of Dalian fisheries college, 1995, 10(3): 58 - 64.

[19] SHI Shangli, FENG Yicheng, ZHENG Lian, et al. Toxicity of ammonia-N in Babylonia areolata at different pH and salinity [J]. Journal of Zhanjiang Ocean University, 2005, 25(6): 36 - 40.

[20] LUO Jie, DU Tao, LIU Chuwu, et al. Toxic effects of ammonia to hemifusus tuba juveniles at

different pH and salinity [J]. Chinese Journal of Zoology, 2010, 45(3): 102 - 109.

[21] YAN Zhenguang, MENG Wei, LIU Zhengtao, et al. Development of aquatic life criteria and lash-up standard for ammonia in Liao River basin [J]. China Environmental Science, 2011, 31(11): 1 829 - 1 835.

[22] SHI Xiaorong, LI Mei, CUI Yibin, et al. Development of aquatic water quality criteria for ammonia in freshwater ecosystem of China based on Lake Tai basin [J]. Acta Scientiae Circumstantiae, 2012, 32(6): 1 406 - 1 414.

[23] Songliao Water Resources Committee. Songhua River Journal (fourth volumes) [M]. Jilin: Jilin People's Press, 2003:145 - 146.

[24] Songliao Water Resources Committee. Liaohe River Journal (fourth volumes) [M]. Jilin: Jilin People's Press, 2003:184.

[25] Haihe River Editorial Committee. Haihe River Journal, First volume [M]. Beijing: China Water Conservancy and Hydropower Press, 1997:41.

[26] Yellow River Water Resources Committee. The Yellow River Journal General Editing Room. Yellow River Journa,Volume 2: Summary of the Yellow River Basin [M]. Zhengzhou: Henan People's Press, 1998: 99 - 106.

[27] Huaihe Water Resources Committee. Huaihe River Editorial Committee. Huaihe River Journal, Volume 2: Summary of Huaihe River Basin [M]. Beijing: Science Press, 2000:19 - 22.

[28] Yangtze River Water Resources Committee. The Yangtze River Journal General Editing Room, Yangtze River Technical and Economic Association. Yangtze River Journa, Volume 1: Summary of Yangtze River Basin [M]. Beijing: Chinese Encyclopedia Press, 2007: 87.

[29] Zhujiang River Water Resources Committee. Zhujiang River Editorial Committee. Zhujiang River Journa, Volume 5 [M]. Guangzhou: Guangdong science and Technology Press, 1994: 225.

[30] WANG Haiying, TENG Jie, ZHANG Ji, et al. Reason analysis of the high DO in winter of Haihe river in Tianjin [J]. Urban Environment & Urban Ecology, 2005, 18(3): 27 - 28.

[31] WANG Keqing, ZENG Yan, XIE Zhiqing, et al. Change trend of temperature and precipitation in Huaihe river basin from 1961 to 2008 [J]. Journal of the Meteorological Sciences, 2012, 32(6): 671 - 677.

[32] SUN Daming, TIAN Huifeng, ZHANG Huan, et al. Minitoring of water temperature and changing relationship between the water temperature and air temperature in the upper Yangtze river [J]. Building Energy Efficiency, 2010, 38(12): 74 - 77.

[33] HU Yingying, ZHAO Liang, GUO Xinyu, et al. Variations of the water temperature offshore the Changjiang river Estuary in winters and springs [J]. Oceanologia Et Limnologia Sinica, 2012, 43(3): 655 - 661.

[34] BAI Zhenying. A new formula for calculating natural water temperature of lakes (reservoirs) [J]. Hydrology, 1999, 3: 29 - 32.

[35] US EPA. Guidelines for deriving numerical national water quality criteria for the protection of

aquatic organisms and their uses [R]. Washington DC: US EPA, Office of Research and Development, 1985.

[36] US EPA. Review of Ecological Risk Assessment Methods. Washington DC: US EPA, 1988.

[37] CAO Hongfa, SHEN Yingwa. Brief review: ecological risk assessmental research [J]. Environmental Chemistry, 1991, 10(3): 26 - 30.

[38] Erickson R J, Stephan C E. Calculating the final acute value for water quality criteria for aquatic organisms [R]. Duluth, MN: US EPA, Environmental Research Laboratory-Duluth, Office of Research and Development, 1984.

[39] Aldenberg T, Jaworska J S. Uncertainty of the hazardous concentration and fraction affected for normal species sensitivity Distributions [J]. Ecotoxicol. Environ. Saf., 2000, 46(1): 1 - 18.

[40] Aldenberg T, Solb W. Confidence limits for hazardous concentrations based on logistically distributed NOEC toxicity data [J]. Ecotoxicol. Environ. Saf., 1993, 25(1): 48 - 63.

[41] State Environmental Protection Administration, General Administration of Quality Supervision, Inspection and Quarantine [S]. Environmental quality standards for surface water. GB3838-2002. Beijing: China Environmental Science Press, 2002.

七大流域氨氮水生生物水质基准与生态风险评估初探

王一喆[1]，闫振广[1*]，郑 欣[1]，赵 莹[2]，张亚辉[1]，杨霓云[1]

（1. 中国环境科学研究院 国家环境保护化学品生态效应与风险评估重点实验室，北京 100012

2. 中国环境科学研究院 机动车排污监控中心，北京 100012）

摘 要：氨氮是我国流域水环境管理的国控指标之一，为评估不同流域的氨氮基准差异性，以七大流域（松花江流域、辽河流域、海河流域、黄河流域、淮河流域、长江流域和珠江流域）为研究对象，基于水质参数对氨氮毒性的影响，借鉴 US EPA（美国国家环境保护局）水环境基准技术方法，分夏季和非夏季 2 种情况推算了各流域氨氮水生生物基准值. 结果显示：a）流域和季节的不同导致氨氮基准值的差异均很明显，不同流域的氨氮基准值差异可超过 6 倍，同一流域不同季节的氨氮基准值差异可超过 2 倍。 b）淮河流域夏季和非夏季氨氮基准值均为最低，夏季氨氮急、慢性基准值分别为 0.37 和 0.06 mg/L，非夏季分别为 0.81 和 0.15 mg/L。c）氨氮暴露生态风险初步评估结果表明，珠江流域风险较小；松花江流域、辽河流域、长江流域次之；黄河流域风险较大；海河流域和淮河流域风险最大，海河 7 个断面中有 2 个存在高风险，淮河 27 个断面中 16 个存在高风险. 根据各流域不同季节氨氮基准值及氨氮暴露生态风险的差异，建议对不同流域、不同季节实行差异化管理。

关键词：七大流域；氨氮；水生生物基准；生态风险评估；风险商值法

A preliminary study on food consumption, preference and day-night predatory difference of *Asterias amurensis* on *Scapharca broughtonii*

ZHANG Tian-wen, LIU Guang-bin, LIU En-fu, ZHENG Yong-yun, QIU Zhao-xing*

Marine Biology Institute of Shandong Province, Qingdao 266002, *China*

Abstract: In order to study the food consumption, preference and day-night predatory difference of *Asterias amurensis* on *Scapharca broughtonii*, the experiments were carried out at the temperatures ranging from 16 ℃ to 20 ℃, salinity of 28.2 ± 2.1, dissolved oxygen of 7.5±0.7 mg/L and pH of 8.0 ± 0.3.The results provided basic data for promoting steady and healthy development of the multiplication and cultivation of *S. broughtonii*. The results of food consumption suggested that the food intake of starfish increased with the density of *S. broughtonii* at all conditions. The food consumption of starfish in different sizes on *S. broughtonii* in the same size had no significant difference ($p>0.05$), but it was significantly different among *S. broughtonii* in different sizes. The starfish had the highest feeding rate on the smallest *S. broughtonii.* Our findings also verified the positive relation between the weight of food intake of starfish in different sizes on the density and size of *S. broughtonii.* The feeding rhythm of starfish on *S. broughtonii* in different sizes showed a certain day-night difference, higher at night than in the day. The maximum food consumption occurred when the size of *S. broughtonii* became larger. The results showed that 30 ind/m^2 was the suitable sea bottom sowing density for *S. broughtonii*. Our data indicated that the ability to avoid predators and rivals increased as the shell length rose. Based on prey selectivity, bivalves that have a lower commercial value may be used to clear away *A. amurensis*.

Keywords: *Asterias amurensis*; *Scapharca broughtonii;* food consumption; food preference; day-night difference

Commonly known as ark shell and baby clam, *Scapharca broughtonii*, belonging to arcidae of lamellibranchia, is a large-scale bivalve mollusk living by burial and dwelling. With delicious taste, rich nutrition, and high economic value, it is always the object caught by fishermen in Yellow Sea and Bohai Sea. In recent decade, the natural resource of *S. broughtonii* shrinks extremely for long-term excessive catch [1]. At present, the natural fishing and catching yield cannot meet the demand in domestic and foreign market, so it is

Received on Apr. 18, 2016

*Corresponding author: zhaoxingqiu@163.com

imperative to develop culture and proliferation and repair the resource [2]. Since 2010, the culture and proliferation of *S. broughtonii* becomes a hotspot in the development and utilization of shallow-sea resource after holothurian culture [3]. There are various factors affecting the effects of *S. broughtonii* culture and proliferation, but the major influencing factor after the bottom sowing is the invasion of harmful organism, starfish [4].

Starfish is one of major predators in the biological system of intertidal zone and subtidal zone [5, 6]. Its ingestion can directly or indirectly affect the distribution and diversity of benthos [7-10]. The starfish distributing in Shandong coastal area is mainly *Amurensis asterias*, belonging to asterias of asteroidean. *A.amuresis* mainly ingests shellfish, crustacea, polychaetes, and small fish [12], especially bivalve. Moreover, it competes with benthos for baits [13, 14]. In the natural environment, *A.amuresis* has extensive feeding habit, but it also has selectivity in food organism. Such selective feeding not only brings more living opportunities, but also plays an important role in adjusting population quantity of food organism [15]. In shellfish culture area, *A.amuresis* can accurately position burial-dwelling shellfish and excavate ingestion according to the smell of shellfish [16, 17]. In 1954, the direct loss in shellfish culture caused by ingestion of *A.amuresis* was up to 4 billion Yen [18]. In 2007, *A.amuresis* bursting out in Qinghai coastal area caused severe loss of bottom-sowing shellfish in Red Island [19]. Studying the ingestion selectivity of *A.amuresis* in different sizes and densities by *A.amuresis* in different sizes and ingestion difference between day and night, this works provided basic data to know more about the ecology of *A.amuresis* to ingest *S. broughtonii*. It is expected to effectively avoid the influence on major harmful organisms, improve the survival rate of *S. broughtonii*, and to better develop the proliferation of *S. broughtonii* by the bottom sowing.

1 Materials and methods

1.1 Experiment polder and management

In Rizhao Institute of Oceanic and Fishery, a pond of sediment substrate was selected for experiment. The ecological method of polder experiment was used to study the capacity of *A.amuresis* to ingest juvenile mollusk of *S. broughtonii* and ingestion difference between day and night. The experiment was developed in 2 m × 2 m polder, and 30-mesh bolting-silk was used as enclosure ecosystem, the lower part of which was embedded into bottom mud for 0.6 m. The whole enclosure ecosystem was set in the pond with timber pile and bamboo as support. 2 days before the experiment, water was flooded for 96h experiment, during which the water depth in pond was 1 ± 0.1 m. After the experiment, the statistics was conducted in the empty pond. In the experiment, water

temperature was 16 ˚C - 20 ˚C, salinity 28.2 ± 2.0, dissolved oxygen (7.5 ± 0.7) mg/L, and pH was 8.0 ± 0.3.

1.2 Experimental materials

The juvenile mollusks of *S.broughtonii* for experiment were offspring seeds by overwintering culture in 2012 from estuary area between 2 cities in Shanhaitian Tourist Resort of Rizhao, Shandong. After being transported to experiment field, the juvenile mollusks were reared for 14 days temporarily with circulating water in the storage pond. During temporary rearing, mangroves and diatom were fed at 06:00, 12:00, 18:00, and 24:00 every day.

The *A.amuresis* for experiment was from the sea area in Rizhao, Shandong. After being transported to experiment field, the *A.amuresis* was reared for 3 days temporarily with circulating water in the storage pond. During the temporary rearing, no bait was fed.

1.3 Experiment design

1.3.1 Food consumption of juvenile mollusks of *S. broughtonii* in different densities and categories by *A.amuresis*

Juvenile mollusks of *S. broughtonii* in four categories with the shell length of 1 ± 0.09 cm and 1.5 ± 0.13 cm were selected and divided into 1 cm group and 1.5 cm group. With 10 ind/m^2, 30 ind/m^2 and 50 ind/m^2 as the experiment density, the weight of soft part was measured for *S. broughtonii* in 4 sizes. *A.amuresis* with peduncle length of 8 cm - 10 cm and density of 1 ind/m^2 was taken for 96h experiment to analyze its capability to ingest *S. broughtonii* in different densities and categories. Four parallels and four blank control groups without *A.amuresis* were set for every group of experiment.

1.3.2 Food consumption of juvenile mollusks of *S. broughtonii* in different categories by *A.amuresis* in different categories

A.amuresis with wrist lengths of 5 cm - 7 cm, 8 cm - 10 cm, and 11 cm - 13 cm was selected as small-scale, middle-scale, and large-scale *A.amuresis*. The density of *S. broughtonii* was 30 ind/m^2, and that of *S. broughtonii* was 1 ind/m^2. During 96h experiment, the difference in capabilities among *A.amuresis* in 3 sizes to ingest *S. broughtonii* in 4 sizes was analyzed. 4 parallels and 4 blank control groups without *A.amuresis* were set in every experiment.

1.3.3 Difference of *A.amuresis* to ingest juvenile mollusks of *S. broughtonii* in different sizes between day and night

In the experiment to analyze the difference of *A.amuresis* to ingest *S. broughtonii* in 4 sizes between day and night, the density of *S. broughtonii* was 30 ind/m^2, and peduncle length and density of *A.amuresis* were 8 cm - 10cm and 1 ind/m^2, respectively. The experiment started at 8:00am and was observed at 1h, 2h, 8h, 12h, 24h, 30h, 46h, 54h, 60h, 72h, and 96h after the experiment. 4 parallels and blank control groups without *A.amuresis* were set for every group of experiment.

1.4 Measurement of experiment indicators

The empty shells of *S. broughtonii* should be counted and natural fatality of seeds was recorded in every enclosure after the experiment about *A.amuresis* in different sizes ingesting *S. broughtonii* in different sizes and densities.

Number of empty shells of *S. broughtonii* in enclosures and that in blank groups were recorded according selected observation time in the experiment about *A.amuresis* in different sizes ingesting *S. broughtonii* in different sizes and densities.

1.5 Data processing and analysis

The food consumption of *S. broughtonii* in different sizes by *A.amuresis* is presented by the number of empty shell of *S. broughtonii* to be ingested.

$$K=E-D$$

where K refers to the number of empty shells of *S. broughtonii* to be ingested, E the number of empty shells of *S. broughtonii* in experiment enclosure, and D the number of empty shells of *S. broughtonii* in blank group without *A.amuresis*.

The difference in food consumption of *S. broughtonii* in different sizes by *A.amuresis* is represented by the percentage of total empty shells accounting for total empty shells of *S. broughtonii*.

$$H_t=(E_t-D_t)/(E-D)$$

where t refers to observation time, H_t the percentage of *S. broughtonii* to be ingested accounting for all *S. broughtonii* to be ingested in experiment at the observation time, E_t empty shells of *S. broughtonii* in experiment enclosure (ind) at the observation time, and D_t the empty shells of *S. broughtonii* in blank control group without *A.amuresis* at that time.

Variance analysis was conducted for experiment data with statistical software SPSS17.0, and multiple comparison conducted by Duncan method. $P>0.05$ means that difference is insignificant, while $P<0.05$ means that difference is significant. Results were represented by lowercases. Data with same letters means that the mutual difference is insignificant ($P>0.05$). During the experiment, the shell length of *S. broughtonii* was denoted by L and the meat weight by W.

2 Experiment results

2.1 Analysis on food consumption of *S. broughtonii* in different sizes and densities by *A.amuresis*

Fig. 1 shows that the food consumption of *S. broughtonii* in different sizes by *A.amuresis* rose with the increase in the density of *S. broughtonii*. When the density of *S. broughtonii* was 30 ind/m^2, the food consumption of *S. broughtonii* by *A.amuresis* increased without significant difference from that when the density of *S. broughtonii* was 10 ind/m^2($P>0.05$). When the density of *S. broughtonii* was 50 ind/m^2, the food consumption of *S. broughtonii* in 4 sizes by *A.amuresis* increased significantly. In the same density, the food consumption of *S. broughtonii* by *A.amuresis* decreased with the increase of shell length of *S. broughtonii*. Food consumption in each density of 2.0 cm group was the smallest. The food consumption of *S. broughtonii* in different sizes by *A.amuresis* was significantly negative correlated to the size of *S. Broughtonii*($r=-0.984\ 5$, $P<0.01$). The fitting formula between both is $K= 35.543e^{-0.457L}$($R^2=0.979\ 3$).

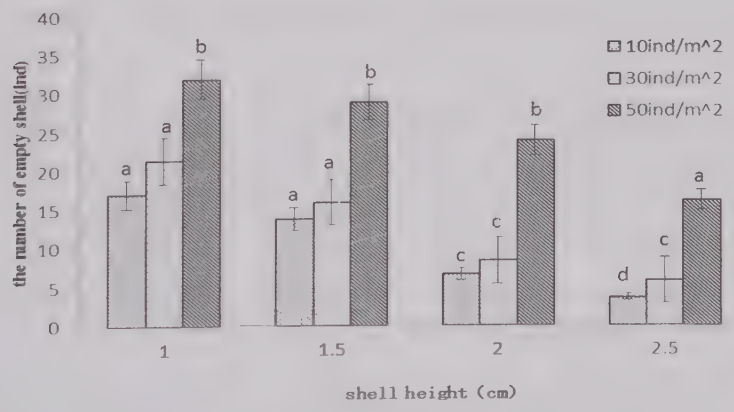

Fig. 1 The amount of food intake of *A.amurensis* on different kinds and densities of *S. Broughtonii*

(Note: Data with the same superscript are not significantly different($P>0.05$))

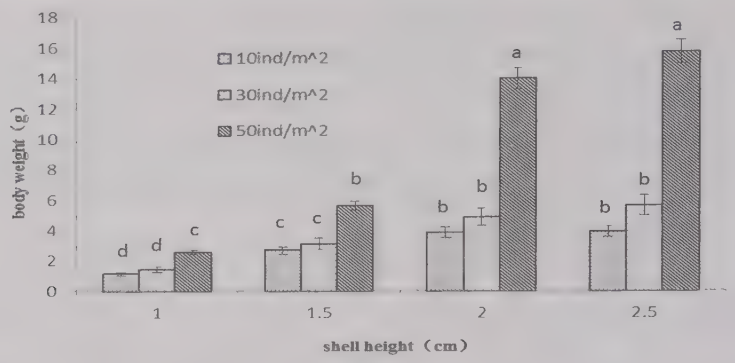

Fig. 2 The weight of food intake of *A.amurensis* on different kinds and density of *S. Broughtonii*

(Note: Data with the same superscript are not significantly different(*P*>0.05))

Fig. 2 shows that the food consumption of *S. broughtonii* by *A.amuresis* with soft part in different densities increased with density increase. The weight of soft part to be ingested was the maximum when the density of *S. broughtonii* in different sizes was 50 ind/m^2. The difference in weight of soft part to be ingested was insignificant when the density was 10 ind/m^2 and 30 ind/m^2. The soft part of *S. broughtonii* in different sizes ingested by *A.amuresis* also tended to increase with the enlargement of *S. broughtonii*. In 3 densities, the food consumption of soft part in 1 cm experiment group was the minimum, while that in 2.5 cm experiment group was the maximum. However, there was no significant difference between 2 cm experiment group and 2.5cm experiment group. The food consumption of soft part of *S. broughtonii* by *A.amuresis* was significantly positive correlated to the size of *S. broughtonii*(r=0.987 3 $p < 0.01$). The fitting formula between both is W=1.486 2 L(R^2=0.972 8).

2.2 Analysis on food consumption *S. broughtonii* in different sizes by *A.amuresis* in different sizes

Fig. 3 shows that there was no significant difference in food consumption of *S. broughtonii* in the same size by *A.amuresis* in different sizes (P>0.05). However, there was difference in the food consumption in different sizes of *S. broughtonii* by *A.amuresis* in the same size to some extent. The difference in food consumption between 1cm group and 1.5 cm group was insignificant. With the enlargement of *S. broughtonii* in experiment group, the food consumption gradually decreased. The food consumption by *A.amuresis* in 3 sizes was the minimum (5 ind at average). In 4 experiment groups, the food consumption of *S. broughtonii* by *A.amuresis* with peduncle length of 5 cm - 7cm was slightly higher than that in groups with peduncle length of 8~10cm and 10 cm - 12 cm without significant difference (P>0.05).

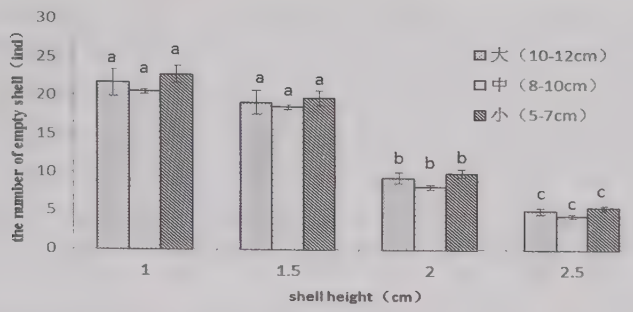

Fig. 3 Feeding intensity of different kinds *A.amurensis* on different kinds *S.broughtonii*

(Note: Data with the same superscript are not significantly different (P>0.05))

2.3 Difference in food consumption of *S. broughtonii* in different sizes by *A.amuresis* between day and night

There was difference in food consumption of *S. broughtonii* in 4 sizes by *A.amuresis* between day and night to some extent because the ingestion time was mainly at night (20:00 - 8:00). The experiment started at 8:00, but *S. broughtonii* in 4 sizes were not ingested by *A.amuresis* in 12 hours (at 20:00 on the first day). When observing at 24h (at 8:00 on the second day), except *S. broughtonii* in 2.5 cm group, those in 3 other sizes were all ingested by *A.amuresis*, and the ingestion ratio in 2 cm group was the largest that is, 14.29%. When observing after 30 hours (at 14:00 on the second day), no *S. broughtonii* was ingested by *A.amuresis* in 3 experiment groups, except 1cm group with a few *S. broughtonii* ingested. When observing after 48 hours (at 8:00 on the third day), *S. broughtonii* in 4 sizes were ingested by *A.amuresis* in large amount with the highest ratio among all observation times. When observing after 54 hours (at 14:00 on the third day), only a few *S. broughtonii* in 1 cm group was ingested, but no new empty shell was found in other 3 experiment groups. When observing after 60 hours (at 20:00 on the third day), except *S. broughtonii* in 2.5 cm group, a few in other 3 groups were ingested. When observing after 72 hours (at 8:00 on the fourth day), *S. broughtonii* in 4 experiment groups were all ingested, but the ingestion ratio was significantly lower than that in 48th hour. When observing after 96 hours (at 8:00 on fifth day), *S. broughtonii* in 4 experiment groups were ingested with the lowest ratio.

3 Discussion

3.1 Analysis on the ingestion of *S. broughtonii* in different densities and categories by *A.amuresis* in different sizes

With wide feeding scope and selectivity, *A.amuresis* is in the top of biogenesis food

chain [20] with ingestion objects, including available food organisms in environment [21]. The selectivity of *A.amuresis* is dependent on the favor to the food organism, as well as the number and availability of such food organism in environment. Studies on the predatory relation and ingestion selectivity of starfish started early in foreign countries, including relevant studies on the selectivity and functional response of *A.amuresis* and Asterias forbesi in the Pacific to the size of scallop and mussel [22-25]. However, there is still no study on the selectivity of *A.amuresis* to ingest *S. broughtonii*.

According to the most suitable recipe model, when food number is up to a certain density, the predator will refuse to ingest the prey with smaller advantage [26]. This experiment found that the soft part in *S. broughtonii* ingested by *A.amuresis* increased with the enlargement of *S. broughtonii* and its density. When the density of bottom sowing was 50ind/m^2, the soft part of *S. broughtonii* in 4 sizes ingested by *A.amuresis* was the largest. When the densities of bottom sowing were 10 ind/m^2 and 30 ind/m^2, there was no significant difference in food consumption of *S. broughtonii* in 4 sizes by *A.amuresis* ($P>0.05$).

In the production of *S. broughtonii* by bottom sowing, the yield and economic benefit will be bad if the density of bottom sowing is as low as 10 ind/m^2 even though there are little harmful organism. If the density is 50 ind/m^2, there will be a large amount of *S. broughtonii* ingested by harmful organism, causing unnecessary economic loss. Therefore, the density of bottom sowing is suggested to be about 30 ind/m^2, which can ensure the number of *S. broughtonii* per unit area, and avoid too much loss for the ingestion of *S. broughtonii* by *A.amuresis* to obtain better effect of culture and proliferation. This suggestive value is close to 15 ind/m^2 - 30 ind/m^2 of the general density for bottom sowing of *S. broughtonii*.

The food selectivity of ingested in marine ecosystem is dependent on the size of food particle [27]. Therefore, the ingestion of shellfish by *A.amuresis* has significant relation with the size of shellfish. According to Kim Y (1968), et al. [18], *A.amuresis* had capability to ingest shellfish in various shell lengths, and the rate to ingest shellfish in appropriate shell length was the largest. In this experiment, there was no significant difference in the food consumption of same *S. broughtonii* by *A.amuresis* in 3 sizes, but there was difference in food consumption of *S. broughtonii* in different sizes. Especially, the food consumption of *S. broughtonii* in 1 cm group and 1.5 cm group was the largest, while that in 2.5 cm group was the smallest. This result is the same as that by Liu Jia (2012) [28] that the food consumption by *A.amuresis* in the group with the smallest shell length was the largest. According to the results in this work, *S. broughtonii* with shell length of 2.0 cm - 2.5 cm is the most suitable as the standard for bottom sowing, which is close to the conclusion by Tang Qisheng et al. (1994) [9]. When developing proliferation by bottom sowing, the larger

the size of *S. broughtonii* is, the more effectively it can defend enemy. Therefore, the size of *S. broughtonii* released in Japan is 2 cm - 3cm, and even 5 cm - 6cm [29]. However, the large size will certainly extend the culture time and increase the cost. Moreover, juvenile mollusks of *S. broughtonii* may be dead from the anoxia in spring, high temperature in summer, and other uncontrollable factors in a large amount [9]. Therefore, the size of *S. broughtonii* for bottom sowing should be determined with the consideration of burrowing, predator, cost, and other factors.

3.2 Difference in ingestion of *S. broughtonii* by *A.amuresis* between day and night

There is difference in the food consumption of *S. broughtonii* in different sizes by *A.amuresis* between day and night. Related to illumination, this ingestion difference between day and night widely exists among aquatic animals [30]. Belonging to low-grade Echinodermata, sterias amurensis is underdeveloped in visual and other sense organs, but many rhombic neurosensory cells with antennal organs and chemical sensors are spread in epithelium. A large quantity of sucking discs in sucker of *A.amuresis* play a role of smell [27]. The visual and smell organ systems of *A.amuresis* are underdeveloped, but ingestion difference between day and night forms for the gradual adaptation to biological factors, including illumination and bait in the long-term evolution [19]. In this work, the food consumption of *S. broughtonii* in 4 sizes by *A.amuresis* was low in the first 24 hours of experiment mainly because *A.amuresis* requires a period to adapt the surrounding environment as other aquatic organisms. From 24^{th} hour to 30^{th} hour (daytime on the second day) and 48^{th} hour to 60^{th} hour (daytime on the third day), only a few *S. broughtonii* in 1 cm was ingested by *A.amuresis*, but *S. broughtonii* in other seizes showed no obvious ingestion. From 30^{th} hour to 48^{th} hour (nighttime on the second day), a large amount of *S. broughtonii* in 1 cm and 1.5 cm group was ingested with the percentage of empty shell increasing from 29.39% and 7.69% to 68.18% and 53.85%, respectively. Moreover, *S. broughtonii* in 2 cm and 2.5 cm group were greatly ingested from the 60^{th} hour to the 72^{th} hour (nighttime on the third day) with percentage increasing from 47.62% and 50% to 85.71% and 100%, respectively. According to results in this work, the food consumption of *S. broughtonii* ingested by *A.amuresis* was large at night on the second day after the bottom sowing if the seed was in the small size (≤1.5 cm), while that was large at night on the third day after the bottom sowing if the seed was in the large size (1.5 cm - 2.5 cm). There is difference in food consumption of *S. broughtonii* in the same size ingested by *A.amuresis* between day and night to some extent. The food consumption at night is larger than that during the daytime, and the larger the size *S. broughtonii* is, the later the time with the largest food consumption will be.

3.3 Strategy to control *A.amuresis* in proliferation of *S. broughtonii* by bottom sowing

A.amuresis is para-oral predator, which can precisely locate the shellfish by the smell. According to the search theory, predator will always choose food organisms with high profitability, and neglect those with low profitability [31]. Tamura thought that the shellfish in shallow water had stronger adductor muscle than that in deep water [32]. In aspect of availability of food organism, *A.amuresis* has much stronger adductor muscle than the shellfish in shallow water, so more energy is required to open them. Therefore, shellfish with low value from shallow water can be caught near the proliferation area to be trap food for the elimination of *A.amuresis.* In this way, the food consumption of *S. broughtonii* by *A.amuresis* can be reduced to obtain better economic benefit.

Acknowledgements

This paper was supported by the National Sea Welfare Project(201205023); China Agriculture Research System(CARS-48) and the earmarked fund for Modern Agro-industry Technology Research System in Shandong Province(SDAIT-14).

References

[1] Wang Xingzhang, Xing Xinze, Zhang Qigang. Effects of several physical and chemical factors on artificial breeding of *S.broughtonii* [J]. Shandong Fisheries, 2003, 20(2): 17

[2] Sun Zhengxing. Cultivation of *S.broughtonii* [J]. Scientific Fish Farming, 1990, 4: 166 - 169.

[3] YU Ruihai, LI Qi. New techniques for bottom sowing multiplication and cultivation of the pollution-free ark shell [J]. Transactions of Oceanology and Limnology, 2009, 03: 87 - 90.

[4] Fu Zhuo, Zheng Guofu. Seeding and aquaculture of *S.broughtonii* [J]. China Fisheries, 2007, 11: 49 - 50.

[5] Sloan N A. Aspects of the feeding biology of asteroids [J]. Oceanogr. Mar. Biol. Ann. Rev., 1980,18: 57 - 124.

[6] Menge B A. Effects of feeding on the environment: Asteroidea [M]. //Jangoux M, Lawrence J M Eds. Echinodern Nutrition FL, USA; CRC Press, 1982: 524 - 551.

[7] Brenchley G A. Mechanisms of spatial competitions in marine soft bottom communities [J]. J. Exp. Mari. Biol. Ecol., 1982, 60: 7 - 33.

[8] Barkai A, McQuaid C. Predator-prey role reversal in a marine benthic ecosystem [J]. Science, 1988, 242: 62 - 64.

[9] Tang Qisheng, Qiu Xianyin. Resource enhancement of arkshell (Scapharca (Anadara) *broughtonii*)

in Shandong off-shore waters [J]. Chinese journal of applied ecology, 1994, 5(4): 396 - 402.

[10] Liu Jia, Zhang Xiu-Mei. Study on the Prey Selection of Sea Stars (*Asterias amurensis*) Preying on Juvenile Oysters(*Crassostrea gigas*), Mussels (*Mytilus edulis*) and Clams (*Ruditapes philippinarum*) [J]. Periodical of ocean university of China, 2012, 42(7-8): 98 - 105.

[11] ZhouXuejia, LiuXinyi, WangShixin, et al. The primary study on the species composition and ecological distribution of Asteroidae in Shandong offshore [J]. Shandong Fhisheries, 1996, 13(1): 41 - 43.

[12] Yang Dejian, Sun Shichun. Marine invertebrate zoology [M]. QingDao: Qingdao Ocean University Press, 1999, 486 - 500.

[13] Hatanaka M, Kosaka M. Biological studies on the population of the starfish, *Asterias amurensis*, in Sendai Bay [J]. Tohoku Journal of Agricultural Research, 1958, 9 (3): 159 - 177.

[14] Davenport S R. Mcloughlin R. Preliminary assessment of the distribution and potential impact of the introduced starfish *Asterias amurensis* in Tasmanian waters: status report to Fisheries Research and Development Corporation [M]. Fisheries Research and Development Corporation (Australia) . Hobart: CSIRO Division of Fisherues, 1993: 38.

[15] Barkai A, McQuaid C. Predator-prey role reversal in a marine benthic ecosystem [J]. Science, 1988, 242: 62 - 64.

[16] Hawkes G, Day R. Review of the biology and ecology of Asterias amurensis: status report to Fisheries Research and Development Corporation [M]. Fisheries Research and Development Corporation(Australia) . Hobart: CSIRO Division of Fisherues, 1993: 38.

[17] Thompson M, Drolet D, Himmelman J H. Localization of infaunal prey by the sea star *Leptasterias* Polaris [J]. Marine Biology, 2005, 146: 887 – 894.

[18] Kim Y S. Histological observation of the annual change in the gonad of the starfish, Asterias amurensis Luken [J]. Bulletin of the Faculty of Fisheries, Hokkaido University, 1968, 19(2): 97 - 108.

[19] DU Mei-rong, FANG Jian-guang, ZHANG Ji-hong, et al. Feeding rate and food preference of Asterias amurensis on four species of bivalves [J]. Fishery Modernization, 2012, 39(2): 25 - 29.

[20] Tamura T, Fuji A, Tanaka S, et al. Injurious effects of the starfish on shellfishes [R]. "Hokusuishi Geppo" (Monthly Report of Hokkaido Fisheries Exp. St.), 1956, 13(6): 25 - 28.

[21] Himmelman J H, Dutil C, Gaymer C F. Foraging behavior and activity budgets of sea stars on a subtidal sediment bottom [J]. J . Exp. Mar. Biol. Ecol., 2005, 322: 153 - 165.

[22] Barbeau M A, Scheibling R E. Behavioral mechanisms of prey size selection by sea stars (*Asterias vulgaris Verrill*) and carbs (Cancer irroratus Say) preying on juvenile sea scallops (*Placopecten magellanicus* (Gmelin)) [J]. J . Exp. Mar. Biol. Ecol., 1994, 180: 103 - 136.

[23] Laudien J, Wahl M. Indirect effects of epibiosis on host mortality: seastar predation on differently fouled mussels [J]. Mar. Ecol., 1990,20(1): 35-47.

[24] Kim Y S. Selective feeding on the several bivalve mollusks by starfish, Asterias amurensis lüken [J].

Bull. Fac. Fish. Hokkaido univ., 1969, 19(4): 244 - 249.

[25] Penney A J, Griffiths C L. Prey selective and the impact of the starfish *Marthasterias glacialis* (L.) and other predators on the mussel *Choromytilus Meridionalis* (Krauss) [J]. J. Exp. Mar. Biol. Ecol., 1984,75(1): 19 - 36.

[26] Shang Yuchang. Behavioural Ecology [M]. Beijing: Peking University Press, 1998, 20 - 22.

[27] Turner E. A northern Pacific seastar, *Asterias amurensis*, in Tasmania [J]. AMSA Bulletin, 1992, 120(9) : 18 - 19.

[28] Liu Jia. Preliminary study of foraging behavior and reproductive biology of the sea star *Asterias amurensis* [D]. Qingdao: China Ocean University Master Thesis, 2012: 47 - 50.

[29] Toyo Takami. A research on the increase of *S.broughtonii* [J]. Aquaculture, 1981, 29(1): 38 - 56.

[30] ZHANG Haifa, LIU Xiaochun, LIN Haoran, et al. Studies on feeding rhythm and daily feeding amount of larval Epinephelus coioides [J]. Journal of fisheries of China, 2004, 28(6): 669 - 674.

[31] Elner R W, Hughes R N. Energy maximization in the diet of the shore crabs, *Carcinus maenas* [J]. J. Anim. Ecol., 1978, 47(1): 103 - 107.

[32] Tamura T. The power of the adductor muscle of the oyster, Ostrea circunpicta Pils [J]. Sci. Rep. Tohoku Imp. Univ., 1929, 4(4): 259 - 279.

多棘海盘车对魁蚶摄食量、选择性及昼夜摄食差异的初步研究

张天文，刘广斌，刘恩孚，郑永允，邱兆星*

（山东省海洋生物研究院 山东 青岛 266002）

摘 要：在水温为 16 ～ 20℃、盐度 28.2 ± 2.1、溶解氧为（7.5 ± 0.7）mg/L、pH 为 8.0 ± 0.3 的条件下，研究了 3 种规格多棘海盘车（*Asterias amurensis*）对 4 种规格魁蚶（*Scapharca broughtonii*）的摄食量、摄食选择性和摄食昼夜差异。研究表明：多棘海盘车对不同规格魁蚶摄食数量均随魁蚶底播密度的增加而上升；不同规格多棘海盘车对同一规格魁蚶摄食数量无显著差异（$p>0.05$），但对不同规格魁蚶摄食数量存在一定差异，对于最小壳长组的摄食数量最大；多棘海盘车对不同规格魁蚶软体部摄食量与魁蚶规格呈成显著正相关；多棘海盘车对不同规格魁蚶摄食数量均存在一定的昼夜差异且夜间的摄食数量大于昼间，魁蚶规格越大，多棘海盘车对魁蚶最大摄食数量时间出现的越晚。结果表明：魁蚶适宜底播密度在 30 ind/m^2 左右，底播规格越大越能有效防御敌害。根据多棘海盘车对贝类捕食特点，可采用浅水低值贝类作为诱捕生物对多棘海盘车进行清除。

关键词：多棘海盘车；魁蚶；摄食量；摄食选择性；昼夜差异

Effects of salinities on the growth and nutrient composition in the muscle of *Exopalaemon carinicauda*

JIANG Ju-feng[1], WU Hui-min[1], GUO Hua-yang[2], ZHANG Zhen-guo[1], LIU Xiao-lian[1], XIA Su-dong[1], ZHUANG Bao-lu[3], FU Zhi-ru[1]

1. *Tianjin Fisheries Research Institute, Tianjin* 300221, *China;*

2. *South China Sea Fisheries Research Institute, Chinese Academy of Fishery Sciences, Key Laboratory of South China Sea Fishery Resources Exploitation & Utilization, Ministry of Agriculture, Guangzhou* 510300, *Guangdong Province, China;*

3. *Fishery Machinery and Instrument Research Institute, Chinese Academy of Fishery Sciences, Shanghai* 200092, *China*

Abstract: The effect of salinity on the growth and muscle nutritional quality of the *Exopalaemon carinicauda* was studied through testing the survival rate, specific growth rate, muscle nutrient composition, amino acid composition and content by the culturing in different salinities(0-30).The results showed that the survival rate of salinity (0-30) had no significant difference ($P>0.05$), and the specific growth rates at salinity 15 and salinity 20 were significantly higher than others($P>0.05$); the muscle moisture content and the crude fat content significantly decreased($P<0.05$), while the muscle crude protein content significantly increased with an increase in the environment salinity from 0 to 30($P<0.05$).The crude ash content with salinity increase had a slight increase; the muscle crude protein content (18.2) at salinity 15 was significantly higher than that at salinity 0,5, or 10($P<0.05$), but there was no significant difference between salinity 15 and salinity 20($P>0.05$). No significant difference was found in total amino acid content or total essential amino acid content from salinity 0 to 30($P>0.05$). Total delicious amino acid content at salinity 15-30 was significantly higher than those at salinity 0-10 ($P<0.05$), while there was no significant difference from salinity 15 to 30($P>0.05$). The results suggest that the suitable salinity for muscle nutritive value ranges from 15 to 30, and the Exopalaemon carinicauda can potentially be cultured above the salinity 15.

Keywords: salinity; *Exopalaemon carinicauda*; survival rate; specific growth rate; nutrient composition

Received on Jun. 26, 2015

Corresponding author: jufengjiang@163.com

Exopalaemon carinicauda Holthuis which is also known as White Shrimp, Five Shrimp and Winter Jasmine Shrimp, et al., attaches to *Curstaea, Decapoda*, *Natantia, Palaemonidae, Palaemon*, *ExoPalaemon.* At present, according to incomplete statistics, *Exopalaemon carinicauda* Holthuis's fishery area is more than 10 000 hectares all around the country and it becomes the main economic shrimp for the single pond cultivating and the polyculture pond with fish, crab and shellfish. In recent years, with the scale expansion of the *Exopalaemon carinicauda* Holthuis's cultivat*ion,* desalting culture has become one of the important patterns for *Exopalaemon carinicauda* Holthuis's faming. However, in some areas of our country, the *Exopalaemon carinicauda* Holthuis of desalting culture shows weak market and low benefit due to its poor quality and bad taste compared with mariculture and wild *Exopalaemon carinicauda* Holthuis. It severely affects the culturist's enthusiasm. Therefore, discussing the best desalting salinity is of great significance to the development in *Exopalaemon carinicauda* Holthuis industry. Now the report on *Exopalaemon carinicauda* Holthuis mainly focuses on breeding the technology, biology and ecology, immune disease, population genetic structure, et al.[1-7]. With regard to the research on the nutrition in *Exopalaemon carinicauda* Holthuis, while it doesn't see any relevant report about the effect of salinity on *Exopalaemon carinicauda* Holthuis's muscle quality except the analysis on differences between natural population and breeding groups[8].

This article is based on *the* test object *of Exopalaemon carinicauda* Holthuis and the research about its corresponding change conditions of the survival rate, nutrient composition of muscle and amino acid composition or content under different salinity breeding of *Exopalaemon carinicauda* Holthuis. From the perspective of growth, muscle nutrition composition and quality, the suitable salinity range of the shrimp farming is discussed so as to provide theoretical basis for the artificial culture.

1 Materials and methods

1.1 Materials

The experimental shrimps were bought from Hongqi wholesale market in Tianjin and transported to the laboratory of Tianjin Fisheries Research Institute by the living water car. They were domesticated breeding in the glass reinforced plastic. During this period, the water temperature ranged from 18 °C to 20 °C, and the salinity was 25‰ and the water was changed every day. After domestication of 7 days, the shrimps were used for the salinity experiment. The method of Hongzheng You, et al. [9] about the salinity control can be a reference for the test water and its control. Choosing the uniform size and strong

individual for the experiment, its body quality was (2.90 ± 0.62) g and length was (5.65 ± 0.45) cm. The glass reinforced plastic(800 mm × 500 mm × 450 mm, with the water of 140 L)was used for the experimental container.

1.2 The design of the experiment and management

Salinity Experiment: In the test, it is divided into seven groups and their salinities are 0, 5, 10, 15, 20, 25 and 30 respectively. Among these seven experimental groups, each group is designed for three parallels. In each tank, 50 shrimps are put randomly. Salinity test is conducted for six weeks.

Daily Management: During the test, the bait is put in twice a day when it is 9:00am and 14:30pm and the bait residues must be cleaned up before feeding every time. In the test, it needs continuous aeration and water temperature is kept at(20±1) °C. The feed for test adopts the *Penaeus vannamei* Boone of Zhengshui Brand from Tianjin Zhenghua Feed CO. LTD and its nutrient composition is as follows: crude protein covers 42%, and crude fat 4.0%, crude ash 15%, crude fiber 5.0%, moisture 12%, calcium 3.0%, lysine 2.1% and the total phosphorus covers 0.9% - 1.45%。

Sampling and Measuring method: After the experiments, the muscles of six farmed shrimps are taken as samples from each of the parallels in the salinity groups respectively. The concrete steps of muscle sampling are as the following: cleaning the sampled shrimps by distilled water, wiping up the water on the surface, taking the muscles after dealing with the head and shell, operating under the ice-bath, taking the samples, and after that, these samples will be put in the refrigerator for further test. After measuring, shearing the shrimp muscles into pieces, mashing, mixing and drying it at 60 °C for constant weight, the samples are divided into two groups, including one used for the nutrient composition measurement and the other for the amino acid composition measurement.

The measurement of content in the crude protein takes the GB/T5009.5-2010 kjeldahl determination for the reference and the measurement of moisture content refers to the GB 5009.3 2010 with 105 °C constant press and temperature drying method. The measurement of crude fat content refers to GB/T 5009.6 2003 soxhlet extraction method. The crude ash content refers to GB/T 5009.4 2010 with 550 °C drying ash content method. The determination of amino acids (except the tryptophan) adopts the method of hydrochloric acid hydrolysis and the determination of tryptophan adopts GB/T 15400-94 fluorescence spectrophotometry.

1.3 Data management and statistical analysis

The SPSS16.0 statistical analysis software is used for the data analysis and the

Duncan method is used for the multiple comparison, and the significant difference is according to $P<0.05$. The descriptive statistics are calculated from the average value ± standard deviation ($\bar{x} \pm s$)).

$SGR=100\times(\ln W_t - \ln W_o)/t$

where W_t is the weight of shrimps at the end of the test, g; W_o is the weight of shrimps at the beginning of the test, g; and t is the time of cultivation, d.

The essential amino acid index (EAAI) is calculated by the following formula [10]:

$$EAAI=\sqrt[n]{\frac{100W_1}{We_1}\times\frac{100W_z}{We_z}\times\cdots\cdots\times\frac{100W_n}{We_n}}$$

where n means the comparative amino acid value, and W_1, W_2, …, W_n mean the content of some essential amino-acid in the protein of samples(mg / g), and $W_{e1}, W_{e2}, \ldots, W_{en}$ mean the content of some essential amino-acid in the egg protein(mg/g).

2 Results

2.1 Effects of salinity on the growth and survival of the *Exopalaemon carinicauda*

At the end of the test, there are only 6 shrimps left in one of the tanks except the salinity group Y0 and there are only 10 shrimps left between the salinity group Y5 and salinity group Y20, while the survival shrimps in other tanks are all above 17. It can be seen from Tab. 1 that in the 42d test, there is no significant difference in text groups and its survival rates of the *Exopalaemon carinicauda* are all above 30%. The highest survival rate is 48.67% in the salinity group Y25 and the lowest survival rate is 32.67% in the salinity group Y20. The survival rates are higher in the salinity groups Y10 and Y15 (47.33% and 46% respectively).

The SGR of *Exopalaemon carinicauda* in the groups Y15 and Y20 is significantly higher than that in other groups($P<0.05$). There is no significant difference among the groups Y5, Y10, Y25, Y30($P>0.05$), but they are all significantly higher than that in group Y0($P<0.05$). The lowest SGR is 0.20 in the salinity group Y0 and the highest SGR is 0.47 in the salinity group Y20, while other groups are all above 0.3. With the increase of the salinity, the SGR is rising in the groups 0-20 and it is reduced in the test groups beyond 20.

Tab. 1 Effects of salinity on the growth and survival of the *Exopalaemon carinicauda*

Item	Test groups						
	Y0	Y5	Y10	Y15	Y20	Y25	Y30
Survival rate /%	34.7±20.5[a]	31.3±9.9[a]	47.3±8.1[a]	46±7.2[a]	32.7±11.1[a]	48.7±8.1[a]	40.7±7.0[a]
SGR /（%/d）	0.20±0.01[c]	0.34±0.11[b]	0.30±0.04[b]	0.46±0.02[a]	0.48±0.01[a]	0.36±0.03[b]	0.33±0.04[b]

Note: in the same row, values with different superscripts are significantly different(P<0.05).

2.2 Effects of salinity on nutrient composition in the muscle of the *Exopalaemon carinicauda*

It can be seen from Tab. 2 and Tab. 3, that with the increase of salinity, the crude protein content in the muscle of *Exopalaemon carinicauda* presents an upward tendency in a straight line(R^2=0.886 1, P<0.05). There is no significant difference among the salinity groups Y0 - Y10 (P>0.05), nor does it in the salinity groups Y15 - Y20(P>0.05), but the significant difference in groups Y15 - Y20 is higher than that in groups Y0 - Y10(P<0.05). The content in the salinity group Y25 is significantly higher than that in the salinity groups Y0 - Y20(P<0.05) and that in the salinity group Y30 is significantly higher than that in any other groups(P<0.05). With the increase of salinity, the content of crude fat presents a linear decrease trend (R^2 = 0.935 8, P<0.01). There is no significant difference among the salinity groups Y0 - Y10 (P>0.05), but that in these groups is higher than that in any other salinity groups (P<0.05). There is no significant difference among the salinity groups Y15 - Y30(P>0.05). With the increase of salinity, the crude ash content presents a gradually linear increase trend. There is no significant difference among the salinity groups Y0 - Y15 (P>0.05), but that in these groups is significantly lower than that in group Y30. There is no significant difference among the salinity groups Y20 - Y25(P>0.05), but it is higher than that in the salinity group Y5(P<0.05). The moisture content in the muscle presents a linear decrease trend with the increase of salinity(R^2 = 0.938 7, P<0.01). There is no significant difference between the salinity groups Y0 - Y10 (P>0.05), but that in these groups is higher than that in any other salinity groups(P<0.05). That content in the group Y15 is significantly higher than that in the salinity groups Y20 - Y30(P<0.05), and that in the group Y20 is significantly higher than that in the salinity groups Y25 - Y30(P<0.05), and the content in the group Y25 is significantly higher than that in the salinity group Y30(P<0.05).

Tab. 2 Nutrient composition in the muscle of the *Exopalaemon carinicauda*

(*n*=3, flesh weight basis, %)

test group	crude protein/%	crude fat/%	crude ash/%	moisture /%
Y0	17.47±0.02^{d}	0.79±0.02^{a}	1.39±0.03^{bc}	80.21±0.02^{a}
Y5	17.47±0.04^{d}	0.76±0.01^{a}	1.36±0.03^{c}	80.20±0.09^{a}
Y10	17.49±0.18^{d}	0.76±0.04^{a}	1.38±0.04^{bc}	80.06±0.18^{a}
Y15	18.02±0.12^{c}	0.70±0.02^{b}	1.40±0.02^{bc}	79.64±0.09^{b}
Y20	18.13±0.09^{c}	0.63±0.03^{c}	1.42±0.01^{ab}	79.23±0.08^{c}
Y25	18.68±0.08^{b}	0.59±0.01^{d}	1.43±0.03^{ab}	79.03±0.01^{d}
Y30	19.15±0.04^{a}	0.55±0.02^{e}	1.47±0.04^{a}	78.61±0.05^{e}

Note: in the same column, values with different superscripts are significantly different(P<0.05).

Tab. 3 Relationship between salinity and nutrient composition in the muscle of the *Exopalaemon carinicauda*

Component	Equation	R^2	*P*
crude protein	y=0.058x+17.193	0.886 1	<0.05
crude fat	y=−0.008 6x+0.812 5	0.935 8	<0.01
crude ash	y= 0.003x+1.361 3	0.550 7	>0.05
moisture	y=−0.056 9x+80.424	0.938 7	<0.01

2.3 Effects of salinity on the amino acid composition and content in the muscle of the *Exopalaemon carinicauda*

It can be seen from Tab. 4, that under different conditions of salinity breeding, 18 kinds of amino acids are tested from the muscle of *Exopalaemon carinicauda*. With the increase of salinity, the contents of the valine, tryptophan, lysine and proline present a gradually decreased trend(P<0.05) and the contents of alanine, isoleucine, histidine and arginine present a gradually increased trend(P<0.05).The contents of the glutamic acid, leucine and phenylalanine don't have a big change with the increase of salinity, and they are kept at the same level (P>0.05). Aspartic acid, threonine, glycine, cystine and tyrosine present the increased trend first, and then they decrease later, but they show different at the falling node. Aspartic acid and cystine begin to reduce in the salinity group Y10. Threonine begins to decrease in the salinity group Y25, and glycine begins to decrease in

the salinity group Y20, and tyrosine in the salinity group Y15. The content of methionine in the salinity groups Y0- Y15 is lower than that in the groups Y20 - Y30($P<0.05$).

There is no significant difference in the total content of amino acids(TAA) and essential amino acids(EAA)($P>0.05$). The total content of the delicious amino acid (DAA) in salinity groups Y15 - Y30 is significantly higher than that in the groups Y0 - Y10($P<0.05$), while there is no significant difference among the salinity groups Y15 - Y30 in the DAA($P>0.05$), and that in the salinity group Y10 is higher than that in the group Y0 ($P<0.05$), but comparing to group Y5, there is no significant difference($P>0.05$). EAA/TAA remain stable (0.45 - 0.46) among the salinity groups Y0 - Y30. The highest EAAI is 79.49 in the salinity group Y20 and the lowest EAAI is 76.24 in the salinity group Y30, and in other groups, EAAI all keeps between 78.16 - 79.23.

3 Discussion

3.1 Effects of salinity on the growth and survival of the *Exopalaemon carinicauda*

Exopalaemon carinicauda is a kind of *euryhaline* shrimps and can grow in a larger salinity range. In this research, the domesticated *Exopalaemon carinicauda* can survive the salinity range from salinity 0 - 30, but the mortality is higher, and the reason for this may be because of tanks and the space is lesser. The results show that the survival rate of salinity (0 - 30) has no significant difference ($P>0.05$), and theY0, Y5, Y20 all have tanks with the higher mortality, which cause the lower survival rate, but the survival rates of other groups are all above 40%, and the survival rates of Y10, Y15 and Y25 are 46% - 48.67%。The specific growth rate of Y0 is lowest, and the specific growth rates of Y15 and Y20 are significantly higher than others($P<0.05$), and the specific growth rates of lower groups are 0.3 - 0.36.

3.2 Effects of salinity on the nutrient composition in the muscle of *Exopalaemon carinicauda*

The nutrient composition in the muscle of the fishes and shrimps will be affected significantly with the change of the salinity in the environment. The research carried out by Shi Yonghai [11] shows that with the increase of the salinity, the content of moisture in the muscle of Parapenaeopsis hardwickii presents the significantly decreased trend and the content of the crude protein presents an increased trend, while the content of the crude fat presents a gradually decreased trend. The content of the crude protein and crude ash in the muscle of the Litopenaeus vannamei cultivated in the seawater is significantly higher than that in the freshwater($P<0.05$), while the moisture content is lower than that cultivated

in the freshwater [12]. The result in this study is similar to the report given above that with the increase of the salinity, the moisture content in the muscle presents a decreased trend and the content of the crude protein presents an increased trend. In the research on the Lateolabrax japonicas[13], it is found that with the increase of salinity, the content of the crude protein and crude fat are increased significantly, while the crude ash and moisture are decreased significantly. With reference to *Scophthalmus maximus*[14], *Channa argus*[15] and *Ctenopharyngodon idellus*[16], it is found that the content of its crude protein and crude fat are decreased with the increase of the salinity ,while the content of moisture is increased. The contents of the moisture and crude protein in the muscle of the *Portunus trituberculatus*[17] don't change obviously with the effect of the salinity in the external environment, however, the content of its crude fat is increased. The contents of the moisture, crude protein and crude fat in the muscle of the *Plectropomus leopardus*[9] and *Epinephelus coioides*[18] don't change obviously under the effect of the salinity. Therefore, with the change of salinity in the external environment, the nutrient composition in the muscle of different aquatic animals changes differently.

In this study, with the increase of the salinity, the possible reason to the result in the moisture content decrease in the muscle of *Exopalaemon carinicauda Holthuis* is that shrimp organism needs to lose parts of its moisture to maintain the osmotic balance in the body under the environment of high salinity, and to the contrary, under the environment of the low salinity, the shrimp organism needs to absorb more moisture[19], this is the same with the result of researching on the *Parapenaeopsis hardwickii*[11].

3.3 Effects of salinity on the amino acid composition and content in the muscle of the *Exopalaemon carinicauda*

The content of the Glycin, Leucine, Phenylalanine and Arginine in the muscle of the *Litopenaeus vannamei* [20] is increased significantly with the increase of the salinity groups 0 - 30($P>0.05$). The contents of the Glycin, Methionine, Proline in the muscle of *Parapenaeopsis hardwickii*[11] are increased significantly with the increase of the salinity groups 12 - 36($P>0.05$). And in the muscle of the *Macrobrachium nipponense*[21], the contents of the valine, methionine, lysine, histidine, glycine, glutamic acid, alanine, serine, tryptophan are gradually increased in the salinity groups 0 - 14 ,while in the salinity groups 14 - 20, they are decreased. In this research, with the increase of the salinity (0-30), the contents of the alanine, histidine, isoleucine, arginine in the muscle of *Exopalaemon carinicauda* Holthuis are significantly increased($P>0.05$). Thus, effects of salinity are not the same on the amino acid composition and content in the muscle of different shrimps.

Tab. 4 Amino acid composition and content in the muscle of the *Exopalaemon carinicauda*

(n=3, dry weight basis, %)

Amino acid composition	Test groups						
	Y0	Y5	Y10	Y15	Y20	Y25	Y30
Aspartic acid^{+}	8.00±0.11^{ab}	8.07±0.07^{a}	8.02±0.08^{ab}	8.02±0.09^{ab}	7.95±0.03^{ab}	7.90±0.07^{b}	7.99±0.06^{ab}
Threonine^{-}	3.00±0.06^{c}	3.03±0.10^{bc}	3.09±0.17^{abc}	3.22±0.04^{abc}	3.29±0.07^{a}	3.23±0.07^{abc}	3.25±0.22^{ab}
Serine	2.80±0.11^{a}	2.41±0.31^{b}	2.41±0.29^{b}	2.29±0.09^{b}	2.22±0.05^{b}	2.26±0.07^{b}	2.23±0.06^{b}
Glutamic acid^{+}	9.64±0.03^{a}	9.68±0.06^{a}	9.66±0.12^{a}	9.59±0.14^{a}	9.55±0.14^{a}	9.63±0.13^{a}	9.43±0.24^{a}
Glycine^{+}	6.44±0.05^{c}	6.55±0.11^{bc}	6.70±0.04^{b}	7.14±0.09^{a}	7.05±0.12^{a}	7.01±0.13^{a}	7.11±0.14^{a}
Alanine^{+}	5.34±0.03^{e}	5.52±0.10^{de}	5.55±0.14^{d}	5.91±0.10^{c}	6.00±0.13^{bc}	6.18±0.10^{ab}	6.22±0.13^{a}
Cystine^{-}	0.66±0.05^{ab}	0.71±0.05^{a}	0.65±0.09^{ab}	0.56±0.03^{bc}	0.51±0.03^{cd}	0.51±0.03^{d}	0.42±0.09^{d}
Valine^{-}	3.62±0.03^{a}	3.57±0.07^{a}	3.46±0.15^{ab}	3.29±0.21^{bc}	3.23±0.18^{bc}	3.10±0.10^{c}	3.09±0.17^{c}
Methionine^{-}	2.04±0.08^{b}	2.00±0.11^{b}	2.09±0.12^{b}	2.19±0.15^{b}	2.42±0.12^{a}	2.61±0.10^{a}	2.57±0.16^{a}
Tryptophan^{-}	1.13±0.03^{a}	1.13±0.06^{a}	1.04±0.11^{ab}	0.98±0.10^{bc}	0.95±0.03^{bc}	0.97±0.03^{bc}	0.89±0.05^{c}
Isoleucine^{-}	3.72±0.03^{b}	3.81±0.06^{b}	3.86±0.10^{b}	4.11±0.07^{a}	4.13±0.08^{a}	4.24±0.13^{a}	4.25±0.13^{a}
Leucine^{-}	5.86±0.05^{a}	5.91±0.11^{a}	5.84±0.24^{a}	5.88±0.20^{a}	5.89±0.08^{a}	5.87±0.01^{a}	5.77±0.10^{a}
Tyrosine^{-}	2.73±0.05^{ab}	2.78±0.04^{a}	2.81±0.12^{a}	2.80±0.04^{a}	2.75±0.09^{ab}	2.62±0.05^{bc}	2.60±0.02^{c}
Phenylalanine^{-}	3.79±0.05^{a}	3.89±0.15^{a}	3.91±0.13^{a}	3.96±0.07^{a}	3.96±0.10^{a}	3.97±0.19^{a}	3.94±0.17^{a}
Lysine^{-}	11.39±0.03^{a}	11.43±0.11^{a}	11.28±0.05^{ab}	11.28±0.14^{ab}	11.09±0.08^{bc}	11.07±0.08^{c}	10.96±0.21^{c}
Histidine	1.89±0.03^{c}	1.99±0.11^{c}	2.09±0.17^{cb}	2.24±0.04^{ab}	2.38±0.12^{a}	2.38±0.09^{a}	2.40±0.24^{a}
Arginine	6.45±0.11^{b}	6.63±0.16^{ab}	6.64±0.26^{ab}	6.76±0.08^{ab}	6.85±0.20^{a}	6.88±0.15^{a}	6.90±0.20^{a}
Proline	4.77±0.14^{a}	4.76±0.05^{a}	4.61±0.07^{ab}	4.42±0.17^{bc}	4.32±0.08^{c}	4.21±0.12^{cd}	4.07±0.16^{d}
TAA	83.25±0.23^{a}	83.87±0.95^{a}	83.73±1.39^{a}	84.65±0.59^{a}	84.53±0.45^{a}	84.66±0.22^{a}	84.66±0.22^{a}
EAA	37.94±0.09^{a}	38.26±0.43^{a}	38.03±0.65^{a}	38.27±0.42^{a}	38.22±0.30^{a}	38.19±0.22^{a}	37.75±0.39^{a}
DAA	29.42±0.08^{c}	29.82±0.21^{bc}	29.94±0.15^{b}	30.66±0.40^{a}	30.55±0.20^{a}	30.73±0.41^{a}	30.75±0.33^{a}
EAA/TAA	0.46	0.46	0.45	0.45	0.45	0.45	0.45
EAAI	78.62	79.23	78.83	78.22	79.49	78.16	76.24

Note: "−" indicates human essential amino acid; "+"indicates delicious amino acid; in the same row, values with different superscripts are significantly different($P<0.05$).

The nutritional value and flavor in the muscle mainly depend on the amino acid composition and the content of the essential amino acids and delicious amino acids in the human body. There is no significant differences between the salinity groups 12 - 36 about the TAA and DAA in the *Parapenaeopsis hardwickii*[11], while the EAA and semi-EAA in the salinity groups 12 - 24 are significantly higher than those in the groups 28 - 36. With regard

to the amino acids in the muscle of the *Macrobrachium nipponense*[21] among salinity groups 0 - 20, the TAA and EAA increase first and then slightly decrease later, while the DAA presents the increased trend.

In this research, there is no significant differences between every group about the TAA and EAA in the *Exopalaemon carinicauda*($P > 0.05$). It can be seen from the TAA and EAA that there is no significant differences among every group about the nutritional value in the muscle. The DAA in the salinity groups Y15 - Y30 is significantly higher than that in the groups Y0 - Y10($P < 0.05$).

While there is no significant differences among the salinity groups Y15 - Y30($P > 0.05$). It can be seen from the DAA, the muscle taste of the *Exopalaemon carinicauda* in the salinity groups Y15 - Y30 is more delicious than that in groups Y 0 - Y10.

4 Conclusion

The domesticated *Exopalaemon carinicauda* can survive the salinity range from Y0 - Y30. The higher the survival rate is in the groups Y10 - Y25, the higher the SGR is in the group Y15 and Y20. The content of the crude protein is 18.02 in the salinity group Y15 and it is significantly higher than that in the salinity groups Y0 - Y10($P<0.05$), while there is no significant difference compared with salinity group Y20($P>0.05$). It is seen from the amino acid composition and EAA in the muscle, that there is no significant difference in all the salinity groups($P>0.05$), but from the perspective of the total content of flavor amino acid, that in the salinity groupsY15 - Y30 is significantly higher than that in Y0 - Y10($P<0.05$) and there is no significant difference in the salinity groups Y15 - Y30($P>0.05$). In conclusion, the lowest salinity value should keep 15 for the desalting culture of *Exopalaemon carinicauda* to ensure its flavor.

Acknowledgements

This work is supported by Fund of Key Laboratory of South China Sea Fishery Resources Exploitation & Utilization, Ministry of Agriculture, P. R. China(LSF2012-05).

References

[1] SHEN Hui, WAN Xihe, WANG Libao, et al. Study on experimental infection of *Exopalaemon carinicauda* Holehuis with white spot syndrome virus [J]. Marine Sciences, 2013, 37(5): 55 - 60.

[2] NI Jianzhong, ZHANG Jie. The Ecological pond aquaculture technology of *Cynoglossus semilaevis*

and *Palaemon (Exopalaemon) carinicauda* [J]. Scientific Fish Farming, 2013,(4): 43 - 44.

[3] JIA Shuwen, LIU Ping, LI Jian, et al. Microsatellite analysis of genetic diversity in 3 wild populations of *Exopalaemon carinicauda* [J]. Journal of Fisheries of China, 2012, 36(12):1 819 - 1 825.

[4] DUAN Yafei, LIU Ping, LI Jitao, et al. Immune gene discovery by expressed sequence tag (EST) analysis of hemocytes in the ridgetail white prawn *Exopalaemon carinicauda* [J]. Fish & Shellfish Immunology, 2013, 34(1): 173 - 182.

[5] DUAN Yafei, LIU Ping, LI Jitao, et al. Expression profiles of selenium dependent glutathione peroxidase and glutathione S-transferase from *Exopalaemon carinicauda* in response to Vibrio anguillarum and WSSV challenge [J]. Fish & Shellfish Immunology, 2013, 35(3): 661 - 670.

[6] ZHANG Chengsong, LI Fuhua, XIANG Jianhai. Effects of salinity on growth and first sexual maturity of *Exopalaemon carinicauda*(Holthuis,1950) [J]. Chinese Journal of Oceanology and Limnology, 2014, 32(1): 65 - 70.

[7] YUAN Hexia, PENG Yanqiang, SUN Bin, et al. Research on ecological efficient technology of mixed farming of Sphyraenus, Exopalaemon carinicauda and Sinonovacula constrzcta [J]. Scientific Fish Farming, 2013, (8): 42 - 43.

[8] SHAO Yinwen, WANG Chunlin, LI Dipin, et al. The nutritional differences of *Exopalaemon carinicauda* between natural population and breeding groups [J]. Reservoir Fisheries, 2008, 28(4): 34 - 37.

[9] YOU Hongzheng, SUN Zhijing, ZHANG Qin, et al. Effects of salinity on feeding, growth and body composition in juvenile leopard coraltrout *Plectropomus leopardus* [J]. Journal of Dalian Ocean University, 2013, 28(1): 89 - 93.

[10] JIANG Jufeng, HAN Xianqin, FU Zhiru, et al. Analysis and Assessment of Muscle Nutritive Composition Between Female and Male Neosalanx brevirostris Pellegrin [J]. Journal of Guangdong Ocean University, 2011, 31(4): 23 – 29.

[11] SHI YongHai, ZHANG GenYu, LIU YongShi, et al. Effects of Salinity on Nutrient Composition, Amino Acid Composition and Content in the Muscle of Parapenaeopsis hardwickii [J]. Chinese Journal of Zoology, 2013, 48(3): 399 – 406.

[12] PENG Yongxing, XU Xiang, CHENG Yulong, et al. Comparative Analysis of Nutrients in Muscles of Pacific White Leg Shrimp Litopenaeus vannamei Cultured in Seawater and Freshwater [J]. Fisheries Science, 2013, 32(8): 435 - 440.

[13] XU Janhe, YAN Bailun, TENG Yajuan, et al. Analysis of nutrient composition and fatty acid profiles of Japanese sea bass Lateolabrax japonicas(Cuvier)reared in seawater and freshwater [J]. Journal of Food Composition and Analysis, 2010, 23: 401 - 405.

[14] ZENG Lin, LEI Jilin, LIU Bin, et al. Effects of salinities on growth and flesh quality of juvenile turbot(Scophthalmus maximus) [J]. Journal of Fisheries of China, 2013, 37(10): 1 535 - 1 541.

[15] LI XiaoQin, LIU XianMin, LENG XiangJun, et al. Effect of salinity on growth and flesh quality of Snakehead channa argus [J]. Oceanologia Et Limnologia Sinica, 2008, 39(5):505 - 510.

[16] LI Xiaoqin, LI Xingxing, LENG Xiangjun, et al. Effect of different salinities on growth and flesh quality of Ctenopharyngodon idellus [J]. Journal of Fisheries of China, 2007, 31(3): 343 - 348.

[17] LV Fu, HUANG Jintian, YU Yebing, et al. Affects of salinity on growth,muscle compostion and protease activity of portunus trituberculatus [J]. Transactions of Oceanology and Limnology, 2010, (4): 137 - 142.

[18] LIN Jianbin, LI Jinqiu, ZHU Qingguo, et al. Effects of salinity on the growth, muscle composition and digestibility of Epinephelus coioides [J]. Marine Sciences, 2009, 33(3): 31 - 35.

[19] HUANG Kai, WANG Wu, LU Jie, et al. Salinity effects on growth and biochemical composition of Penaeus vannamei [J]. Marine Sciences, 2004, 28(9): 20 - 25.

[20] LIANG Meng-qing, WANG Shi-wen, WANG Jia-lin, et al. Effects of different salinities on free amino acid composition in muscle and hemolymph of the shrimp *Litopenaeus vannamei* [J]. Progress in Fishery Sciences, 2009, 30(2): 34 - 39.

[21] WANG Weina, WANG Anli, BAO Lai, et al. Changes of protein-bound and free amino acids in the muscle of the freshwater prawn Macrobrachium nipponense in different salinities [J]. Aquaculture, 2004, 233: 561 - 571.

盐度对脊尾白虾生长和肌肉营养成分影响的研究

姜巨峰[1]，吴会民[1]，郭华阳[2]，张振国[1]，刘肖莲[1]，夏苏东[1]，庄保陆[3]，付志茹[1]

（1. 天津市水产研究所，天津 300221；2. 中国水产科学研究院南海水产研究所，农业部南海渔业资源开发利用重点实验室，广东 广州 510300；3. 中国水产科学研究院渔业机械仪器研究所，上海 200092）

摘 要：为研究盐度对脊尾白虾（*Exopalaemon carinicauda*）生长及肌肉营养品质的影响，对不同盐度（0～30）环境下养殖的脊尾白虾存活率、特定生长率及肌肉营养成分进行了分析比较。结果显示，各盐度组脊尾白虾存活率差异不显著（P<0.05）；15、20 盐度组脊尾白虾特定生长率显著高于其它各组（P＜0.05）；肌肉的水分和粗脂肪随环境盐度升高出现显著下降（P<0.05），而粗蛋白含量随环境盐度升高而升高（P<0.05）；粗灰分含量随盐度升高有一定的上升趋势；脊尾白虾肌肉粗蛋白含量在盐度 15 时为 18.02，显著高于 0～10 盐度组（P<0.05），与盐度 20 组差异不显著（P>0.05）。肌肉氨基酸总量和必需氨基酸总量，各盐度组差异不显著（P>0.05），而风味氨基酸总量，15～30 盐度组显著高于 0～10 盐度组（P<0.05），且盐度组 15～30 之间均没有明显差异（P >0.05）。因此，脊尾白虾淡化养殖最低盐度应该保持在 15 以上，以保证其风味。

关键词：盐度；脊尾白虾；存活率；特定生长率；营养成分

Distribution of heavy metals in suspension in Bohai Bay

DONG Yu-bo

Fisheries Research Institute of Tianjin, Tianjin 300221, *China*

Abstract: Selecting suspension sample 51 stations in Bohai Bay contents of heavy metals(Fe, Mn, Si, Ba) analysis, studied the distribution of the suspension of heavy metals. It Showed that in the study area, the content of iron was the highest, silicon content was lowest; in descending order: Fe>Mn>Ba>Si; the coefficient of variation is between 7.60 and 110.35; except barium greater the degree of dispersion (coefficient of variation is greater than 100).With the samples of stations, the 4 kinds of heavy metals are from low to high, from the south to the north. Silicon content was the highest in 51 stations. The other 3 elements appeared in 50 stations.

Keywords: Bohai Sea, heavy metals, distribution

Suspended solids as main habitat of phytoplankton, zooplankton and nekton in recent years has been the focus of scientific research of the marine environment, and as an important place of primary productivity of photosynthesis, and growing concern. In recent years, with the rapid development of industrialization, industrial wastewater discharge has caused heavy metal pollution. In Bohai Bay, diatoms are the dominant species of phytoplankton, and sometimes the main index of the silicon element is the main factor of the monitoring, the manganese and iron are the essential trace elements for the growth of zooplankton.

1 The sources of data

The datas in this paper were from suspension of Bohai Bay of summer in 2014 . Each station acquisition surface seawater for 1 L, back to the lab, filtrating by 0.45 um membrane, membranes were digested by microwave, then by ICP-MS for the determination of the content of heavy metals (Fe, Mn, Si, Ba) in suspension.

Received on Oct. 25, 2015

Corresponding author: dongyubo2006@163.com

2 Figures of stance

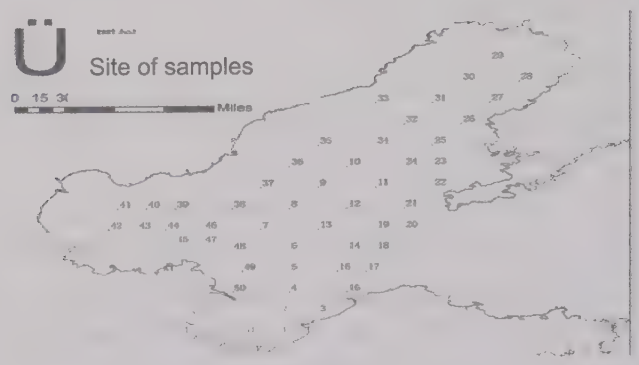

Fig. 1 Sampling Stations bitmap

3 Infusions and analysis

3.1 Index for heavy metals

Collectting and summarizing the data of heavy metals in 2014 for Bohai Bay, Statistical characteristics of the suspension of heavy metals contents were shown in Tab. 1.

Tab. 1 Statistical characteristics of heavy metal contents in suspension(ug/L, n=51)

Project	Fe	Mn	Si	Ba
Maximum	24 291.07	2 022.54	1.76	1 037.06
Minimum	277.42	48.52	0.20	22.24
Mean	7 945.62	609.47	1.60	282.14
Standard Deviation	5 902.52	510.34	0.12	311.34
Coefficient of Variation	74.29	83.74	7.60	110.35

Note: The Coefficient of Variation: CV=(SD/MN)*100%; SD is Standard deviation; MN is Mean.

According to Tab. 1, the average of heavy metals in the study area , the content of iron was the highest, silicon content was lowest; in descending order: Fe>Mn>Ba>Si; the coefficient of variation is between 7.60 and 110.35; except barium greater the degree of dispersion (coefficient of variation is greater than 100), the other elements of Fe, Mn and Si; the coefficient of variation of less than 50; the coefficient of variation of Si was smaller, more uniform spatial distribution, discrete small; and Ba spatial variation coefficient greater

than 50, indicating that the content of Ba in the uneven distribution of space, a large degree of dispersion.

Fig. 2 Distribution characteristics of heavy metals in different stations in suspension

3.2 Distribution of heavy metals

From Fig. 2, the 4 kinds of heavy metals are from low to high, from the south to the north. Silicon content was the highest in 51 stations. The other 3 elements appeared in 50 stations, 50 and 51 stations in the 4 kinds of heavy metal pollution of other stations seriously. Lowest value of Si and Mn elements appear in the 6 stations; Fe elements appear in the station No. 1; barium element is No. 10 stations; this shows that in the southern Gulf of Bohai Sea seston Si, Mn, Fe contamination from light; BA element pollution in the Central Bay of Bohai Sea light.

4 Conclusions

(1) The results showed that 4 heavy metals in the study area, the content of iron was the highest, silicon content was lowest; in descending order: Fe>Mn>Ba>Si; the coefficient of variation is between 7.60 and 110.35.

(2) The 4 kinds of heavy metals are from low to high with the sample of satations, from the south to the north in Bohai Bay. Silicon content was the highest in 51 stations. The

other three elements appeared in 50 stations.

(3) Bohai Bay had potential ecological risk.

Acknowledgments

This research is financially supported by Key Laboratory of Marine Oil Spill Identification and Damage Assessment Technology, State Oceanic Administration (201214) and Key Laboratory of Pollution Processes and Environmental Criteria (Nankai University), Ministry of Education (KL-PPEC-2013-09), and Tianjin aquatic Bureau Youth Fund (J-2014-08).

Reference

[1] YU Tao, ZHANG Yuan, ZHANG Yan. Distribution and bioavailability of heavy metals in different particle-size fractions of sediments in Taihu Lake, China [J]. Chemical Speciation and Bioavailability, 2012, 24(4): 205 - 215.

[2] GONG M, WU L, BI X Y, et al. Assessing heavy-metal contamination and sources by GIS-based approach and multivariate analysis of urban-rural topsoils in Wuha, central China [J]. Environmental Geochemistry and Health, 2010, 32(1) : 59 - 72.

[3] Bhuiyan M A H, Parvez L, Islam M A, et al. Heavy metal pollution of coal mine-affected agricultural soils in the northern part of Bangladesh [J]. J. Hazard Mater, 2010, 173(1) : 384 - 392.

[4] WU J R, Ember R, JIN M, et al. Isotopic evidence for the source oflead in the North Pacific abyssal water [J]. Geochimica et Cosmochimica Acta, 2010, 74(16) : 4 629 - 4 638.

渤海湾悬浮物中重金属的分布特征

董玉波

（天津市水产研究所，天津 300221）

摘 要：对 2014 年夏季渤海湾 51 个站位悬浮物样品中 4 种重金属（Fe、Mn、Si 和 Ba）含量进行了分析，研究了该海域悬浮物中重金属元素分布特征及其控制因素。结果显示，该海域中，重金属铁含量最高；硅含量最低；其他依次为：Fe>Mn>Ba>Si。钡的变异系数最大，超过 100，其他重金属的变异系数在 7.60 - 110.35 之间。所有采样站位中，四种重金属的含量，从南到北，显示由低到高的趋势。硅的最高浓度站位在 51 号站位；其他均在 50 号站位。

关键词：渤海湾；重金属；分布特征；控制因素

海 洋 通 报（英文版）

HAIYANG TONGBAO

2016 年 5 月 第 18 卷 第 1 期

目 次

黄河口海域潮汐、潮流、余流、切变锋数值模拟 …… 高 佳 等 (08)

2010年东亚季风月内尺度振荡特征及其与西南地区冬季气温的关系……齐冬梅 等 (28)

液化粉质土波动压力试验研究 …… 黄 哲 等 (42)

无居民海岛保护和利用规划中开发空间的确定方法 …… 姬厚德 等 (54)

七大流域氨氮水生生物水质基准与生态风险评估初探……王一喆 等 (68)

多棘海盘车对魁蚶摄食量、选择性及昼夜摄食差异的初步研究 ……张天文 等 (80)

盐度对脊尾白虾生长和肌肉营养成分影响的研究 …… 姜巨峰 等 (92)

渤海湾悬浮物中重金属的分布特征 …… 董玉波 (96)

Marine Science Bulletin

Marine Science Bulletin publishes papers on marine science and technology including physical oceanography, chemical oceanography, marine biology, marine geology, environmental oceanography, estuarine & coastal sciences, marine technology, digital ocean, coastal zone management, ocean engineering, marine economics, etc., and aims to promote international academic exchange.

Editor-in-Chief: SHI Sui-xiang (石绥祥)
Associate Editor-in-Chief: XIANG Wen-xi (相文玺) LI Xue (李雪)
Executive Editor: QIU Wen-jing (邱文静)
Editor: DONG Yi (董 艺) LI Xiao-guang (李晓光) YUAN Ze-yi (袁泽轶)

English proofed by: WANG Qi (王 琦)

Semi-annually (started in 1999, sum 35)
Publication date: May 15th and Oct. 15th

Marine Science Bulletin **(Vol. 18, No. 1, May 2016)**

Responsible Institution:
State Oceanic Administration of China
Sponsored by:
National Marine Data and Information Service
Edited by:
Office of Marine Science Bulletin (English edition)
Printed by:
Printery of National Marine Date and Information Service

Published by:
Office of Marine Science Bulletin (English edition)
E-mail: msb1999@163.com
Tel: (022) 24011287
Address: 93 Liuwei Rd., Hedong District, Tianjin 300171, China

---

ISSN1000-9620
CN12-1271/N

ISSN 1000-9620

Price: $ 30.00 / ￥40.00 Per year